ATTITUDE CONTROL OF SPINNING SATELLITES USING ENVIRONMENTAL FORCES

by

KAILASH CHANDRA PANDE
B.Sc. Eng. (Hons.), Banaras Hindu University, 1966
M.Sc., University of Saskatchewan, 1969

A THESIS SUBMITTED IN PARTIAL FULFILMENT OF
THE REQUIREMENTS FOR THE DEGREE OF
DOCTOR OF PHILOSOPHY

in the Department
of
Mechanical Engineering

We accept this thesis as conforming to the
required standard

THE UNIVERSITY OF BRITISH COLUMBIA

November, 1973

In presenting this thesis in partial fulfilment of the requirements for an advanced degree at the University of British Columbia, I agree that the Library shall make it freely available for reference and study. I further agree that permission for extensive copying of this thesis for scholarly purposes may be granted by the Head of my Department or by his representatives. It is understood that publication, in part or in whole, or the copying of this thesis for financial gain shall not be allowed without my written permission.

KAILASH CHANDRA PANDE

Department of Mechanical Engineering

The University of British Columbia,
Vancouver 8, Canada

Date February 11, 1974

ABSTRACT

The feasibility of utilizing the environmental forces for three-axis librational damping and attitude control of spinning satellites is investigated in detail. An appreciation of the environmental influence is first gained through a librational dynamics study of spinning, axisymmetric, cylindrical satellites in the solar radiation pressure field. The highly nonlinear, nonautonomous, coupled equations of motion are analyzed approximately using the method of variation of parameters. The closed form solution proves to be quite useful in locating periodic solutions and resonance characteristics of the system. A numerical parametric analysis, involving large amplitude motion, establishes the effect of the radiation pressure to be substantial and destabilizing.

Next, a possibility of utilizing this adverse influence to advantage through judiciously located rotatable control surfaces is explored. A controller configuration for a dual-spin spacecraft is analyzed first. The governing equations, in the absence of a known exact solution, are solved numerically to evaluate the effect of system parameters on the performance of the control system. The available control moments are found to be sufficient to

compensate for the rotor spin decay, thus dispensing with the necessity of energy sources maintaining the spin rate. The controller is able to damp extremely severe disturbances in a fraction of an orbit and is capable of imparting arbitrary orientations to a satellite, thus permitting it to undertake diverse missions.

The development of an efficient yet structurally simple controller configuration is then considered. A logical approach for solar controller design is proposed which suggests a four-plate configuration. Its performance in conjunction with a bang-bang control law is studied in detail. The utilization of maximum available control moments leads to a substantial improvement of the damping characteristics.

Attention is then focussed on using the earth's magnetic field interaction with onboard dipoles for attitude control. Magnetic torquing, however, is unable to provide first order pitch control in near equatorial orbital planes. The shortcoming is overcome by hybridizing the concepts of magnetic and solar control. Two magnetic controller models, employing a single rotatable dipole or two fixed dipoles, are proposed in conjunction with a solar pitch controller. The system performance is evaluated for a wide range of system parameters and initial conditions. Although high spin rates lend considerable gyroscopic stiffness to the

spacecraft, the controllers continue to be quite effective even in the absence of any spin. Even with extremely severe disturbances, damping times of the order of a few orbital degrees are attainable. As before, the concept enables a satellite to change the desired attitude in orbit.

The effectiveness of the controllers at high altitudes having been established, the next logical step was to extend the analysis to near-earth satellites in free molecular environment. A hybrid control system, using the solar pressure at high altitudes and the aerodynamic forces near perigee, is proposed. The influence of important system parameters on the bang-bang operation of the controller is analyzed. The concept appears to be quite effective in damping the satellite librations. Both the orbit normal and the local vertical orientations of the axis of symmetry of the satellite are attainable. However, for arbitrary pointing of the symmetry axis, small limit cycle oscillation about the desired final orientation results.

Finally, the time-optimal control, through solar radiation pressure, of an unsymmetrical satellite executing planar pitch librations is examined analytically. The switching criterion, synthesized for the linear case, is found to be quite accurate even when the system is subjected to large disturbances.

Throughout, the semi-passive character of the system promises an increased life-span for a satellite.

TABLE OF CONTENTS

Chapter Page

Chapter Page

Chapter Page

LIST OF TABLES

LIST OF FIGURES

Figure | Page

ACKNOWLEDGEMENT

The author wishes to express his gratitude to Dr. V.J. Modi for the guidance given throughout the preparation of the thesis. His encouragement, help and patience have been invaluable.

The investigation reported in this thesis was supported by the National Research Council of Canada Grant No. A-2181.

LIST OF SYMBOLS

A, A_i	area of single control plate, i=1,2,3,4
$\bar{B}$	geomagnetic induction vector
B_i, B_j, B_k; B_{xn}, B_{yn}, B_{zn}	components of $\bar{B}/D_m$ along the x,y,z and x_n, y_n, z_n axes, respectively
C, C_i	solar parameter, i=1,2,3,4
$\bar{C}, \bar{C}_i$	$2\rho p_o R_p^3 A_i \epsilon_i/\mu$, i=1,2,3,4
C_m	magnetic parameter
D_m	geomagnetic dipole moment, M_e/R^3; $M_e = 8.1 \times 10^{25}$ gauss-cm^3
$E(\theta)$	$(1+e)^3/(1+e\cos\theta)^4$
G	solar aspect ratio
I	inertia parameter of axisymmetric ($I_y=I_z$) satellite, I_x/I_y
I_x, I_y, I_z	principal moments of inertia of the satellite
I_{xp}, I_{xr}	moment of inertia of the platform and the rotor about the axis of symmetry of the satellite, respectively
J	platform inertia fraction, I_{xp}/I_x
$J(\theta)$	$\{(1+e)^2(1+2e\cos\theta+e^2)/(1+e\cos\theta)^4\}[\{R_p(1+e)/(1+e\cos\theta)-R_e\}/(R_p-R_e)]^n$
K	viscous damping parameter, $K_d(R_p^3/\mu)^{1/2}/I_y$
K_d	viscous damping coefficient

K_i	inertia parameter of unsymmetrical satellite, $(I_z-I_y)/I_x$
O	center of force
P	pericenter
Q_i	total generalized force, $i=\alpha,\beta,\gamma,\lambda,\psi$
Q_{is}	generalized force due to solar radiation pressure, $i=\alpha,\beta,\gamma,\lambda$
Q_{im}	generalized force due to magnetic interaction, $i=\beta,\gamma,\lambda$
Q_{ia}	generalized force due to aerodynamic forces, $i=\beta,\gamma,\lambda$
R	distance between the satellite center of mass and the center of force
R_e	radius of the earth
R_p	distance between the pericenter and the center of force
S	center of mass of the satellite
S_i	switching function, $i=\beta,\gamma,\lambda$
T	kinetic energy
U_g	gravitational potential energy
U,U_1,U_2	polarity
V	velocity of the satellite center of mass
e	orbit eccentricity
h	distance between the satellite center of mass and the hinge point T, Figure 3.11a

h_m^2	dipole strength
h_α, h_θ	constants of motion
h_p	perigee altitude
i, i_m	inclinations of the orbital plane from the ecliptic and the equatorial planes, respectively
$\bar{i}, \bar{j}, \bar{k}$	unit vectors along x,y and z axes, respectively
ℓ, r	length and radius of cylindrical satellite, respectively
m	bang-bang control system gain
m_s	mass of the satellite
n_e, n_r	rates of the earth's rotation and regression of the line of nodes, respectively
n	$(3K_i \cos 2\psi_e)^{1/2}$, $-\pi/4 < \psi_e < \pi/4$
$\bar{p}, \bar{p}_1, \bar{p}_2$	unit vector along dipole orientation, $\bar{p} = p_i \bar{i} + p_j \bar{j} + p_k \bar{k}$
p_o	solar radiation pressure, 4.65×10^{-5} dynes/cm^2
$\bar{r}$	position vector of area element from the center of mass of the satellite
t	time
$\bar{u}$	unit vector in the direction of the sun, $u_i \bar{i} + u_j \bar{j} + u_k \bar{k}$
u_i	$\cos\phi(\sin\gamma\cos\beta\cos\eta + \sin\beta\sin\eta) + \sin\phi\{\cos i(\sin\gamma\cos\beta \sin\eta - \sin\beta\cos\eta) - \sin i \cos\beta\cos\gamma\}$
u_j	$\cos\phi\cos\gamma\cos\eta + \sin\phi(\cos i\cos\gamma\sin\eta + \sin i\sin\gamma)$

u_k	$\cos\phi(\sin\gamma\sin\beta\cos\eta-\cos\beta\sin\eta)+\sin\phi\{\cos i(\sin\gamma\sin\beta\sin\eta+\cos\beta\cos\eta)-\sin i\sin\beta\cos\gamma\}$
$\underline{u}$	control vector
$\bar{v}$	unit vector in the direction of atmospheric flow relative to the satellite center of mass, $v_i\bar{i}+v_j\bar{j}+v_k\bar{k}$
v_i	$\{\sin\beta+e(\sin\beta\cos\theta-\cos\beta\sin\gamma\sin\theta)\}/(1+2e\cos\theta+e^2)^{1/2}$
v_j	$-e\cos\gamma\sin\theta/(1+2e\cos\theta+e^2)^{1/2}$
v_k	$-\{\cos\beta+e(\cos\beta\cos\theta+\sin\beta\sin\gamma\sin\theta)\}/(1+2e\cos\theta+e^2)^{1/2}$
x_n,y_n,z_n	inertial coordinate system with x_n normal to the orbital plane and y_n along the line of nodes referred to the equatorial plane
x',y',z'	inertial coordinate system with x' normal to the orbital plane and y' along the pericenter
x_o,y_o,z_o	rotating orbital coordinate system with x_o normal to the orbital plane and y_o along the local vertical
x_1,y_1,z_1; x_2,y_2,z_2	intermediate body coordinates resulting from rotations γ and β about z_o and y_1 axes, respectively
x_p,y_p,z_p	platform-fixed coordinate system
Φ	coning angle of the axis of symmetry, $\cos^{-1}(\cos\beta\cos\gamma)$
$\Phi(\theta)$	state-transition matrix (Equation 6.8)
Ω,Ω_m	angles between the vernal equinox and the lines of nodes referred to the ecliptic and the equatorial planes, respectively

$\alpha,\beta,\gamma,\lambda$	attitude angles
α_1,α_2	constants in Chapter 2 and Appendices I and II; longitude and latitude of the plate support arm in the xyz-reference, respectively (Figure 3.11a)
$\beta_c,\gamma_c,\lambda_c$	position control parameters
$\beta_f,\gamma_f,\lambda_f$	final desired attitude
β_m	longitude of the plane containing both the geographic and geomagnetic polar axes from the vernal equinox (Figure 4.1)
δ,δ_i	control plate rotation, i=1,2,3,4
ε	distance between the center of pressure and the center of mass of the satellite (Chapter 2); distance between the center of pressure of the control plate and the hinge point T of the support arm (Chapter 3)
ε_i	distance between the center of pressure of control plate and the satellite center of mass, i=1,2,3,4
ε_m	geomagnetic polar axis declination, 11.4°
ζ	$\eta+\psi-\tan^{-1}(\tan\phi\cos i)$
η,η_m	$(\omega+\theta)$ and $(\omega_m+\theta)$, respectively
θ	orbital angle
θ_m	angular position of unit vectors $\bar{p}$ and $\bar{p}_1$ from the y_p axis (Figure 4.2)
θ_s,θ_f	switching time and final time, respectively

λ_i	characteristic multipliers, i=1,2,3,4
μ	gravitational constant
μ_i, ν_i	gains of linear controller with saturation constraints
ξ, ξ_i	angle of incidence, $\xi = \cos^{-1}(\bar{u}\cdot\bar{n})$; i=1,2,3,4
ξ_a, ξ_{ai}	angle between the direction of relative flow and plate normal, $\xi_a = \cos^{-1}(\bar{v}\cdot\bar{n})$; i=1,2,3
ρ, τ	reflectivity and transmissibility of satellite surface or control plate, respectively
ρ_a, ρ_{ap}	atmospheric density and its value at the perigee altitude h_p, respectively
σ	spin parameter
τ_d	damping time
ϕ	solar aspect angle, angle between the sun-line and the line of nodes referred to the ecliptic plane
ϕ_m	$\beta_m - \Omega_m$
ψ	planar pitch attitude of unsymmetrical satellite
ψ_e	nominal pitch attitude of unsymmetrical satellite
ω, ω_m	arguments of the perigee referred to the ecliptic and the equatorial planes, respectively

ω_n	average nodding frequency of the satellite axis of symmetry
ω_1, ω_2	frequencies of the high and low frequency periodic motion, respectively

Dots and primes indicate differentiation with respect to t and θ respectively. The subscript o indicates initial condition.

1. INTRODUCTION

1.1 Preliminary Remarks

Success of a vast majority of space missions depends on the ability of a spacecraft to point accurately in the desired direction. Even a correctly positioned satellite tends to deviate in time from its preferred orientation due to environmental influences, such as, micrometeorite impacts, solar radiation pressure, aerodynamic forces, gravitational and magnetic field interactions, etc. Fortunately, several methods of attitude control are available which damp the resulting undesirable librations. These procedures may be broadly classified as active, passive and semi-passive (or semi-active).

Active stabilization procedures involve mass expulsion schemes and/or components requiring a large amount of energy, an expensive commodity aboard a spacecraft, leading to increased weight and space requirements with a reduced satellite life-span. The main advantage of the technique is its ability to achieve a specified orientation with almost any desired degree of accuracy.

Stabilization techniques requiring no power consumption are termed passive. This is generally achieved by designing satellites with physical characteristics which

interact with the environmental forces in a manner so as to attain a specific equilibrium position. Spin stabilization presents an alternative that relies on the inherent tendency of a spinning body to maintain its attitude in space. The pointing accuracies attained through passive methods, however, are limited and deteriorate due to the influence of environmental forces.

The semi-passive methods attempt to utilize the environmental forces, through the introduction of appropriate controllers, and thereby achieve attitude control. The possibility of attaining high pointing accuracies with low power consumption promises an increased satellite life-span. The design of suitable controller configurations, however, requires a thorough understanding of the system dynamics under the influence of the environmental force used for control.

The development and analysis of several semi-passive control systems, with particular reference to spinning satellites, forms the main objective of this thesis.

1.2 Literature Review

Spinning bodies have received,in the past decade, considerable attention owing to their particular stability properties. For rigid axisymmetric bodies under the

influence of gravity forces and with the axis of spin perpendicular to the orbital plane, Thomson[1] (1962) presented a stability criterion using linearized analysis while Pringle[2] (1964) investigated motion in the large employing the Hamiltonian as a Lyapunov function. Asymmetry was taken into account by Kane and Shippy[3] (1963) applying the Floquet theory. The same method was used later by Kane and Barba[4] (1966) to deal with motion in the small for arbitrary eccentricity. Wallace and Meirovitch[5] (1967) studied the same problem by an asymptotic analysis in conjunction with Lyapunov's direct method. Neilson and Modi[6-9] (1968-72) gave insight into the problem of stability in the large by making use of the integral manifold concept.

According to classical mechanics, the stable rotational motion of a rigid body in absence of external forces is possible only if the axis of rotation is a principal axis of least or greatest inertia. If the body is not rigid and energy is dissipated by the cyclic forces acting on it while under nutation, then only the motion about the axis of maximum inertia is stable. It turns out that for slowly spinning rigid satellite, the internally dissipated energy is such as to overcome the stabilizing influence of gravity and the system ends up in a state of tumbling about the axis of maximum moment of inertia: the classical example is that of Explorer I[10].

The constraint of "major axis spin rule" was subsequently removed by the introduction of the dual-spin concept which allows two sections to nominally rotate about a common axis at different rates relative to inertial space. An early paper by Roberson[11] (1958) had anticipated that torques generated by a disc rotating about an axis fixed in a rigid body could substantially affect its motion. However, the first fundamental contribution to the feasibility of dual-spin stabilization was by Landon and Stewart[12] (1964): an energy-sink method indicated no constraints on inertias when energy dissipation took place on the slowly-rotating part of the system. Iorillo[13], a year later, extended this concept to the case where energy dissipation occurs on both bodies.

Likins[14] (1967) developed, for a specific configuration involving an axisymmetric rotor and an asymmetric body containing a ball-in-tube damper constrained to move parallel to the rotor axis, an accurate stability criterion based on the Routh analysis. Mingori[15] (1969) took a more general approach which involved two dissipative sections. The Floquet analysis stressed the sensitivity of the system behaviour to the relative effectiveness of the sources of energy dissipation. Pringle[16] (1969) extended his theorems on Lyapunov stability to the case of dual-spin spacecraft and gave a rigorous proof of the "maximum moment of inertia spin-axis" rule. Cloutier[17] (1968) investigated the

stability and performance of a nutation damper consisting of mass shifting perpendicular to the spin-axis: again, it led to no restrictions on inertia ratios or damper size when dissipation occurs on a despun platform. In another paper[18] (1969), the author extended the analysis to a damper involving two degrees of freedom in a plane perpendicular to the spin axis. An approximate solution was derived for the nutation angle and its decay was optimized in terms of system parameters. Sen[19] (1970) studied a four mass nutation damper whose design constraints were not as severe as those of Likins. Vigneron[20] (1971) applied the method of averaging to obtain a closed-form first approximation solution for a dual-spin system containing both platform and rotor mounted dampers. Bainum et al.[21] (1970) conducted a stability and performance analysis of the dual-spin Small Astronomy Satellite (SAS-A) and found that asymmetry noticeably deteriorates the performance of the nutation damping system. In a subsequent paper[22] (1972), the authors included the effect of damping in the momentum wheel by permitting the plane of the wheel to flex with two degrees of freedom with respect to the hub. The analysis established stability criteria for the SAS-A satellite.

Although passive methods for attenuating nutation are generally reliable and conceptually simple, their effectiveness may be limited. A device containing an actively controlled mass, capable of attaining any nutation

angles, was studied by Kane and Scher[23] (1969). Mingori et al.[24] (1971) analyzed both semi-passive and active nutation dampers for dual-spin spacecraft, the former involving single axis control moment gyros (CMG's) whose rotational motion relative to the spacecraft was restrained passively by a spring and dashpot. The active damper was realized by controlling the CMG's in accordance with the information from a rectilinear accelerometer. Both devices were found to be capable of reducing nutation several times faster than passive dampers of equal mass.

Studies which take the gravity torque into account are rare but offer, nevertheless, valuable results. Of particular interest is the conclusion by Kane and Mingori[25] (1965) that the stability of undamped axisymmetric dual-spin satellites is equivalent to that of rigid spinning bodies. White and Likins[26] (1969) extended the research to slightly asymmetric system by making use of asymptotic expansions and resonance lines. The efforts of Roberson et al.[27,28] (1966, 1969) and Yu[29] (1969) should also be noted who analyzed the equilibrium positions of a single rigid body containing a symmetric, constant speed, fixed axis rotor, also called a gyrostat, in presence of gravity forces.

The concept of dual-spin spacecraft gained sufficient recognition by 1967 to be considered seriously as a design alternative[30]. The first flight data for a prolate dual-spin satellite (Tacsat 1), however, became publicly available

only recently[31] (1970). It was found that the spacecraft did not maintain the nominal inertial attitude but executed stable limit cycle in a nearby state of free precession. None of the previous analyses employing linear models for the energy dissipation mechanisms could explain this anomaly. In a recent paper, Likins et al.[32] (1971) found, via the 'energy-sink' method, the limit cycle oscillation to be a consequence of nonlinearities in the damping forces. On the other hand, the possibility of constant or variable amplitude limit cycles due to nonlinear restoring forces has been indicated by Mingori et al.[33] (1972).

It should be emphasized that although several authors have recognized the importance of environmental forces, they were ignored in the analyses of spinning spacecraft discussed above.

Although extensive volume of literature exists on the librational dynamics of gravity stabilized satellites[34,35,et al.], serious efforts at analyzing the influence of environmental forces and exploiting them for attitude control are relatively recent. Roberson[36] (1958) gave a general outline of the problem and Wiggins[37] (1964) presented estimates of the relative magnitudes of these forces. Clancy and Mitchell[38] (1964) and Modi et al.[39,40] (1971) investigated the influence of solar radiation pressure on the attitude motion of satellites. The effect of the atmosphere on satellite librations was the subject of

study by Debra[41] (1959), Schrello[42] (1961), Garber[43] (1963), Meirovitch and Wallace[44] (1966), et al. The environmental effect, in general, was found to be detrimental to the satellite performance.

On the other hand, the environmental forces offer an exciting possibility of trajectory and attitude control through the introduction of a carefully designed controller. As no mass expulsion or active gyros requiring large power consumption are involved, these schemes are essentially semi-passive and hence promise an increased satellite life-span.

The use of solar radiation pressure for propulsion within the solar system was first proposed by Garwin[45] (1958). Sohn[46] (1959) suggested a specific configuration using plates of large surface areas to orient the satellite with respect to the sun. Galitskaya and Kiselev[47] (1965) studied, qualitatively, the principle of libration control of space probes about three axes. Mallach[48] (1966) presented a system for solar damping of gravity oriented satellites and gave a simplified analysis using average torques. Modi and Flanagan[49] (1971) examined the planar attitude control of a gravity gradient system in an ecliptic orbit using the solar pressure as a damping torque. Modi and Tschann[50] (1971) extended the analysis by the introduction of a displacement and velocity sensitive controller enabling the satellite to attain any desired orientation. Modi and

Kumar[51] (1973) further generalized the concept for the case of three degree of freedom motion. Their analysis demonstrated the feasibility of achieving general three-axis librational damping and attitude control.

Literature on the use of solar pressure for attitude control of spinning vehicles appears to be rather limited. Ule[52] (1963) was the first to consider aligning the spin axis along the sun-satellite line employing a corner mirror array fixed to the spacecarft. Similar devices were further explored by Peterson[53] (1966), Colombo[54] (1966), Falcovitz[55] (1966), et al. Crocker[56] (1970) considered the same problem using spacecraft-fixed and spring-mounted paddles. An adequate nutation damper was assumed so that the angular momentum vector remained close to the spin axis. A possibility of using the solar pressure for general three-axis librational damping and attitude control of spinning satellites remains virtually unexplored.

It would be appropriate to mention here the experiment aboard Mariner IV spacecraft[57], conducted on depletion of the attitude control gas, to align the roll axis along the sun-line using passive solar radiation control. Each of the four solar panels was provided with a rotatable solar pressure vane for this purpose. Unfortunately, one of the vanes proved to be inoperative during a major portion of the mission. However, subsequent reactivation of the vane enabled the solar pressure control system, in con-

junction with active gyros, to maintain the spacecraft attitude within 1° of the sun-line.

Generation of control torques through the interaction of onboard electromagnetic dipoles and the earth's magnetic field appears to be particularly attractive as the system reliability is enhanced by the elimination of moving parts.

Libration damping of gravity oriented satellites was considered by Alper and O'Neill[58] (1967) who proposed a passive hysteresis damper. Bainum and Mackison[59] (1968), on the other hand, considered three mutually perpendicular electromagnets controlled according to the sample and hold concept. Although time constants of approximately one to two orbits for roll-yaw damping were achieved, the inadequacy of the system for pitch control in equatorial orbits, where the geomagnetic field is nearly parallel to the orbit normal, became apparent.

The problem of maintaining the spin axis of a satellite perpendicular to the orbital plane has been a subject of considerable study by Vrablik et al.[60] (1965), Sonnabend[61] (1967) and many others. Fischell[62] (1966) considered the possibility of using magnetic control for regulating the spin rate of a satellite. Wheeler[63] (1967) investigated the use of a single dipole along the spin axis for both attitude control and nutation damping. The analysis, however, assumes the desired final orientation

to be inertially fixed and the spin rate constant during the control maneuver. Sorensen[64] (1971) applied the Kalman filter technique to estimate pointing errors for a system with limited attitude determination capabilities and developed the minimum energy control law using these estimates. In a recent paper, Shigehara[65] (1972) studied a control law, based on the asymptotic stability criterion, for the spin-axis and the spin rate using dipoles along the axis and perpendicular to it, respectively. The first operational magnetically controlled satellites, the TIROS wheels, were discussed by Hecht and Manger[66] (1964) and Lindorfer and Muhlfelder[67] (1966).

The use of aerodynamic forces for attitude control of satellites in near-earth orbits was a subject of several early discussions by Wall[68] (1959), Schrello[69] (1961), et al. In practice, however, it has been used successfully only for the pitch control of COSMOS-149, with the other degrees of freedom governed by gyroscopic forces[70]. Ravindran[71] (1971) optimized, through linearization, a set of controller flaps for a satellite in a circular orbit. Modi and Shrivastava[72] (1971), on the other hand, have proposed several schemes of semi-passive aerodynamic controllers. Their nonlinear analysis showed the system to be effective in damping severe disturbances in a fraction of an orbit. The performance of the controller appeared promising even in elliptic orbits where the corrective

moments are available only over a portion of the trajectory. In a subsequent paper[73] (1973), the authors optimized the performance of the controller in both circular and elliptic orbits, using the damping time and the steady state pointing error as the respective criteria.

1.3 Purpose and Scope of the Investigation

From the foregoing, it is evident that the influence of environmental forces on the attitude motion of spinning satellites and their utilization for attitude control has received little attention in the past. On the other hand, the importance of such a study becomes apparent when one recognizes the fact that the majority of the communications, applied technology and scientific satellites are indeed spin stabilized. The thesis aims at filling this gap by systematically analyzing environmental effects and exploiting them to advantage over a wide range of operational altitudes.

The influence of solar radiation pressure, constituting the dominant environmental force at high altitudes, on the librational motion is examined first. Both analytical and numerical techniques are employed to study the system response. Stability of the periodic solutions is ascertained using the Floquet theory. Numerical results establish regions of nontumbling motion in the system parameter space.

Next, the possibility of using solar radiation pressure for general three-axis libration damping and attitude control of a dual-spin system is explored. The results establish the effectiveness of the concept. Effort is then directed towards devising a solar controller model that is structurally simple and operationally efficient.

This is followed by an investigation of attitude damping and control utilizing the earth's magnetic field. A comparative study of two controller models is conducted. For the reason pointed out earlier, the magnetic controllers fail to provide first order pitch control in synchronous orbits. To compensate for this, the magnetic controllers are hybridized with a solar pitch controller.

Attitude control of near-earth satellites in elliptic trajectories, normally preferred to minimize degeneration of the orbit due to atmospheric drag, is considered next. A hybrid control system, utilizing the aerodynamic forces at low altitudes and solar radiation pressure when beyond the atmosphere, is proposed. Finally, the problem of time-optimal pitch control of satellites using the radiation pressure is examined analytically.

Figure 1.1 schematically presents the plan of study.

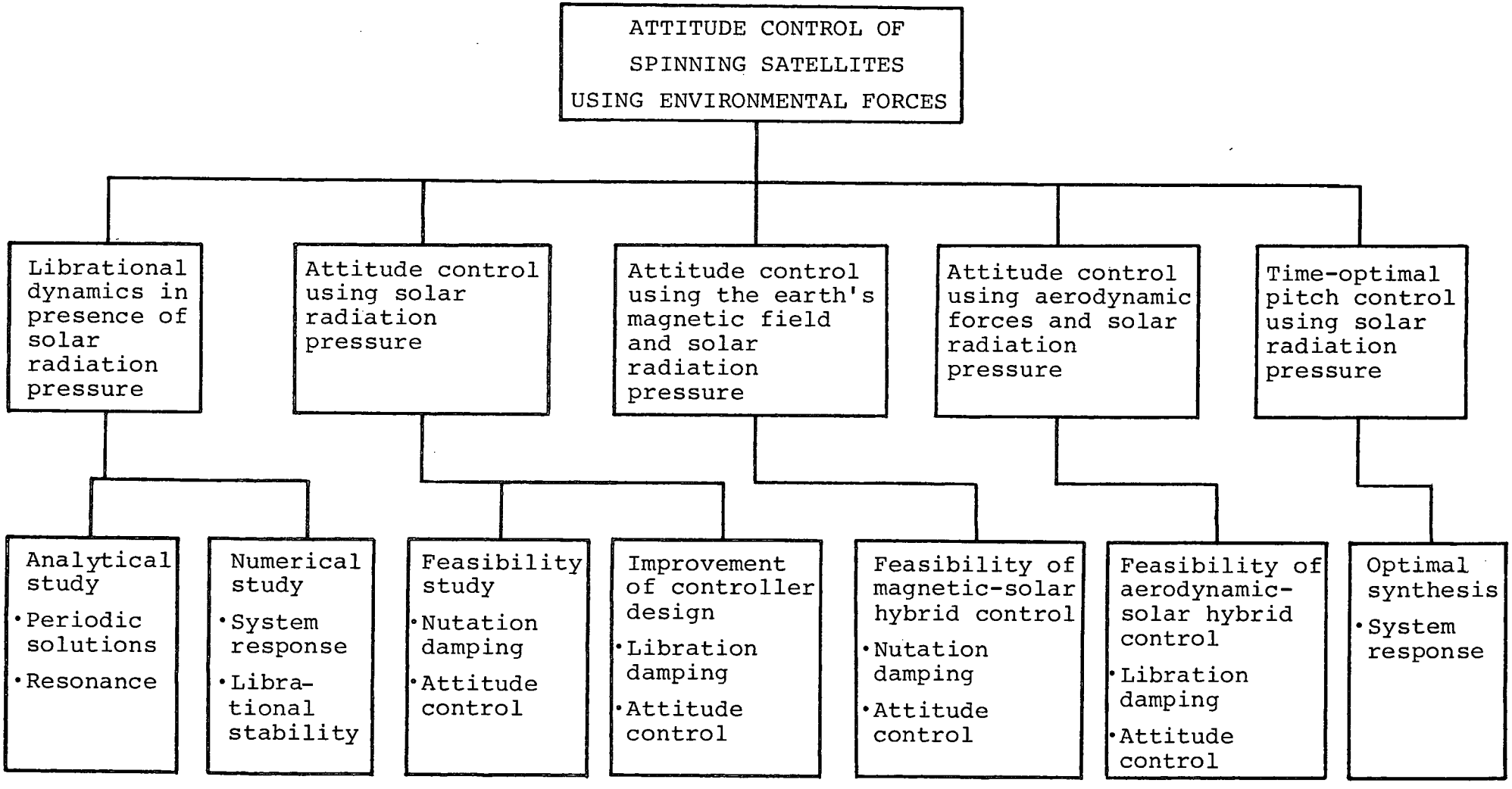

Figure 1.1 Schematic diagram of the proposed plan of study

2. LIBRATIONAL DYNAMICS OF SPINNING AXISYMMETRIC SATELLITES IN PRESENCE OF SOLAR RADIATION PRESSURE

This chapter investigates the attitude dynamics of axisymmetric, cylindrical, spinning satellites under the influence of solar radiation pressure and gravity gradient torques. The equations of motion of the system are obtained first using the classical Lagrangian formulation followed by an evaluation of the generalized forces due to the radiation pressure.

As the nonlinear, nonautonomous, coupled equations of motion do not possess a known closed-form solution, an approximate study is undertaken using Butenin's extension of the method of slowly varying parameters[74]. The approximate analytical solution proves to be an excellent tool in locating periodic solutions of the system, whose importance in the attitude dynamics study of satellites has been well emphasized [9,75,76]. The Floquet theory[77] is employed to examine the variational stability of the periodic solutions. The possibility of resonant oscillations of the system in presence of the solar torque is also investigated.

The quasi-linear analytical method, however, fails to describe the large amplitude motion of the system. To this end, the governing equations are analyzed numerically

and the librational response is studied as a function of the system parameters. The available information is condensed in the form of design plots, which clearly emphasize the importance of the solar parameter characterizing the radiation pressure torque, and should prove useful during the design of an attitude control system.

2.1 Formulation of the Problem

Figure 2.1 shows an axisymmetric cylindrical satellite with the center of mass S moving in a Keplerian orbit about the center of force O. The spatial orientation of the axis of symmetry of the satellite is completely specified by two successive rotations γ and β, referred to as roll and yaw, respectively, which define the attitude of the satellite principal axes x,y,z with respect to the inertial reference frame x',y',z'. The satellite spins in the x,y,z reference with angular velocity $\dot{\alpha}$. In terms of these modified Eulerian rotations, the expressions for the potential and kinetic energies to $O(1/R^3)$ are obtained as:

$$U_g = -\mu m_s/R - \mu\{(I_x/2R^3)(I-1)/I\}(1-3\sin^2\gamma\cos^2\beta) \qquad (2.1)$$

$$T = (m_s/2)(\dot{R}^2+R^2\dot{\theta}^2)+(I_x/2I)\{I(\dot{\alpha}-\dot{\gamma}\sin\beta+\dot{\theta}\cos\beta\cos\gamma)^2 + (\dot{\beta}-\dot{\theta}\sin\gamma)^2 + (\dot{\gamma}\cos\beta+\dot{\theta}\sin\beta\cos\gamma)^2\} \qquad (2.2)$$

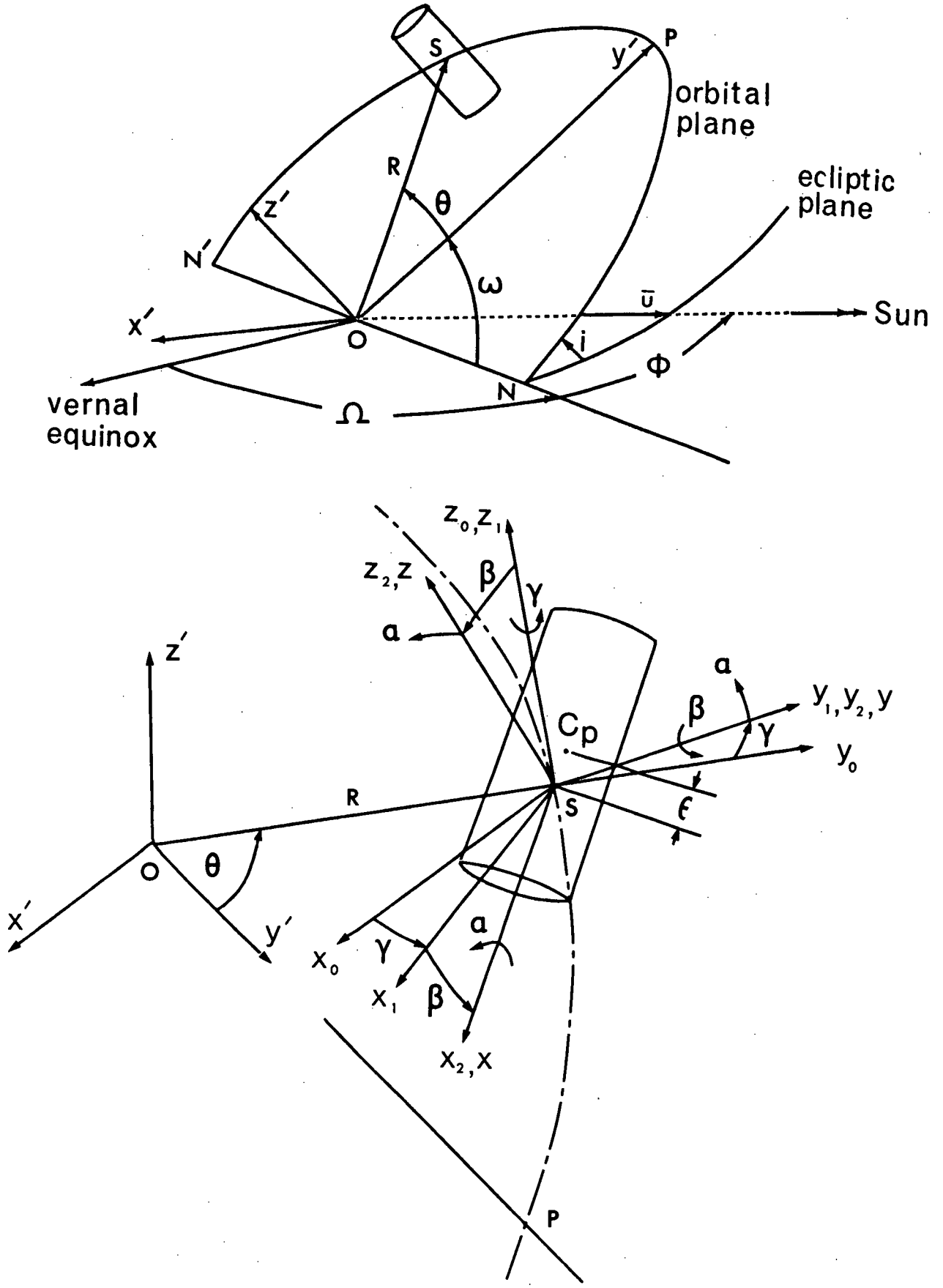

Figure 2.1 Geometry of motion of spinning satellite in the solar pressure environment

Neglecting orbital perturbations due to the librational motion[78,79], the classical Lagrangian formulation yields the governing equations of motion in the roll, yaw and spin degrees of freedom as:

$$(d/dt)\{-I(\dot{\alpha}-\dot{\gamma}\sin\beta+\dot{\theta}\cos\beta\cos\gamma)\sin\beta+(\dot{\gamma}\cos\beta+\dot{\theta}\sin\beta\cos\gamma)\cos\beta\}$$
$$+I(\dot{\alpha}-\dot{\gamma}\sin\beta+\dot{\theta}\cos\beta\cos\gamma)\dot{\theta}\cos\beta\sin\gamma+(\dot{\beta}-\dot{\theta}\sin\gamma)\dot{\theta}\cos\gamma$$
$$+(\dot{\gamma}\cos\beta+\dot{\theta}\sin\beta\cos\gamma)\dot{\theta}\sin\beta\sin\gamma+3(\mu/R^3)(I-1)\times$$
$$\sin\gamma\cos\gamma\cos^2\beta = Q_\gamma/I_y \qquad (2.3a)$$

$$(d/dt)(\dot{\beta}-\dot{\theta}\sin\gamma)+(\dot{\gamma}\cos\beta+\dot{\theta}\sin\beta\cos\gamma)\{I(\dot{\alpha}-\dot{\gamma}\sin\beta+\dot{\theta}\cos\beta\cos\gamma)$$
$$+(\dot{\gamma}\sin\beta-\dot{\theta}\cos\beta\cos\gamma)\}-3(\mu/R^3)(I-1)\sin^2\gamma\sin\beta\cos\beta$$
$$= Q_\beta/I_y \qquad (2.3b)$$

$$(d/dt)(\dot{\alpha}-\dot{\gamma}\sin\beta+\dot{\theta}\cos\beta\cos\gamma) = Q_\alpha/I_x \qquad (2.3c)$$

where $Q_i (i=\gamma,\beta,\alpha)$ represent the generalized forces due to solar radiation pressure.

Consider an area element dA, of the curved surface of the satellite, of length dx, angular width $d\Theta$ and located at an axial distance x from the center of mass S such that the surface normal $\bar{n}$ makes an angle Θ with the y axis (Figure 2.2a). The force acting on the area element due to solar radiation pressure is given by,

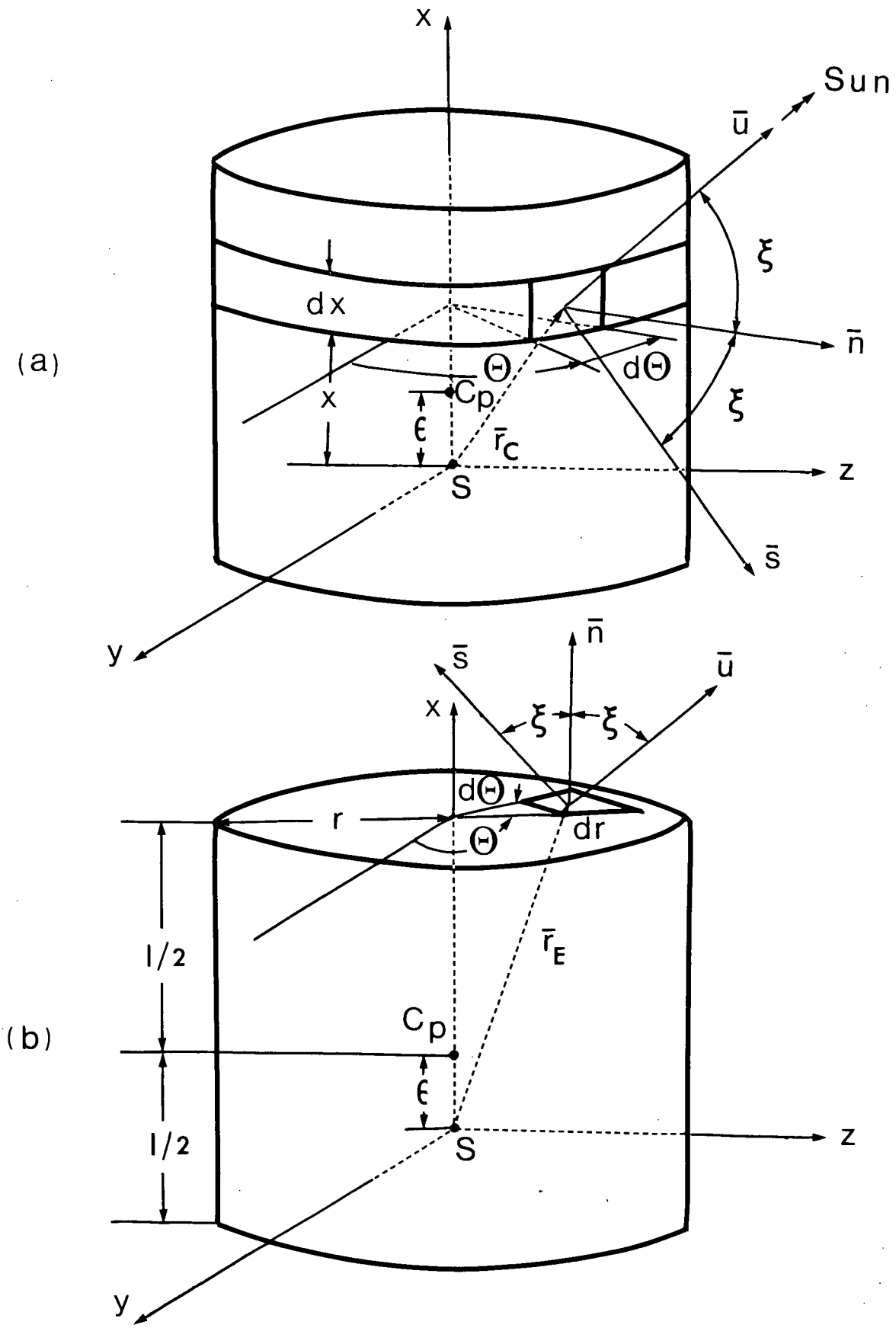

Figure 2.2 Evaluation of generalized forces due to solar radiation pressure: (a) curved surface; (b) flat ends

$$d\bar{F} = -p_o dA|\cos\xi|\{(1-\tau)\bar{u}+\rho\bar{s}\} \tag{2.4}$$

with the resulting moment about the satellite center of mass as

$$\bar{M}_C = \int_A \bar{r}_C \times d\bar{F} \tag{2.5}$$

where the integration extends over the entire curved surface "seen" by the sun. The limits of integration for x are $-(\ell/2-\varepsilon)$ to $(\ell/2+\varepsilon)$ and those for Θ are $\tan^{-1}(-u_j/u_k)$ to $\{\pi+\tan^{-1}(-u_j/u_k)\}$, which correspond to $\xi=\pi/2$.

Evaluation of the integral in Equation (2.5), after considerable algebraic manipulations, leads to

$$\bar{M}_C = \{-(\pi/2)p_o\ell r^2(1-\tau-\rho)u_i u_k+2(1-\tau+\rho/3)p_o r\ell\varepsilon u_k\sqrt{u_j^2+u_k^2}\}\bar{j}$$
$$+\{(\pi/2)p_o\ell r^2(1-\tau-\rho)u_i u_j-2(1-\tau+\rho/3)p_o r\ell\varepsilon u_j\sqrt{u_j^2+u_k^2}\}\bar{k} \tag{2.6}$$

The expression for the moment due to the flat ends of the cylindrical satellite (Figure 2.2b) is obtained in a similar manner,

$$\bar{M}_E = \{(\pi/2)p_o\ell r^2(1-\tau-\rho)u_i u_k+\pi p_o r^2\varepsilon(1-\tau-\rho)u_k|u_i|\}\bar{j}$$
$$-\{(\pi/2)p_o\ell r^2(1-\tau-\rho)u_i u_j+\pi p_o r^2\varepsilon(1-\tau-\rho)u_j|u_i|\}\bar{k} \tag{2.7}$$

The total moment due to solar radiation pressure is thus given by

$$\bar{M} = \bar{M}_C + \bar{M}_E$$

$$= 2(1-\tau+\rho/3)p_o r\ell\varepsilon u_k[\sqrt{u_j^2+u_k^2}+(\pi r/2\ell)\{(1-\tau-\rho)/(1-\tau+\rho/3)\}|u_i|]\bar{j}-2(1-\tau+\rho/3)p_o r\ell\varepsilon u_j \times$$

$$[\sqrt{u_j^2+u_k^2}+(\pi r/2\ell)\{(1-\tau-\rho)/(1-\tau+\rho/3)\}|u_i|]\bar{k} \qquad (2.8)$$

The application of the principle of virtual work yields the generalized forces in the γ,β and α degrees of freedom as:

$$Q_\gamma = -2(1-\tau+\rho/3)p_o r\ell\varepsilon u_j[\sqrt{u_j^2+u_k^2}+(\pi r/2\ell)\times \{(1-\tau-\rho)/(1-\tau+\rho/3)\}|u_i|]\cos\beta \qquad (2.9a)$$

$$Q_\beta = 2(1-\tau+\rho/3)p_o r\ell\varepsilon u_k[\sqrt{u_j^2+u_k^2}+(\pi r/2\ell)\times \{(1-\tau-\rho)/(1-\tau+\rho/3)\}|u_i|] \qquad (2.9b)$$

$$Q_\alpha = 0 \qquad (2.9c)$$

The generalized force in the α degree of freedom being zero, a first integral of motion defining the satellite spin rate $\dot{\alpha}$ is furnished by Equation (2.3c),

$$\dot{\alpha}-\dot{\gamma}\sin\beta+\dot{\theta}\cos\beta\cos\gamma = h_\alpha \qquad (2.10)$$

As h_α is a measure of the spin rate, a dimensionless spin parameter σ, defined as

$$\sigma = (\dot{\alpha}/\dot{\theta})\Big|_{\theta=\beta=\gamma=0} = (h_\alpha/\dot{\theta})\Big|_{\theta=0} - 1 \qquad (2.11)$$

may be used to eliminate the cyclic coordinate α. Changing the independent variable from t to θ, through the Keplerian orbital relations

$$R = h_\theta^2/\mu(1+e\cos\theta) \qquad (2.12a)$$

$$\dot{\theta} = h_\theta/R^2 \qquad (2.12b)$$

and making use of the spin parameter σ, the governing equations of motion in the roll and yaw degrees of freedom (Equations 2.3a and b, respectively) transform to:

$$\begin{aligned}\gamma'' &-2\beta'\gamma'\tan\beta+2\beta'\cos\gamma-I(\sigma+1)\{(1+e)/(1+e\cos\theta)\}^2\times\\ &(\beta'-\sin\gamma)\sec\beta+\{3(I-1)/(1+e\cos\theta)-1\}\times\\ &\sin\gamma\cos\gamma-\{2e\sin\theta/(1+e\cos\theta)\}(\gamma'+\cos\gamma\tan\beta)\\ &=-\{(1+e)^3/(1+e\cos\theta)^4\}Cu_j\{\sqrt{u_j^2+u_k^2}+G|u_i|\}\sec\beta \qquad (2.13a)\end{aligned}$$

$$\begin{aligned}\beta'' &-\gamma'\cos\gamma+[I(\sigma+1)\{(1+e)/(1+e\cos\theta)\}^2\\ &+(\gamma'\sin\beta-\cos\beta\cos\gamma)](\gamma'\cos\beta+\cos\gamma\sin\beta)\\ &-\{3(I-1)/(1+e\cos\theta)\}\sin^2\gamma\sin\beta\cos\beta\end{aligned}$$

$$-\{2e\sin\theta/(1+e\cos\theta)\}(\beta'-\sin\gamma)$$

$$=\{(1+e)^3/(1+e\cos\theta)^4\}Cu_k\{\sqrt{u_j^2+u_k^2}+G|u_i|\} \qquad (2.13b)$$

where the solar parameter C and the solar aspect ratio G are defined as:

$$C = (2R_p^3/\mu I_y)p_o r\ell\varepsilon(1-\tau+\rho/3)$$

$$G = (\pi r/2\ell)(1-\tau-\rho)/(1-\tau+\rho/3) \qquad (2.14)$$

2.2 Analytical Results

2.2.1 Approximate analytical solution

In absence of a known, exact, closed form solution to such a complex system, it was decided to analyze the problem approximately using Butenin's extension of the method of variation of parameters. The case of $\omega=\phi=0$ is analyzed here which leads to a considerable reduction in algebra without affecting the physics of the problem.

Replacing the trigonometric functions of the dependent variables by their series expansions, ignoring fourth and higher order terms in β,γ, and their derivatives as well as terms of $O(e^2)$, Equations (2.13) take the form:

$$\gamma'' + n_1^2\gamma - \ell_1\beta' = 2Ce - C(1+3e)\cos\theta + 2Ce\cos 2\theta + f(\gamma,\gamma',\beta,\beta',\theta) \tag{2.15a}$$

$$\beta'' + n_2^2\beta + \ell_2\gamma' = -C(1+3e)\sin\theta + 2Ce\sin 2\theta + g(\gamma,\gamma',\beta,\beta',\theta) \tag{2.15b}$$

where

$$n_1^2 = 3I - 4 + I(\sigma+1)(1+2e)$$

$$n_2^2 = I(\sigma+1)(1+2e) - 1$$

$$\ell_1 = \ell_2 = I(\sigma+1)(1+2e) - 2 \tag{2.16}$$

and the nonlinear functions f and g are defined as

$$\begin{aligned} f = {} & C(1+3e-4e\cos\theta)[\gamma^2\cos\theta/2 + \beta^2\sin\theta\cos\theta/2 \\ & + \gamma^2\cos^3\theta/2 + \gamma\beta\sin\theta\cos^2\theta - G|\gamma\cos\theta + \beta\sin\theta|\cos\theta] \\ & - 2I(\sigma+1)(\beta'-\gamma)e\cos\theta + 3(I-1)\gamma e\cos\theta + 2(\gamma'+\beta)e\sin\theta \\ & + I(\sigma+1)(1+2e-2e\cos\theta)(\gamma^3 + 3\beta'\beta^2 - 3\gamma\beta^2)/6 \\ & + 2\beta\beta'\gamma' + \beta'\gamma^2 + (2/3)\{(3I-4) - 3(I-1)e\cos\theta\}\gamma^3 \\ & + (\beta^3/3 - \beta\gamma^2/2)2e\sin\theta \end{aligned}$$

$$\begin{aligned} g = {} & C(1+3e-4e\cos\theta)[\gamma\beta\cos\theta + \beta^2\sin^3\theta/2 + \gamma^2\sin\theta\cos^2\theta/2 \\ & + \gamma\beta\sin^2\theta\cos\theta - G|\gamma\cos\theta + \beta\sin\theta|\sin\theta] + 2I(\sigma+1) \times \end{aligned}$$

$$\times(\gamma'+\beta)e\cos\theta+2(\beta'-\gamma)e\sin\theta+I(\sigma+1)(1+2e-2e\cos\theta)(3\gamma'\beta^2+3\gamma^2\beta+\beta^3)$$

$$-2\gamma'\beta^2-\beta\gamma^2-\gamma'^2\beta-\gamma'\gamma^2-2\beta^3/3+3(I-1)(1-e\cos\theta)\gamma^2\beta+\gamma^3 e\sin\theta/3 \tag{2.17}$$

The solution for the corresponding linear system (i.e., f=g=0) is given by

$$\gamma = a\sin(k_1\theta+\beta_1)+b\sin(k_2\theta+\beta_2)+A_o+A_1\cos\theta+A_2\cos 2\theta \tag{2.18a}$$

$$\beta = \alpha_1 a\cos(k_1\theta+\beta_1)+\alpha_2 b\cos(k_2\theta+\beta_2)+B_1\sin\theta+B_2\sin 2\theta \tag{2.18b}$$

where a, b, β_1, β_2 are constants to be determined from initial conditions and the characteristic frequencies k_1 and k_2 ($k_1>k_2$) are the roots of the equation

$$k^4-(n_1^2+n_2^2+\ell_1\ell_2)k^2+n_1^2n_2^2 = 0 \tag{2.19}$$

The constants α_i, A_i and B_i are defined as:

$$\alpha_i = (k_i^2-n_1^2)/\ell_1 k_i, \quad i = 1,2$$

$$A_o = 2Ce/n_1^2$$

$$A_1 = C(1+3e)(1-n_2^2-\ell_1)/(1-k_1^2)(1-k_2^2)$$

$$A_2 = 2Ce(n_2^2+2\ell_1-4)/(4-k_1^2)(4-k_2^2)$$

$$B_1 = C(1+3e)(1-n_1^2-\ell_2)/(1-k_1^2)(1-k_2^2)$$

$$B_2 = 2Ce(n_1^2+2\ell_2-4)/(4-k_1^2)(4-k_2^2) \qquad (2.20)$$

A solution of the similar form is sought for the nonlinear system, however, allowing the amplitude and phase to be functions of θ, i.e.,

$$\gamma = a(\theta)\sin(k_1\theta+\beta_1(\theta))+b(\theta)\sin(k_2\theta+\beta_2(\theta))+A_o$$
$$+A_1\cos\theta+A_2\cos 2\theta \qquad (2.21a)$$

$$\beta = \alpha_1 a(\theta)\cos(k_1\theta+\beta_1(\theta))+\alpha_2 b(\theta)\cos(k_2\theta+\beta_2(\theta))$$
$$+B_1\sin\theta+B_2\sin 2\theta \qquad (2.21b)$$

As the four unknown functions defining the variable amplitude and phase cannot be determined from four initial conditions alone, the solution in the present form is over-specified. Hence four constraint relations must be obtained.

Keeping the first derivatives of γ and β to be the same as that of the linear system gives two of the constraint relations:

$$a'\sin\psi_1+b'\sin\psi_2+a\beta_1'\cos\psi_1+b\beta_2'\cos\psi_2 = 0 \qquad (2.22a)$$

$$\alpha_1 a'\cos\psi_1+\alpha_2 b'\cos\psi_2-\alpha_1 a\beta_1'\sin\psi_1-\alpha_2 b\beta_2'\sin\psi_2 = 0 \qquad (2.22b)$$

where

$$\psi_1 = k_1\theta+\beta_1(\theta),\ \psi_2 = k_2\theta+\beta_2(\theta)$$

Equations of motion (2.15) in conjunction with the assumed solution(2.21) yield the other two constraint relations as:

$$k_1a'\cos\psi_1+k_2b'\cos\psi_2-k_1a\beta_1'\sin\psi_1-k_2b\beta_2'\sin\psi_2 = f^* \qquad (2.23a)$$

$$\alpha_1k_1a'\sin\psi_1+\alpha_2k_2b'\sin\psi_2+\alpha_1k_1a\beta_1'\cos\psi_1+\alpha_2k_2b\beta_2'\cos\psi_2 = -g^* \qquad (2.23b)$$

where f^*, g^* are the modified nonlinear functions.

Solving Equations (2.22) and (2.23) simultaneously for a', b', β_1' and β_2' yields:

$$a' = -\{\ell_1g^*\sin\psi_1-(\ell_2/\alpha_1)f^*\cos\psi_1\}/(k_1^2-k_2^2)$$

$$b' = \{\ell_1g^*\sin\psi_2-(\ell_2/\alpha_2)f^*\cos\psi_2\}/(k_1^2-k_2^2)$$

$$\beta_1' = -\{\ell_1g^*\cos\psi_1+(\ell_2/\alpha_1)f^*\sin\psi_1\}/\{a(k_1^2-k_2^2)\}$$

$$\beta_2' = \{\ell_1g^*\cos\psi_2+(\ell_2/\alpha_2)f^*\sin\psi_2\}/\{b(k_1^2-k_2^2)\} \qquad (2.24)$$

Equations (2.24) represent an exact transformation of the two second order equations of motion (2.15) into four

first order differential equations. For small amplitude motion, f^* and g^* are small. Consequently, a, b, β_1 and β_2 are slowly varying parameters. Using their average values over one period gives:

$$a' = -\{1/8\pi^3(k_1^2-k_2^2)\} \int_0^{2\pi}\int_0^{2\pi}\int_0^{2\pi} \{\ell_1 g^* \sin\psi_1 - (\ell_2/\alpha_1) f^* \cos\psi_1\} d\psi_1 d\psi_2 d\theta$$

$$b' = \{1/8\pi^3(k_1^2-k_2^2)\} \int_0^{2\pi}\int_0^{2\pi}\int_0^{2\pi} \{\ell_1 g^* \sin\psi_2 - (\ell_2/\alpha_2) f^* \cos\psi_2\} d\psi_1 d\psi_2 d\theta$$

$$\beta_1' = -\{1/8\pi^3 a(k_1^2-k_2^2)\} \int_0^{2\pi}\int_0^{2\pi}\int_0^{2\pi} \{\ell_1 g^* \cos\psi_1 + (\ell_2/\alpha_1) f^* \sin\psi_1\} d\psi_1 d\psi_2 d\theta$$

$$\beta_2' = \{1/8\pi^3 b(k_1^2-k_2^2)\} \int_0^{2\pi}\int_0^{2\pi}\int_0^{2\pi} \{\ell_1 g^* \cos\psi_2 + (\ell_2/\alpha_2) f^* \sin\psi_2\} d\psi_1 d\psi_2 d\theta \qquad (2.25)$$

Solving Equations (2.25) for a, b, β_1 and β_2, and substituting in Equations (2.21), the solution takes the form:

$$\gamma = a\sin(\omega_1\theta+c_1)+b\sin(\omega_2\theta+c_2)+A_o+A_1\cos\theta+A_2\cos 2\theta \quad (2.26a)$$

$$\beta = \alpha_1 a\cos(\omega_1\theta+c_1)+\alpha_2 b\cos(\omega_2\theta+c_2)+B_1\sin\theta+B_2\sin 2\theta \quad (2.26b)$$

where

$$a = [\{(\beta_o'+\alpha_2\omega_2(\gamma_o-A_o-A_1-A_2)-B_1-2B_2)/(\alpha_1\omega_1-\alpha_2\omega_2)\}^2 + \{(\alpha_2\gamma_o'-\omega_2\beta_o)/(\alpha_1\omega_2-\alpha_2\omega_1)\}^2]^{1/2} \quad (2.27a)$$

$$b = [\{(\beta_o'+\alpha_1\omega_1(\gamma_o-A_o-A_1-A_2)-B_1-2B_2)/(\alpha_1\omega_1-\alpha_2\omega_2)\}^2 + \{(\alpha_1\gamma_o'-\omega_1\beta_o)/(\alpha_1\omega_2-\alpha_2\omega_1)\}^2]^{1/2} \quad (2.27b)$$

$$c_1 = \tan^{-1}[\{(\beta_o'+\alpha_2\omega_2(\gamma_o-A_o-A_1-A_2)-B_1-2B_2)/(\alpha_1\omega_1-\alpha_2\omega_2)\}/ \{(\alpha_2\gamma_o'-\omega_2\beta_o)/(\alpha_1\omega_2-\alpha_2\omega_1)\}] \quad (2.27c)$$

$$c_2 = \tan^{-1}[\{(\beta_o'+\alpha_1\omega_1(\gamma_o-A_o-A_1-A_2)-B_1-2B_2)/(\alpha_1\omega_1-\alpha_2\omega_2)\}/ \{(\alpha_1\gamma_o'-\omega_1\beta_o)/(\alpha_1\omega_2-\alpha_2\omega_1)\}] \quad (2.27d)$$

The frequencies ω_1 and ω_2 are represented by rather lengthy functions (Appendix I) of librational amplitudes and system parameters,

$$\omega_1 = f_1(a,b,I,\sigma,e,C,G) \tag{2.28a}$$

$$\omega_2 = f_2(a,b,I,\sigma,e,C,G) \tag{2.28b}$$

2.2.2 Periodic solutions of the system

The approximate, closed-form solution shows the system response to be characterized by three distinct components: response at 'high' frequency ω_1, 'low' frequency ω_2 and the orbital frequency. The resulting motion would, in general, be non-periodic except in the special situation when the frequencies ω_1 and ω_2 assume rational values for non-zero C, or, the ratio ω_1/ω_2 is a rational number with C = 0. A search extending over a reasonable range of system parameters and initial conditions showed such frequency combinations to be rare indeed.

On the other hand, the solution indicates that the system would execute periodic motion subject to initial conditions which excite only one of the three frequencies. Various relationships exist in the initial condition space for which the resulting motion is periodic. The high and low frequency periodic librations in the absence of solar radiation pressure (C = 0) are discussed first, followed by the solar pressure excited periodic oscillations of orbital frequency.

(a) High frequency oscillations (C = 0)

In the absence of solar radiation pressure, $A_i = B_i = 0$. Hence, the system would execute high frequency periodic motion for b = 0. This is satisfied by two sets of initial conditions. The oscillations of type I result with

$$\gamma_o = \beta_o' = 0$$

$$\gamma_o' = (\omega_1/\alpha_1)\beta_o \qquad (2.29a)$$

The corresponding amplitude and frequency of motion are obtained from Equations (2.27a) and (2.28a), respectively, as:

$$a = \beta_o/\alpha_1$$

$$\omega_1 = k_1 + \bar{f}_1(\beta_o/\alpha_1, I, \sigma, e) \qquad (2.29b)$$

The other set of initial conditions, leading to high frequency oscillations of type II, is readily found to be,

$$\gamma_o' = \beta_o = 0$$

$$\beta_o' = -\alpha_1\omega_1\gamma_o \qquad (2.30a)$$

with the amplitude and the frequency of motion,

$$a = \gamma_o$$

$$\omega_1 = k_1 + \bar{f}_1(\gamma_o, I, \sigma, e) \qquad (2.30b)$$

Relations (2.29) and (2.30), governing the initial conditions for high frequency periodic oscillations and the resulting frequency (oscillations per orbit), are plotted in Figure 2.3 for typical values of satellite parameters. The system behaves as a hard-spring oscillator showing an increase in the frequency with amplitude. Note that the change in satellite's configuration from spherical (I = 1) to disc-like (I = 2) results in a corresponding increase in frequency. An increase in orbital eccentricity also has similar effect.

(b) Low frequency oscillations (C = 0)

The low frequency periodic oscillations result from initial conditions leading to a = 0. As in the case of the high frequency oscillations, two distinct relationships between the initial states are found to yield periodic motions of low frequency.

Periodic motion of type I is obtained with,

$$\beta_o' = \gamma_o = 0$$

$$\gamma_o' = (\omega_2/\alpha_2)\beta_o \qquad (2.31a)$$

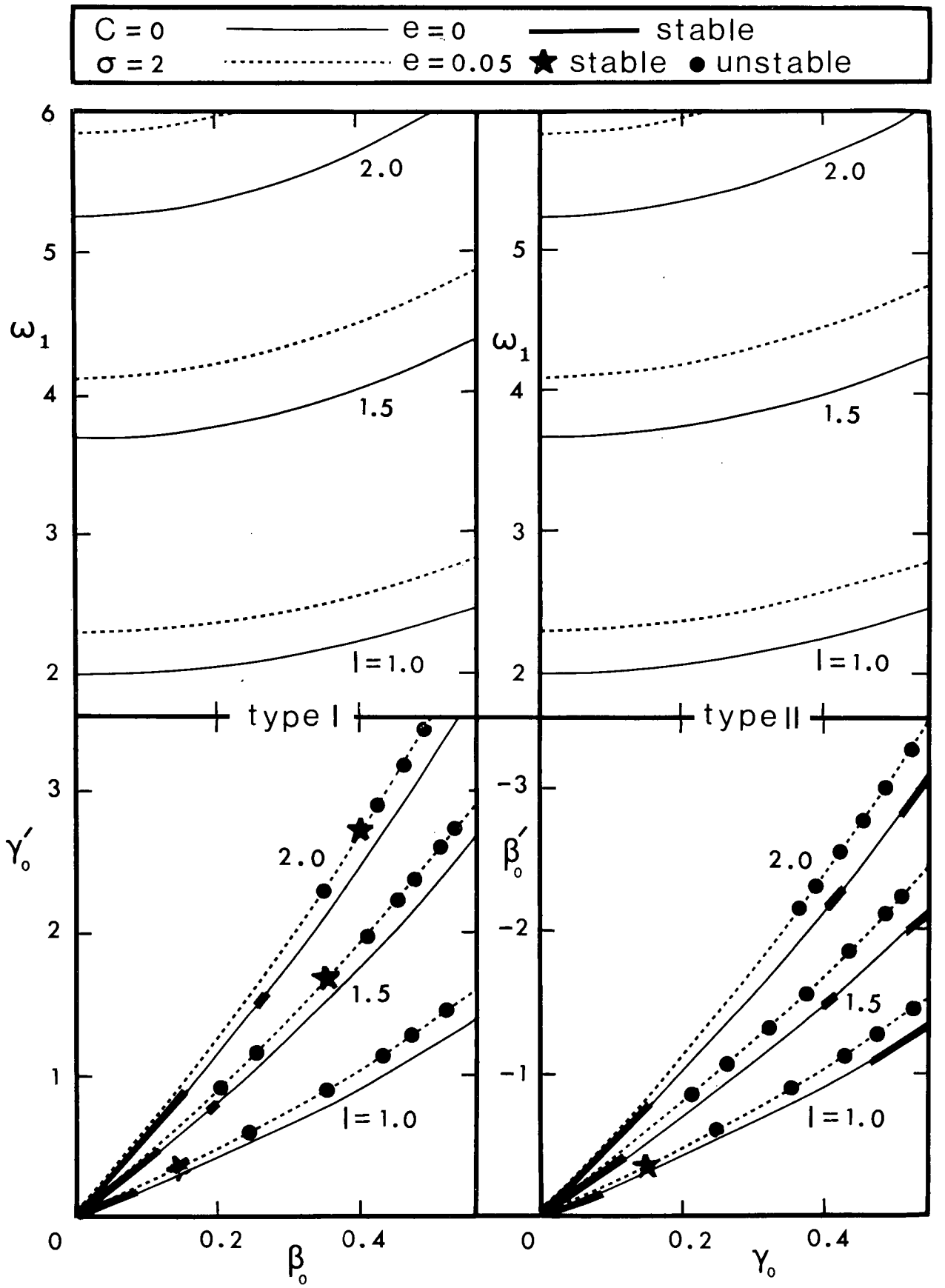

Figure 2.3 Frequency and initial conditions for high frequency periodic motion

with amplitude and frequency as

$$b = \beta_o/\alpha_2$$

$$\omega_2 = k_2 + \bar{f}_2(\beta_o/\alpha_2, I, \sigma, e) \qquad (2.31b)$$

while that of type II is governed by the conditions,

$$\gamma_o' = \beta_o = 0$$

$$\beta_o' = -\alpha_2\omega_2\gamma_o \qquad (2.32a)$$

leading to

$$b = \gamma_o$$

$$\omega_2 = k_2 + \bar{f}_2(\gamma_o, I, \sigma, e) \qquad (2.32b)$$

Relations (2.31) and (2.32) are presented in Figure 2.4 for typical values of the system parameters. The variation of the frequency is found to be relatively small. The slight decrease in its value with increasing amplitude indicates a soft-spring type of nonlinear effect over the range of initial conditions considered. Influence of the inertia parameter follows essentially the same trend as before. On the other hand, an increase in eccentricity tends to reduce the frequency of motion.

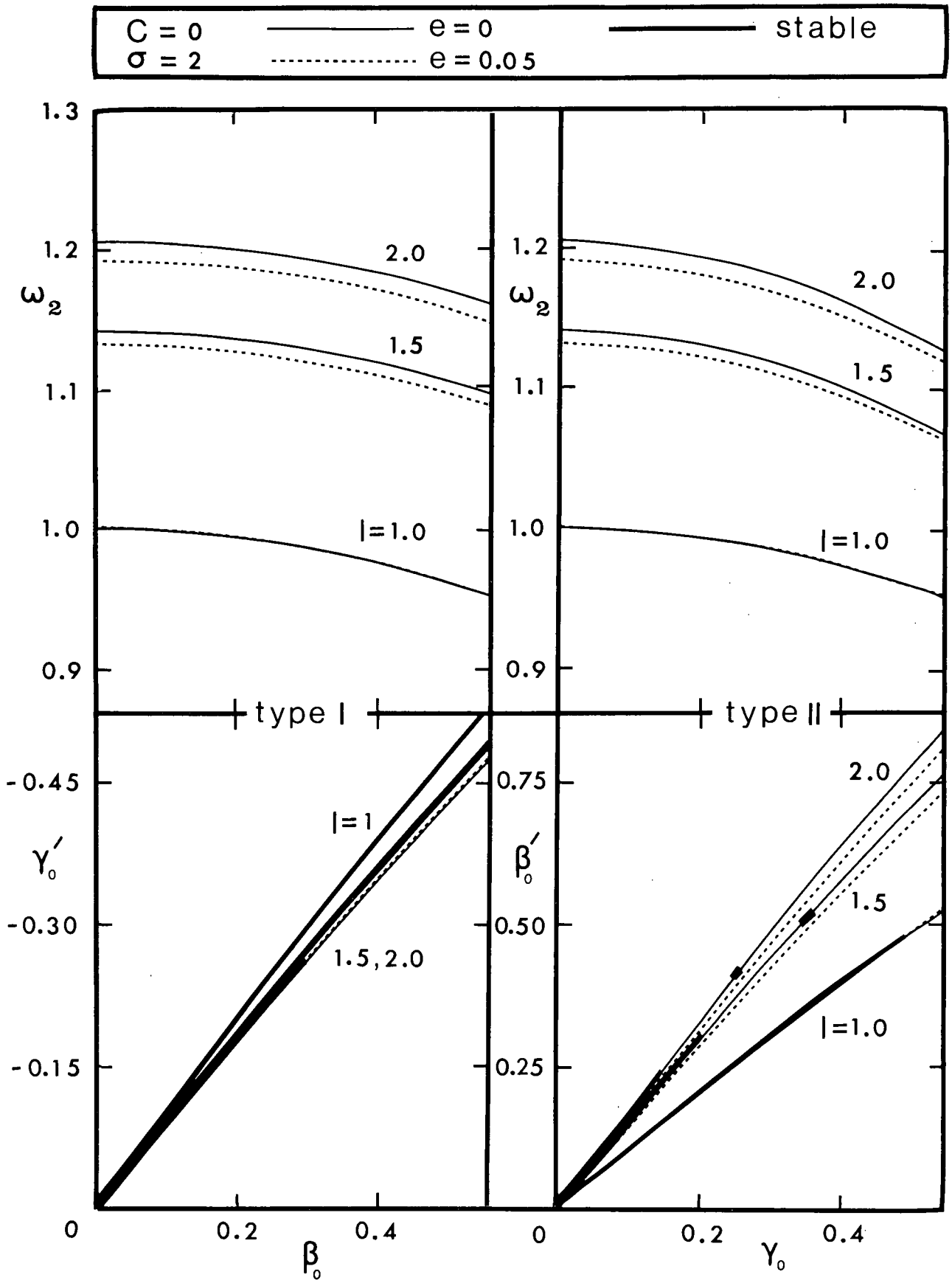

Figure 2.4 Frequency and initial conditions for low frequency periodic motion

(c) Solar pressure excited oscillations ($C \neq 0$)

For the solar pressure excited periodic solutions, having the same frequency as that of the orbital motion, $a = 0$, $b = 0$. Substituting these conditions in Equations (2.27a and b) results in the initial state,

$$\gamma_o = A_o + A_1 + A_2$$

$$\gamma_o' = 0$$

$$\beta_o = 0$$

$$\beta_o' = B_1 + 2B_2 \qquad (2.33)$$

Figure 2.5 shows the variation of the initial conditions γ_o and β_o' with the satellite spin parameter for both circular and noncircular orbital motion. The influence of the solar parameter C is to raise the initial conditions for periodic motion. The initial state appears to be highly sensitive to the spin rate for slowly spinning satellites, however, it asymptotically approaches a constant value with increasing spin parameter. In general, the effect of eccentricity is to increase the magnitude of the initial conditions except at the lower end of the spin parameter spectrum.

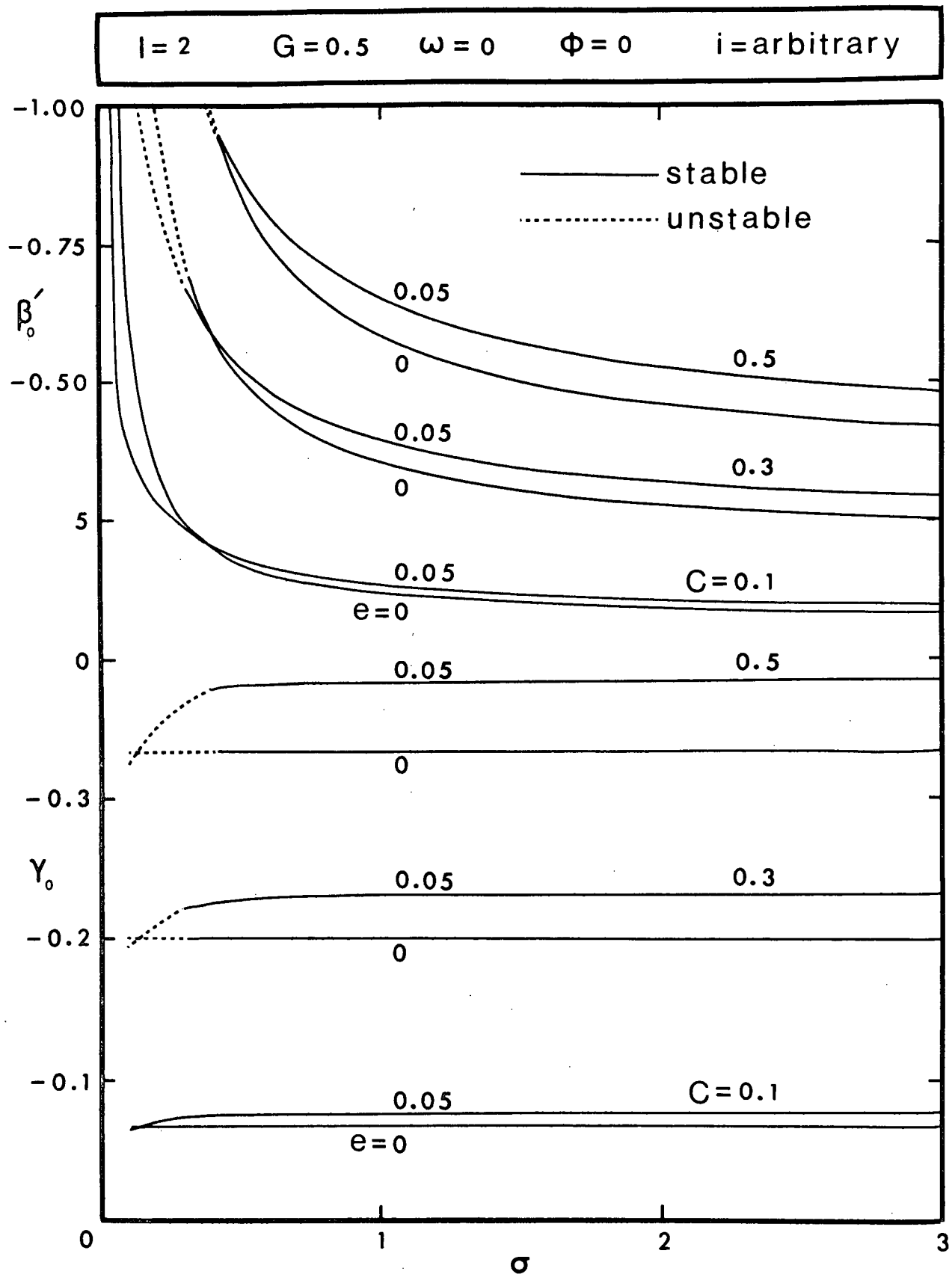

Figure 2.5 Initial conditions leading to solar pressure excited periodic motion

(d) Accuracy of the analytical solution

To assess the accuracy of this analytical procedure in predicting the periodic solutions, the governing equations of motion (2.13) were integrated numerically with initial conditions derived from the analytical solution. Typical responses are presented in Figure 2.6.

In circular orbits, the librational response is observed to be periodic with insignificant error. The frequency of oscillations is also predicted very accurately, thus demonstrating the effectiveness of the approximate, closed-form analysis.

The method continues to predict the periodic motions quite accurately even in elliptic orbits. The accuracy, however, was found to deteriorate with increasing e. Results showed the amplitude and frequency of the numerically generated response to be within five percent of their analytically predicted values for $e \leq 0.1$, the normal range of interest.

(e) Stability of periodic solutions

The stability of periodic solutions can be studied using variational analysis. The variational equations are obtained by letting

$$\gamma = \gamma_P + \gamma_v$$

$$\beta = \beta_P + \beta_v$$

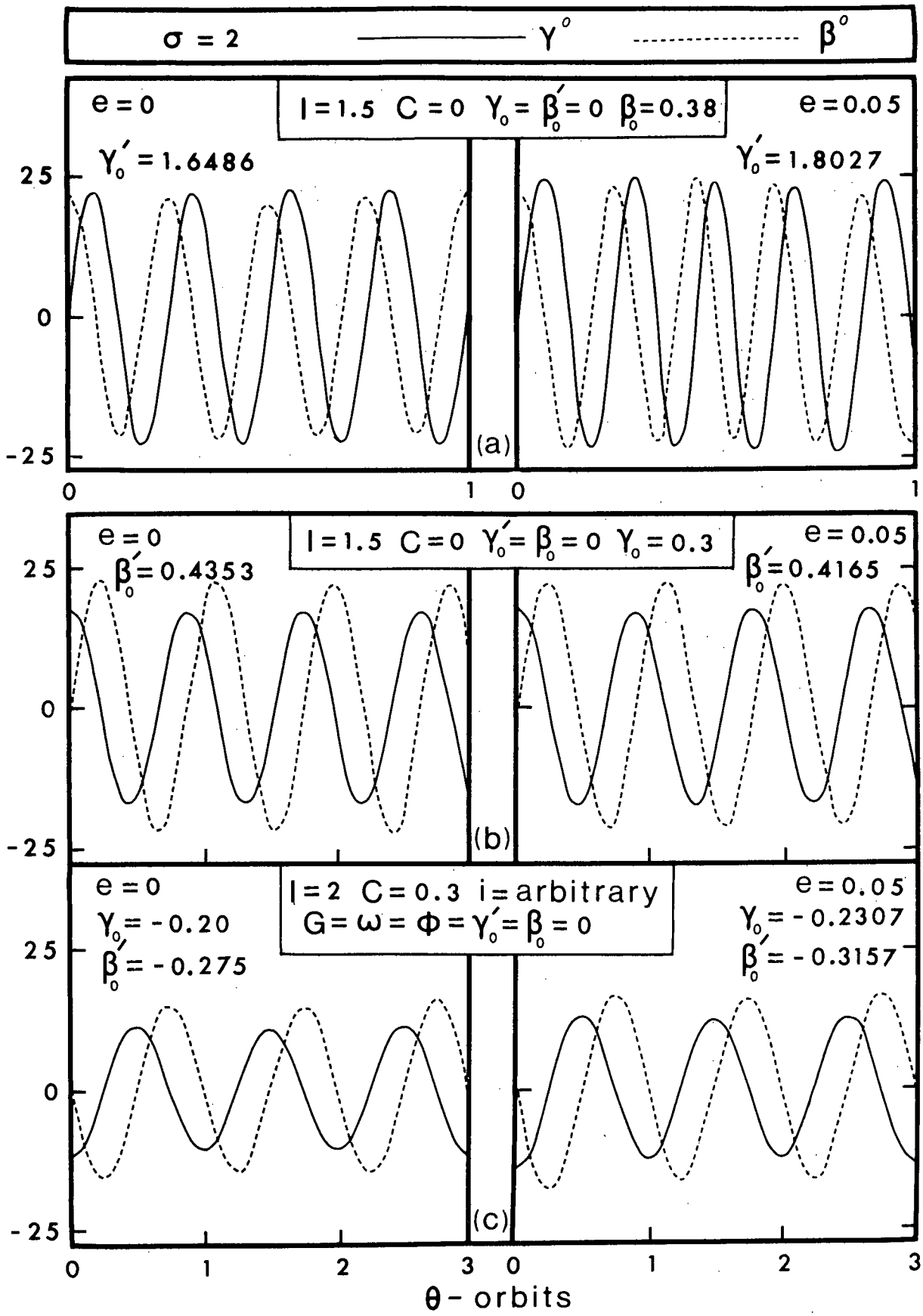

Figure 2.6 Typical periodic solutions of the system

where γ_p, β_p represent a periodic solution and γ_v, β_v are small perturbations. Substituting in Equations (2.13) and linearizing with respect to γ_v and β_v leads to:

$$\gamma_v'' = F_1\gamma_v + F_2\gamma_v' + F_3\beta_v + F_4\beta_v'$$

$$\beta_v'' = G_1\gamma_v + G_2\gamma_v' + G_3\beta_v + G_4\beta_v' \qquad (2.34)$$

where the details of lengthy functions

$$F_i = F_i(\gamma_p,\beta_p,\theta), \quad i = 1,2,3,4$$

$$G_i = G_i(\gamma_p,\beta_p,\theta), \quad i = 1,2,3,4 \qquad (2.35)$$

are given in Appendix II.

For circular orbital motion, the functions F_i and G_i assume the form $F_i = F_i(\gamma_p,\beta_p)$, $G_i = G_i(\gamma_p,\beta_p)$ and hence have periodicity of the solution. The Floquet theory can thus be applied to investigate the stability of the variational system (2.34). The stability criteria for distinct roots can be expressed as:

$$|\lambda_i| \leq 1, \ i = 1,2,3,4; \text{ stable}$$

any of the $|\lambda_i| > 1$, $i = 1,2,3,4$; unstable $\qquad (2.36)$

For satellite librations in noncircular orbits, the functions F_i and G_i are periodic only if the solution period is a rational multiple of the orbital period. The Floquet theory may again be used to assess the variational stability of these solutions. Figures 2.3 - 2.5 also show the results of this analysis.

The stable motion at smaller values of the initial conditions is, of course, anticipated. What is of particular significance is the possibility of periodic motions of large amplitudes. The amount of computational effort involved for stability analysis in an eccentric trajectory is enormous. Large values of the common period of the librational and orbital motion lead to extended integration limiting the stability investigation to isolated points (Figure 2.3). Of course, the solar pressure excited motion of the orbital period does not present this problem (Figure 2.5). The ability of the approximate closed form solution to predict nonlinear character of the system is indeed promising.

2.2.3 Resonance

It is of particular relevance to recognize here several possibilities of solar pressure excited resonance (Equations 2.15). Equivalence of k_1 or k_2 to the frequency of one of the forcing terms implies existence of certain combinations of the satellite inertia parameter I, spin

parameter σ and the orbital eccentricity e which would lead to unbounded motion.

In circular orbits, the condition k_1 and/or k_2=1 results in the resonance conditions,

$$I = 1$$

$$\text{or,} \quad I(\sigma + 1) - 2 = 0 \tag{2.37}$$

The conditions for resonance in elliptic orbits are obtained, for one of the frequencies k_1, k_2 assuming the value 1 or 2, as:

$$I = 1$$

$$\text{or,} \quad I(\sigma + 1)(1 + 2e) - 2 = 0$$

$$\text{or,} \quad 2I(\sigma+1)(1+2e) - (I+1) \pm \sqrt{I^2 - 18I + 33} = 0 \tag{2.38}$$

Figure 2.7 shows resonance conditions (2.37) and (2.38) in the system parameter space with typical responses presented in Figure 2.8. The large amplitude beat phenomenon in some cases indicates near resonant conditions. The value of C is purposely taken here to be small to emphasize the destabilizing effect of the radiation pressure. Larger values of the solar parameter as often observed in practice ($C \simeq 1.5$ for Anik, 2 for the CTS) would magnify the amplitude build-up. This clearly indicates the need for avoiding such

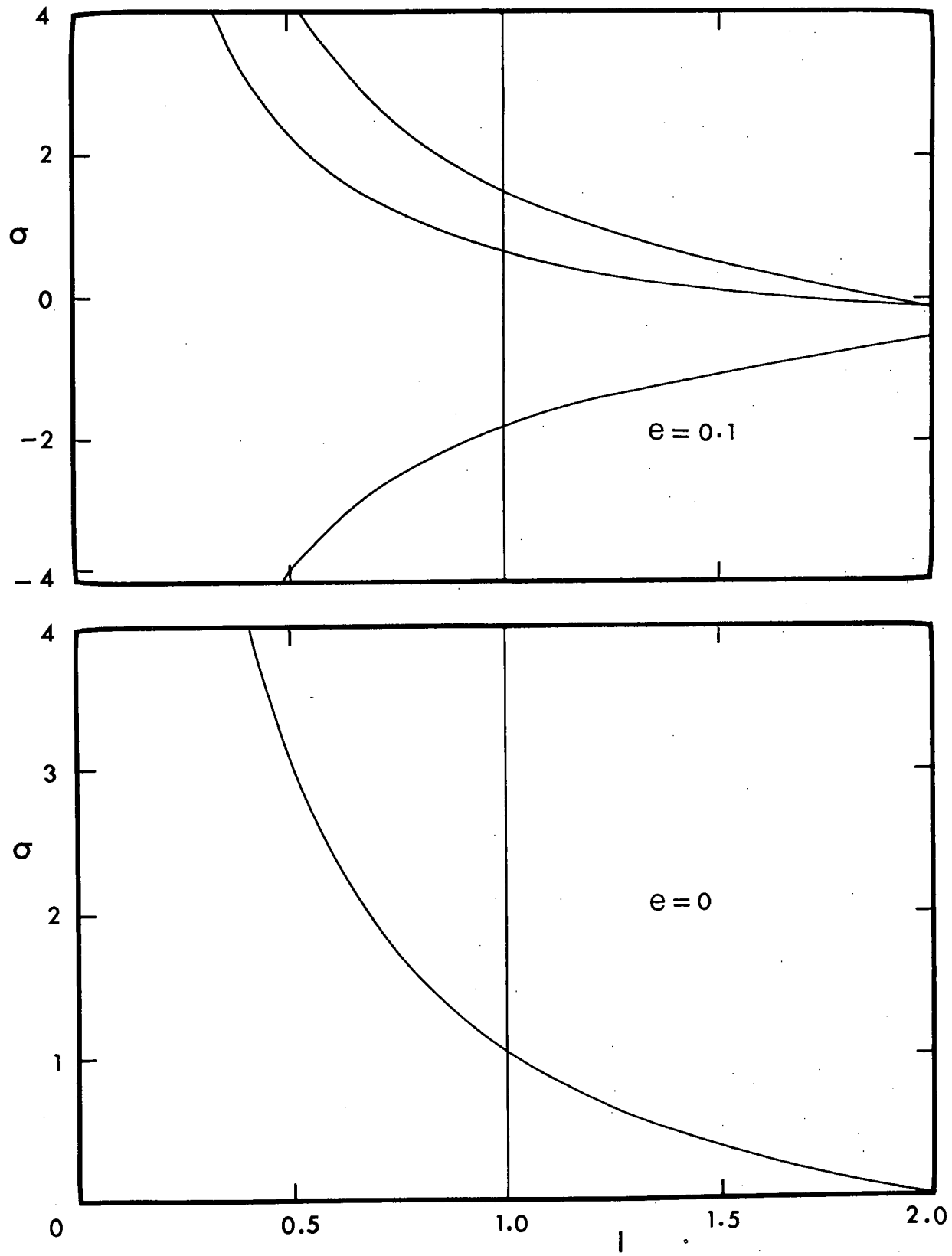

Figure 2.7 Resonance conditions in system parameter space

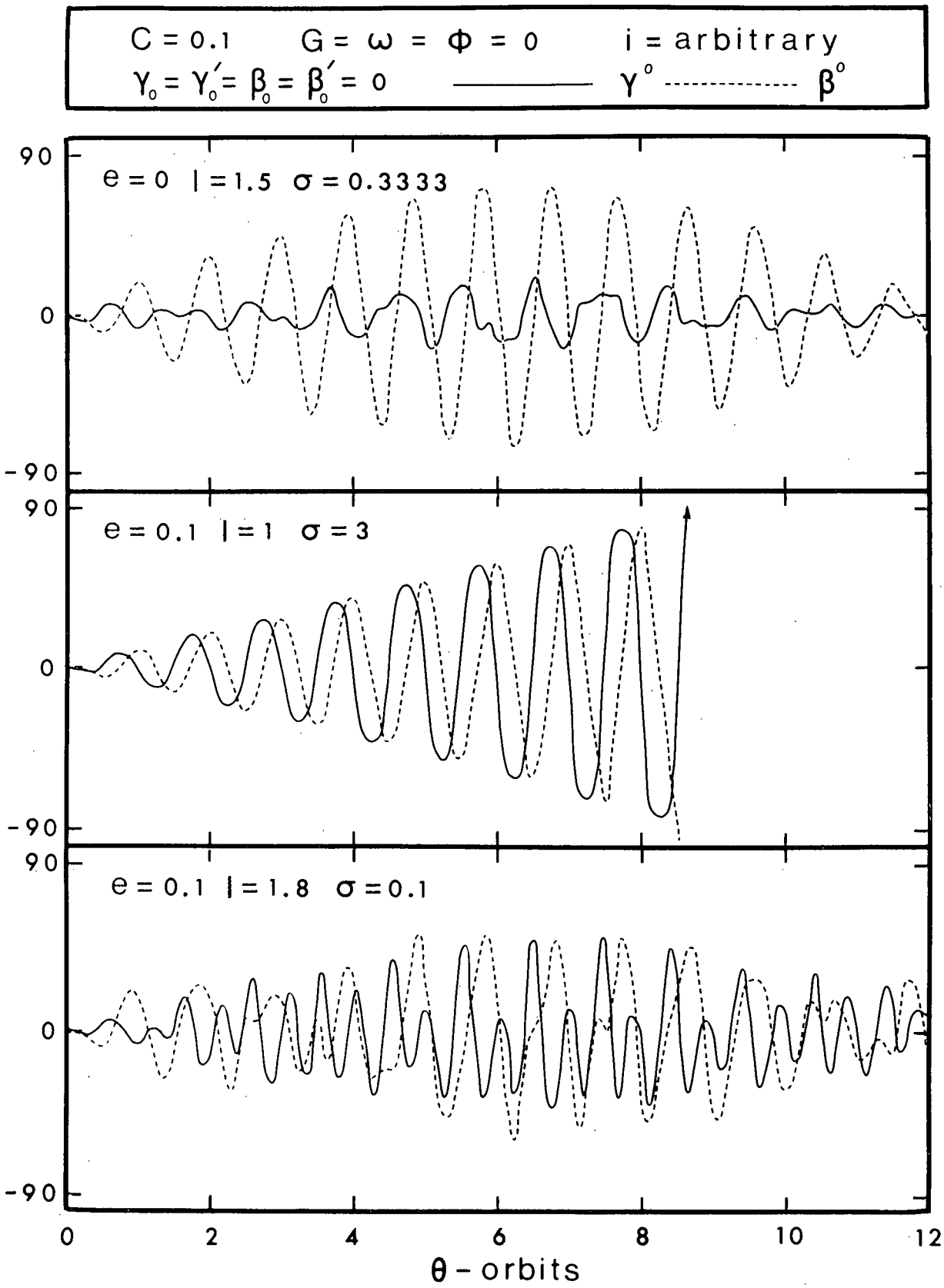

Figure 2.8 Typical responses under resonant conditions

critical combinations of system parameters for a safe satellite design.

2.3 Numerical Results

The quasi-linear character of the analytical solution limits its usefulness to the study of small amplitude motion. As anticipated, with large amplitudes, its accuracy was found to deteriorate due to the increased effect of system nonlinearities. A parametric study of the system was, therefore, carried out by numerically integrating the governing equations of motion. The Adams-Bashforth predictor-corrector quadrature with the Runge-Kutta starter was used, in conjunction with a step size of 3°, which gave results of sufficient accuracy without involving excessive computational effort.

2.3.1 Significant system parameters

The significance of the inertia parameter I, the spin parameter σ and the orbital eccentricity e in the librational dynamics of spin stabilized satellites cannot be overemphasized. Sensitivity of the system response to these parameters is vividly demonstrated in Figure 2.9. It shows the variation of Φ, the angular deviation of the axis of symmetry of the satellite from the orbit normal, against θ, the position of the satellite in an orbit. It is apparent that a judicious choice of parameter values is essential to avoid tumbling motion ($\Phi > \pi/2$).

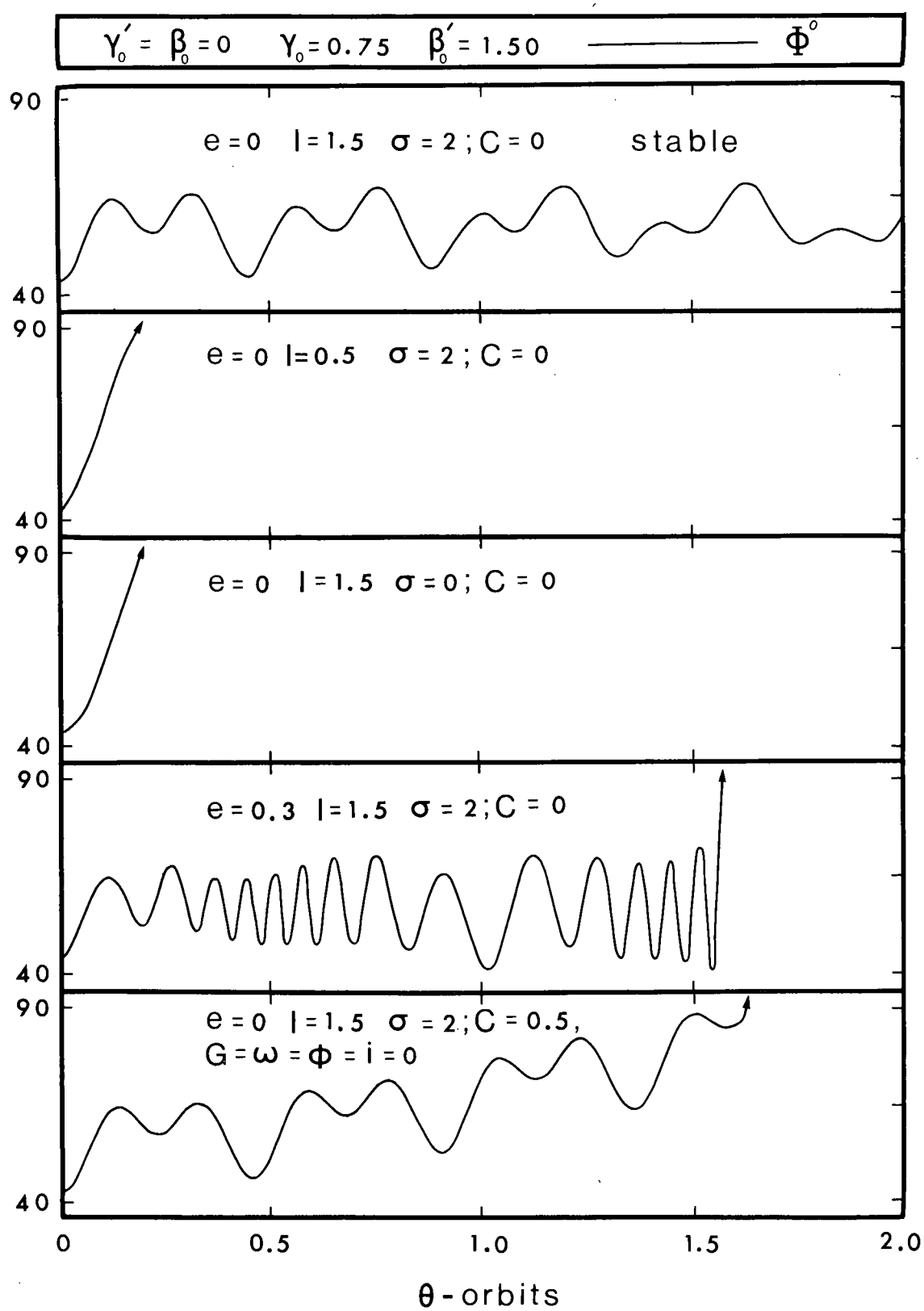

Figure 2.9 Typical unstable responses demonstrating the significance of system parameters

Of particular interest is the disturbing influence of solar radiation pressure. Note that the value of C as small as 0.5, which would physically correspond to $\varepsilon = 0.1$ ft for INTELSAT IV category of satellites at synchronous altitude, causes the satellite to tumble over. The critical values of eccentricity, intertia and spin parameters would only accentuate this behaviour. Of course, in actual practice, a higher spin rate and/or active control system would counter this tendency. Nevertheless, the analysis clearly brings out the fact that the solar parameter C is of the same importance as I, σ and e in the design of the satellite attitude control system.

2.3.2 System plots

In order to better understand the solar pressure excited dynamical behaviour of the satellite, the system parameters were varied over the desired range and the librational response observed. To isolate and emphasize the influence of the radiation pressure no other disturbances in the form of initial conditions were introduced. The resulting information was condensed in the form of system plots.

Figure 2.10a shows the effect of the satellite inertia parameter I on the coning amplitude Φ_{max} and the average "nodding" frequency of the axis of symmetry, ω_n, expressed as oscillations per orbit, for different values of

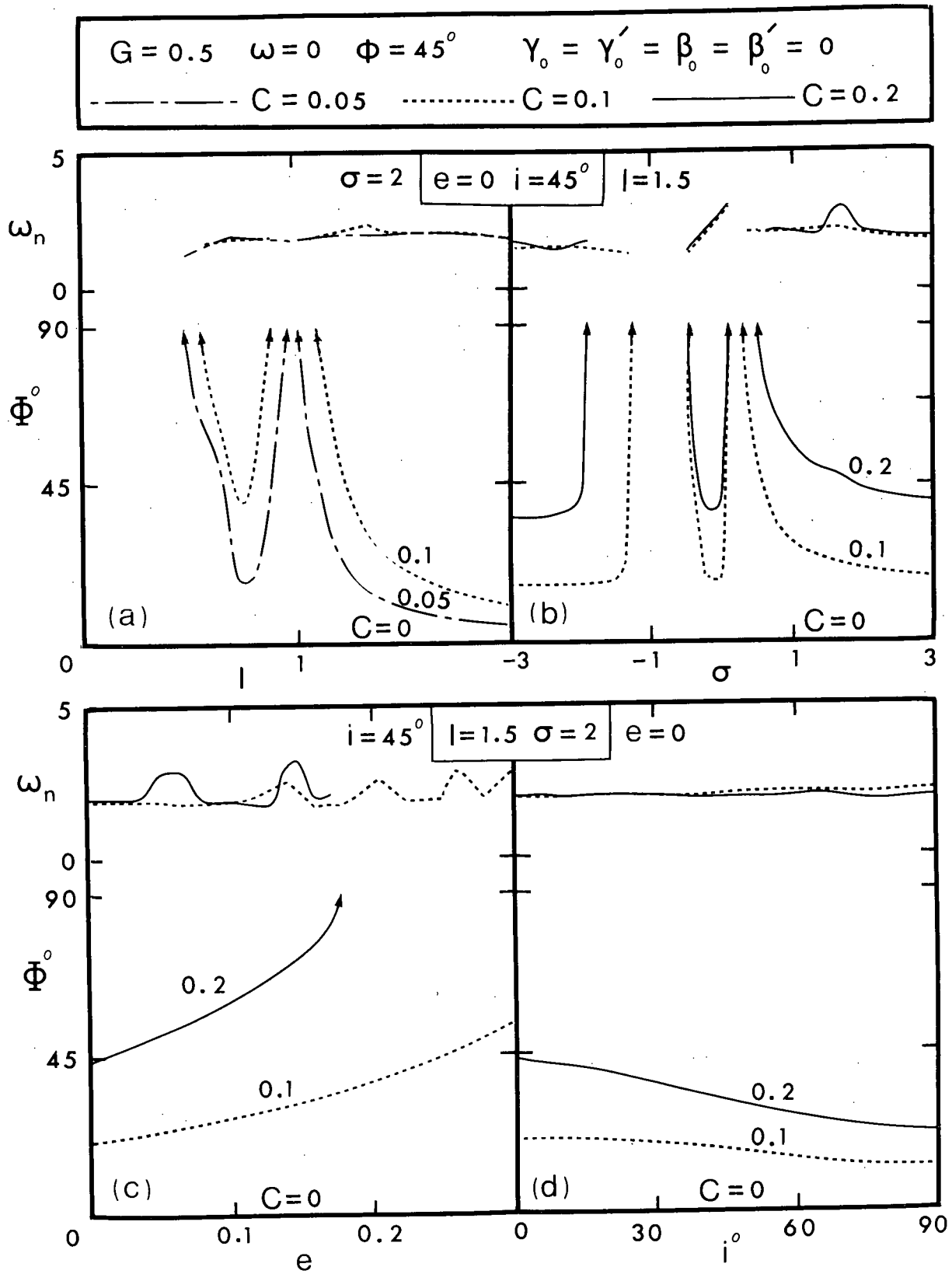

Figure 2.10 System plots showing the coning angle and average nodding frequency as affected by: (a) inertia parameter; (b) spin parameter; (c) orbit eccentricity; (d) orbit inclination

the solar parameter C. It may be observed that a satellite, when the solar pressure effects are neglected, remains in the equilibrium position (Φ = o). However, with non-zero C (say, C = 0.05), the librational motion is excited which increases in amplitude with increasing C. It is of interest to recognize the presence of a critical value of I = 1 leading to large amplitude motion finally resulting in instability. This amplitude build-up was found to occur even for very small values of the solar parameter C, thus confirming the resonant behaviour at these critical combinations of the system parameters predicted earlier by the analytical method. On the other hand, the average nodding frequency of the axis of symmetry appears to be relatively unaffected by changes in the inertia or solar paremeter.

The effect of the spin parameter σ on the librational behaviour is indicated in Figure 2.10b. Here again, critical values of the spin parameter exist for which the satellite tumbles over. A large value of the spin parameter, in general, leads to smaller coning angles as anticipated.

Figure 2.10c shows the influence of the orbit eccentricity on the attitude motion. In general, higher values of the orbit eccentricity result in larger amplitude motion. Unlike the effect of the inertia and the spin parameters, no resonant behaviour is noticed for the typical values of system parameters considered here.

The influence of the significant orbital parameters, such as i, ϕ, ω and the solar aspect ratio G, on the satellite performance was also investigated. The amplitude of oscillation was found to reduce gradually with an increase in the orbital inclination from the ecliptic (Figure 2.10d). Changes in the solar aspect angle ϕ, which depends upon the location of the line of nodes and the apparent position of the sun, did not affect the amplitude of librations and their frequency. The influence of the perigee position ω and the solar aspect ratio G was also found to be insignificant.

2.3.3 Design plots

From design considerations, it would be desirable to assess the magnitude of the solar pressure torque that a satellite can withstand without exceeding the permissible bound of libration as governed by the mission requirements. This bound then would establish a criterion for stability. Here, the stability limit is purposely taken as a large value of $\Phi = \pi/2$ to emphasize the vulnerability of the satellite's performance to the solar pressure torque.

Figure 2.11a shows a typical stability chart for librational motion in a circular orbit with the radiation pressure as the only excitation. The equations of motion (2.13) were integrated over 15-20 orbits for a range of values of satellite inertia and spin parameters. The result-

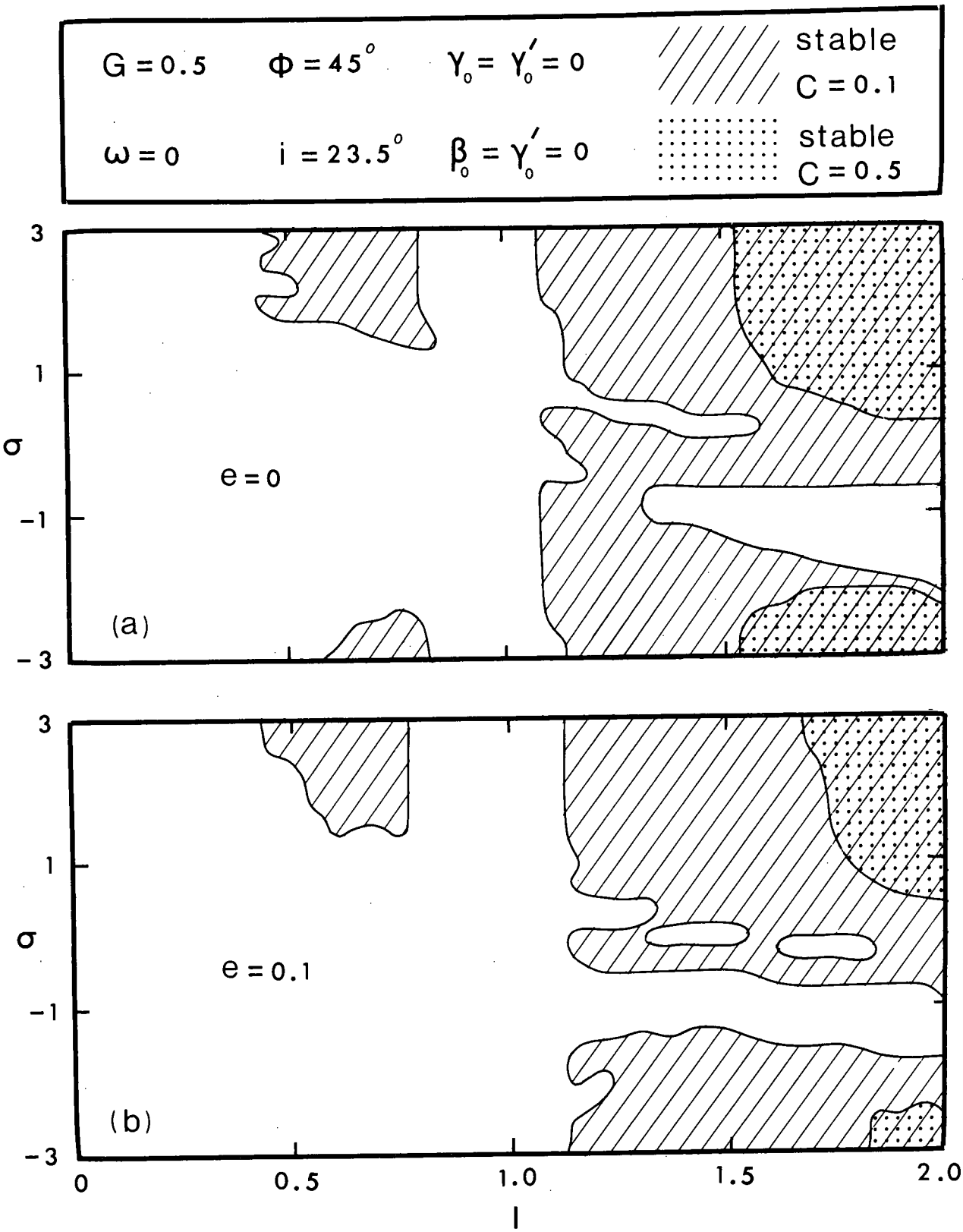

Figure 2.11 Typical stability charts showing adverse influence of solar radiation pressure: (a) e = 0; (b) e = 0.1

ing information about the maximum amplitude of the coning angle Φ_{max} was then condensed in the form of stability plots in the I-σ space. The analysis shows that in addition to the main stable region for high inertia parameter values, there also exist small isolated stable areas. However, there are substantial unstable regions even for positive spin or large inertia parameters. It is observed that the stable areas reduce drastically, as expected, with an increase in the value of the solar parameter.

The effect of the orbital eccentricity on the stability of librational motion is presented in Figure 2.11b. An increase in orbital eccentricity further enhances the destabilizing influence of the solar pressure. The effect appears to be more pronounced for satellites with the retrograde spin.

2.4 Concluding Remarks

The important features of the analysis and the conclusions based on them may be summarized as follows:

(i) The approximate analytical solution developed using the method of slowly varying parameters proves to be an excellent tool in establishing the periodic solutions of the system. The closed form character of the solution provides considerable insight into the system behaviour.

(ii) The analytical method predicts the system response and frequency quite accurately in circular orbits. Even for noncircular orbital motion ($e \leq 0.1$), the errors are confined to less than 5%.

(iii) The influence of the solar pressure on the satellite librations, in general, is adverse. The analysis shows, however, that the system can execute stable periodic motions of considerable magnitude in the solar pressure field under suitable initial conditions.

(iv) There exist combinations of system parameters for which large amplitude oscillations result, even in the presence of a very small solar torque, due to resonant interaction.

(v) The solar parameter affects stability of the motion substantially and hence merits equal consideration with the satellite inertia and spin parameters and the orbital eccentricity.

3. ATTITUDE CONTROL USING SOLAR RADIATION PRESSURE

The analysis of the last chapter clearly establishes the substantial adverse influence of solar radiation pressure on satellite librations. On the other hand, the findings of earlier investigations of gravity oriented systems[49-51] suggest that the radiation force can provide effective damping torques to maintain a satellite in a desired attitude. However, as pointed out in the literature review, available analyses of solar pressure control of spinning satellites are only of a preliminary nature. This is unfortunate because, in many space applications, a satellite with a directional sensor has a preferred orientation which is normally achieved by mounting the device on a stabilized platform aboard the spinning satellite. The spin, through a gyroscopic moment, provides stability while the platform, despun by control moments, tracks a given object in space. The concept of solar pressure control provides an exciting possibility of stabilizing the entire system through a semipassive approach.

This chapter investigates the feasibility of the general three-axis nutation damping and attitude control of spinning satellites using a solar controller sensitive to angular displacement and velocity errors. The analysis

is kept quite general to accommodate eccentric orbits and arbitrary inclinations of the orbital plane with respect to the ecliptic. The nonlinear, nonautonomous, coupled equations of motion are analyzed numerically and the influence of system parameters on the response studied.

In the latter part of the chapter, a logical approach for controller design is developed. Analytical solutions for the control variables are obtained which suggest reduced software requirements. Several examples using representative satellites illustrate the effectiveness of the control system and help gain an appreciation as to the controller size required for a desired performance.

3.1 Feasibility of Solar Pressure Control

3.1.1 Equations of motion

Figure 3.1 shows an axisymmetric ($I_y = I_z$) satellite with the center of mass S moving in a Keplerian orbit about the center of force O. The satellite consists of a central body I, spinning at a constant average angular velocity, connected to a stabilized platform II through a viscous damper effective in axial rotation. The spatial orientation of the axis of symmetry, as stated before, is specified by two successive rotations γ and β, referred to as roll and yaw, respectively, which define the attitude of the satellite principal axes x,y,z with respect to the inertial

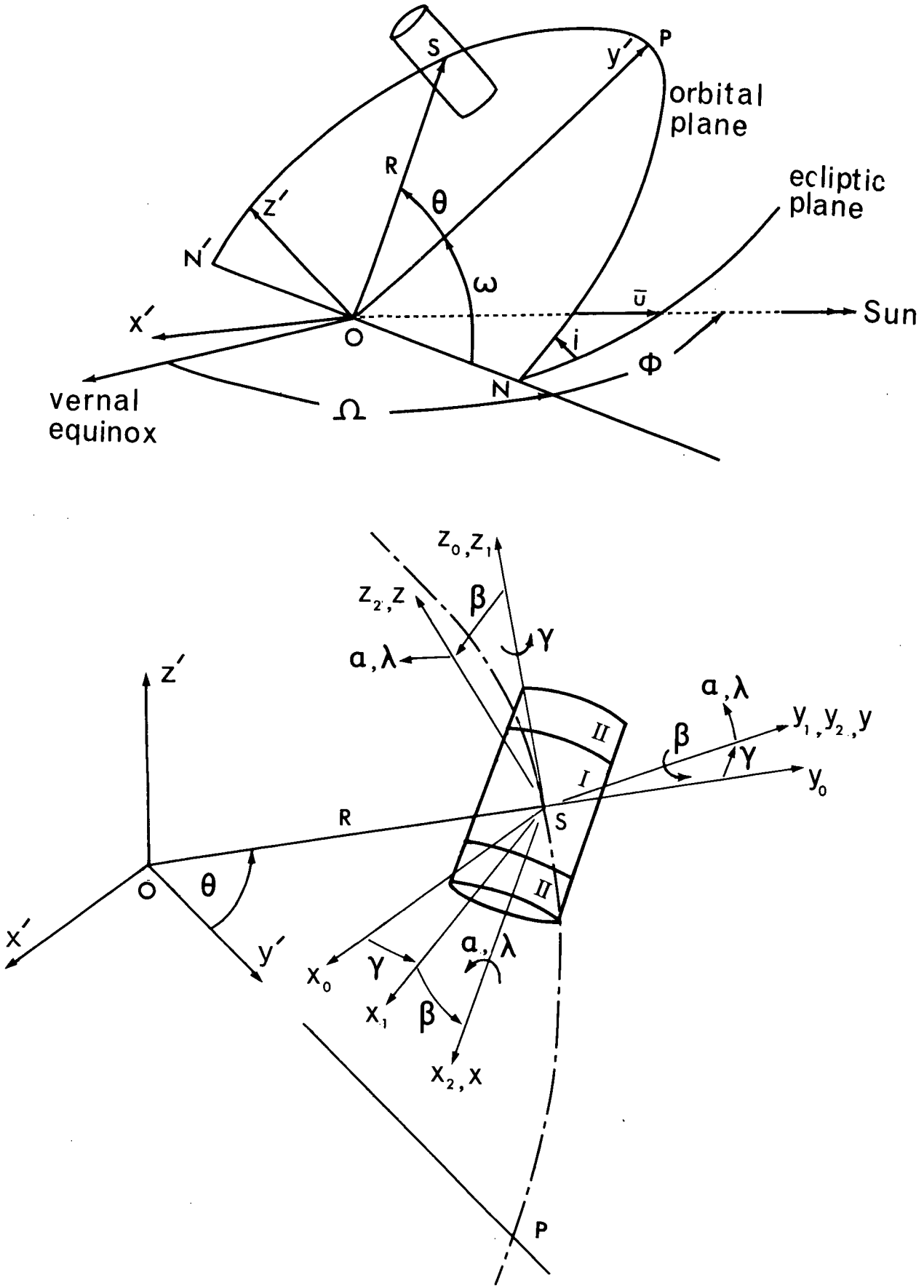

Figure 3.1 Geometry of motion of dual-spin satellite in the solar pressure environment

reference frame x', y', z'. The rotor and the platform spin in the x,y,z reference with angular velocities $\dot{\alpha}$ and $\dot{\lambda}$, respectively. In terms of these modified Eulerian rotations, the expressions for the potential and kinetic energies to $O(1/R^3)$ are obtained as:

$$U_g = -\mu m_s/R-\mu\{(I_x/2R^3)(I-1)/I\}(1-3\sin^2\gamma\cos^2\beta) \qquad (3.1)$$

$$\begin{aligned} T = {} & (m_s/2)(\dot{R}^2+R^2\dot{\theta}^2)+(I_x/2I)\{(1-J)I(\dot{\alpha}-\dot{\gamma}\sin\beta+\dot{\theta}\cos\beta\cos\gamma)^2 \\ & + JI(\dot{\lambda}-\dot{\gamma}\sin\beta+\dot{\theta}\cos\beta\cos\gamma)^2+(\dot{\beta}-\dot{\theta}\sin\gamma)^2 \\ & +(\dot{\gamma}\cos\beta+\dot{\theta}\sin\beta\cos\gamma)^2\} \end{aligned} \qquad (3.2)$$

The Rayleigh dissipation function is given by

$$F = (1/2)K_d(\dot{\lambda}-\dot{\alpha})^2 \qquad (3.3)$$

Using the Lagrangian formulation, the equation of motion in the α degree of freedom becomes,

$$(d/dt)\{I_{xr}(\dot{\alpha}-\dot{\gamma}\sin\beta+\dot{\theta}\cos\beta\cos\gamma)\}+K_d(\dot{\alpha}-\dot{\lambda}) = Q_\alpha \qquad (3.4)$$

As the rotor is considered to spin at a constant average spin rate (i.e., no spin decay), the usual assumption in the analysis of dual-spin spacecraft,

$$Q_\alpha = K_d(\dot{\alpha}-\dot{\lambda}) \tag{3.5}$$

This is equivalent to assuming an energy source countering the bearing drag on the rotor. The first integral

$$\dot{\alpha}-\dot{\gamma}\sin\beta+\dot{\theta}\cos\beta\cos\gamma = h_\alpha \tag{3.6}$$

may now be used to eliminate the cyclic coordinate α through the spin parameter σ defined as,

$$\sigma = (\dot{\alpha}/\dot{\theta})\Big|_{\theta=\beta=\gamma=0} = (h_\alpha/\dot{\theta})\Big|_{\theta=0} - 1 \tag{3.7}$$

Neglecting orbital perturbations due to librational motion[78,79] and making use of the spin parameter, the Lagrangian formulation yields the governing equations of motion in the roll, yaw and pitch degrees of freedom. Changing the independent variable from t to θ through the Keplerian orbital relations, they finally take the form:

$$\gamma'' - 2\beta'(\gamma'\tan\beta-\cos\gamma) - (\beta'-\sin\gamma)\sec\beta[(1-J)I(\sigma+1)\times$$

$$\{(1+e)/(1+e\cos\theta)\}^2 + JI(\lambda'-\gamma'\sin\beta+\cos\beta\cos\gamma)]$$

$$+\{3(I-1)/(1+e\cos\theta)-1\}\sin\gamma\cos\gamma-\{2e\sin\theta/(1+e\cos\theta)\}\times$$

$$(\gamma'+\cos\gamma\tan\beta) = Q_\gamma \tag{3.8a}$$

$$\beta'' - \gamma'\cos\gamma - \{2e\sin\theta/(1+e\cos\theta)\}(\beta' - \sin\gamma) + (\gamma'\cos\beta + \cos\gamma\sin\beta) \times$$

$$[(1-J)I(\sigma+1)\{(1+e)/(1+e\cos\theta)\}^2 + JI(\lambda' - \gamma'\sin\beta + \cos\beta\cos\gamma)$$

$$+ (\gamma'\sin\beta - \cos\beta\cos\gamma)] - 3\{(I-1)/(1+e\cos\theta)\}\sin^2\gamma\sin\beta\cos\beta = Q_\beta \qquad (3.8b)$$

$$\lambda'' - \gamma''\sin\beta - \{2e\sin\theta/(1+e\cos\theta)\}(\lambda' - \gamma'\sin\beta + \cos\beta\cos\gamma)$$

$$- \beta'\gamma'\cos\beta - \gamma'\cos\beta\sin\gamma - \beta'\cos\gamma\sin\beta + (K/JI) \times$$

$$\{(1+e)^{3/2}/(1+e\cos\theta)^2\}[\lambda' - \gamma'\sin\beta + \cos\beta\cos\gamma - (\sigma+1) \times$$

$$\{(1+e)/(1+e\cos\theta)\}^2] = Q_\lambda \qquad (3.8c)$$

where $Q_i (i = \gamma, \beta, \lambda)$ represent the generalized forces due to solar radiation pressure.

3.1.2 Controller configuration

A controller, in general, consists of light, rigid, highly reflective plates (membranes) suitably mounted on the platform to be stabilized. The control moments resulting from the solar radiation force on the plates may be varied by changing any one of the following:

(i) the distance between the center of pressure and the satellite center of mass by translating the plate support;

(ii) the area of the membrane through wrapping or unfurling portions of it;

(iii) the projected area of the plate as 'seen' by the sun by rotating the plate.

Practical considerations make the last alternative the most attractive, especially, when servomotors can be located within the controlled environment of the spacecraft. In order that the three degrees of freedom of the system, namely the roll γ, the yaw β and the platform pitch λ, be controlled independently, it is necessary to provide at least three independent plate rotations δ_1, δ_2, and δ_3.

Various controller configurations were studied which, in general, yield expressions for the generalized forces of the form:

$$Q_\gamma = Q_\gamma(\delta_1, \delta_2, \delta_3)$$

$$Q_\beta = Q_\beta(\delta_1, \delta_2, \delta_3)$$

$$Q_\lambda = Q_\lambda(\delta_1, \delta_2, \delta_3) \qquad (3.9)$$

where the functions in the right hand side are transcendental.

As the rotations δ_1, δ_2, and δ_3 are real, the simultaneous maxima $|Q_\gamma|_{max}$, $|Q_\beta|_{max}$ and $|Q_\lambda|_{max}$, for which the set of Equations (3.9) possesses a real solution,

represent the physical limit on the generalized forces that a particular controller configuration can yield. The problem of determining the maximum values of Q_γ, Q_β, and Q_λ, which would satisfy the above criterion is, in general, a complex one. Any attempt to simplify the problem, through the choice of controllers yielding completely decoupled moments, would lead to increased hardware complexities. One is, therefore, forced to compromise by selecting a controller configuration resulting in a partial uncoupling of the Q_i.

Figure 3.2 shows the schematic diagram of the proposed semi-passive controller. It consists of five sets of plates $P_i (i = 1,2,3)$ and $P'_j (j = 1,2)$ with their axes mounted on the platform. The plates are permitted rotations $\delta_i (i = 1,2,3)$ about these axes. The angles $\delta_i (i = 1, 2)$ are measured from the yz-plane and δ_3 is measured from a platform-fixed reference line at an angle λ from the y axis. At a given instant, the set P_3, controlling the λ motion, operates in conjunction with the sets $P_i (i = 1,2)$ or $P'_j (j = 1,2)$ or $P_i P'_j (i \neq j)$, which provide corrective torques in the γ and β degrees of freedom.

The determination of the moments due to solar radiation pressure is somewhat involved. Figure 3.3 shows a plate in an arbitrary orientation with respect to the sun. The force on an elemental plate area dA is given by

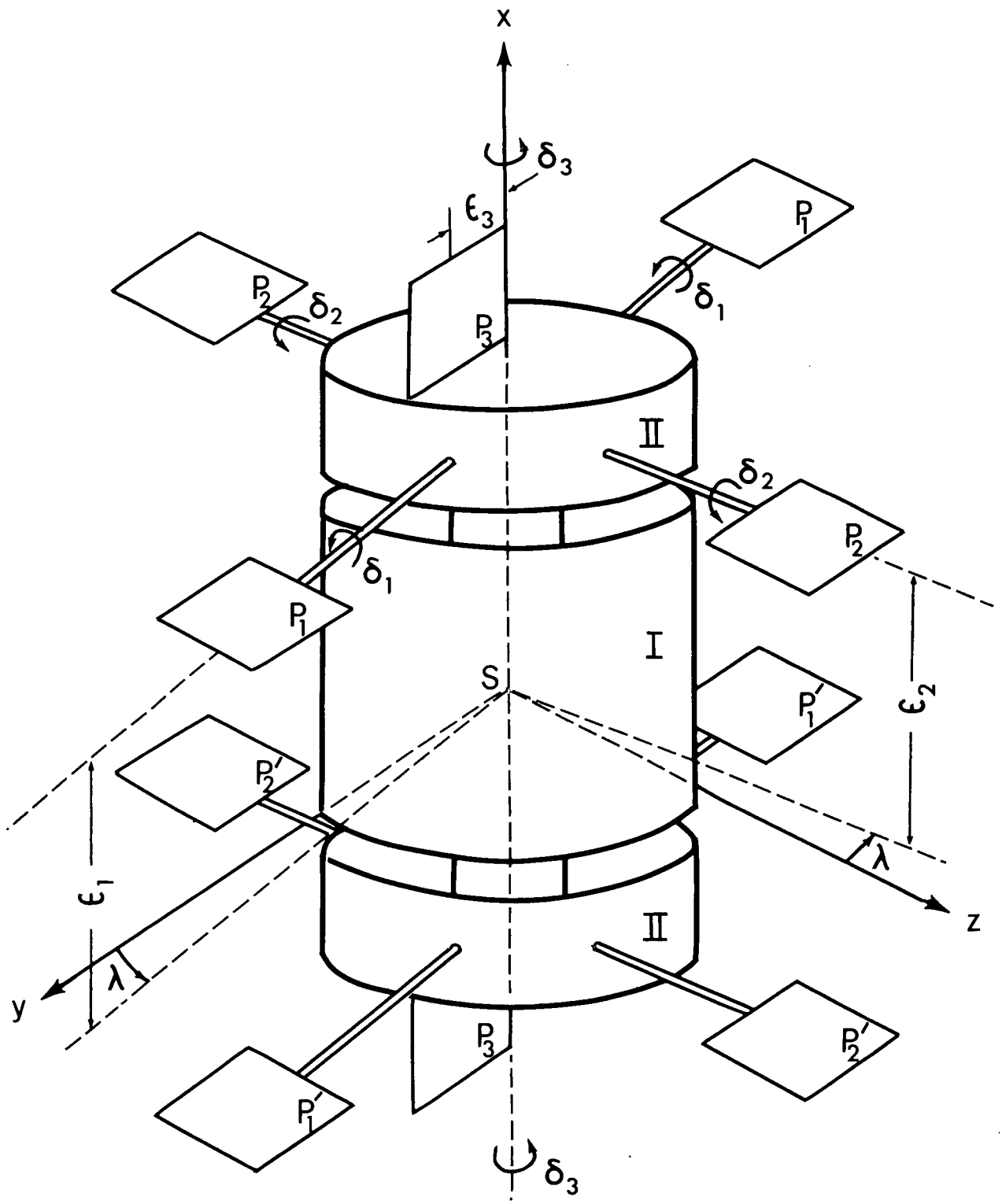

Figure 3.2 Solar controller configuration

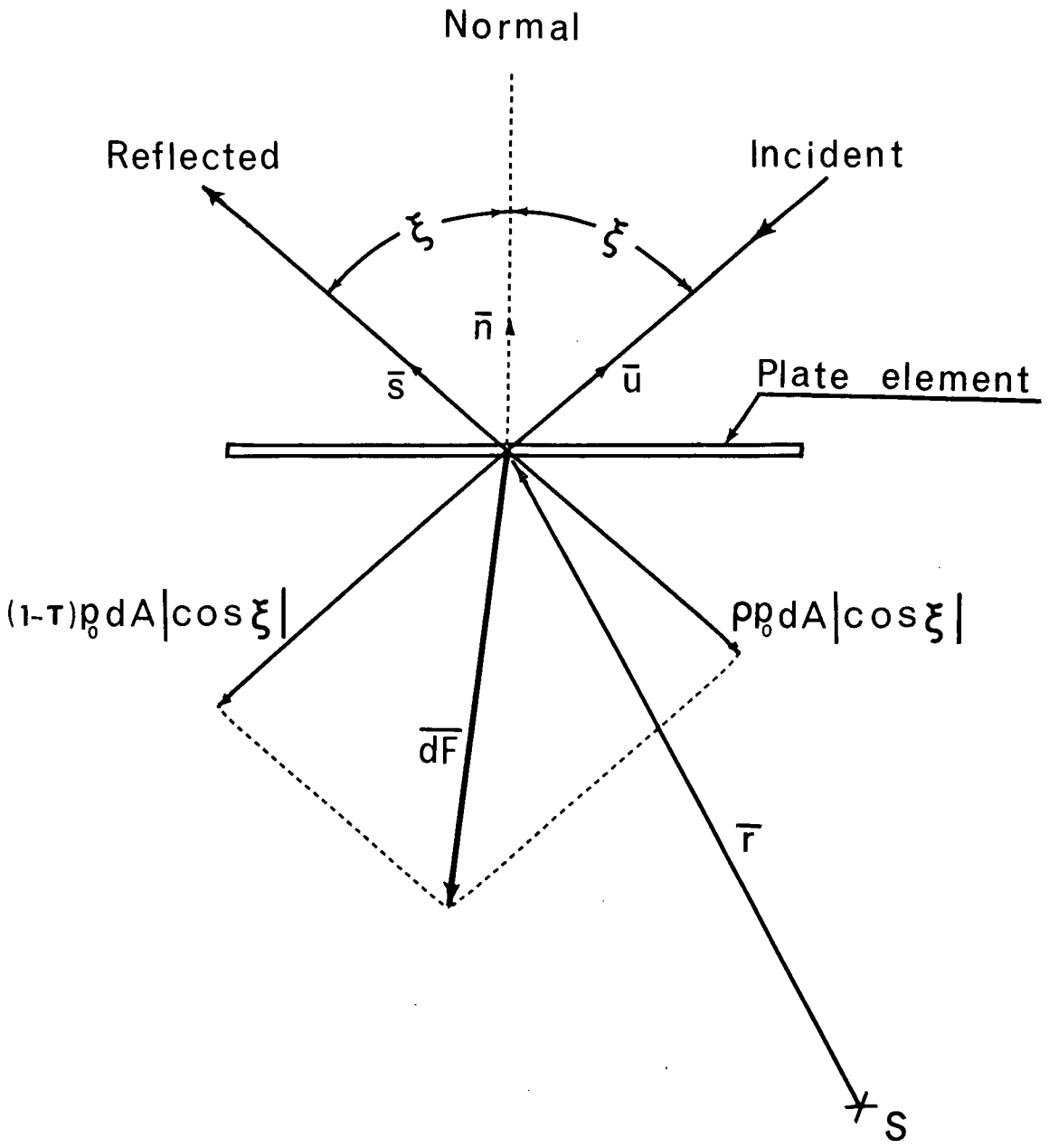

Figure 3.3 Radiation force on a plate element

$$d\bar{F} = -p_o dA|\cos\xi|\{(1-\tau)\bar{u}+\rho\bar{s}\} \tag{3.10}$$

with the resulting moment about the satellite center of mass as

$$\bar{M} = \int_A \bar{r} \times d\bar{F} \tag{3.11}$$

Expressing the angle of incidence ξ and the unit vectors $\bar{u}$ and $\bar{s}$ as functions of the attitude angles, the solar aspect angle ϕ and the plate rotations δ_i, and evaluating the integral in Equation (3.11) yield the desired expression for $\bar{M}$. The application of the principle of virtual work finally leads to the generalized forces Q_i. The expressions are rather lengthy, however, ignoring the terms of order $(1-\tau-\rho)/2\rho$ compared to unity, which is justifiable for surfaces of high reflectivity, results in a considerable similification:

$$\begin{aligned} Q_\gamma = \; & -E(\theta)[U_1C_1|\cos\xi_1|\cos\xi_1\sin\delta_1\sin\lambda \\ & +U_2C_2|\cos\xi_2|\cos\xi_2\sin\delta_2\cos\lambda]\sec\beta \end{aligned} \tag{3.12a}$$

$$\begin{aligned} Q_\beta = \; & -E(\theta)[U_1C_1|\cos\xi_1|\cos\xi_1\sin\delta_1\cos\lambda \\ & -U_2C_2|\cos\xi_2|\cos\xi_2\sin\delta_2\sin\lambda] \end{aligned} \tag{3.12b}$$

$$Q_\lambda = -E(\theta)(C_3/J)|\cos \xi_3| \cos \xi_3 \qquad (3.12c)$$

where

$$U_i = +1 \text{ for } P_i, \ -1 \text{ for } P_i'; \ i = 1,2$$

$$\cos \xi_1 = u_i \cos\delta_1 + (u_j \sin\lambda - u_k \cos\lambda)\sin\delta_1$$

$$\cos \xi_2 = u_i \cos\delta_2 + (u_j \cos\lambda + u_k \sin\lambda)\sin\delta_2 \qquad (3.13)$$

$$\cos \xi_3 = -u_j \sin(\delta_3+\lambda) + u_k \cos(\delta_3+\lambda)$$

The solar parameters, C_i, are defined as

$$C_i = (4\rho p_o R_p^3/\mu I_y) A_i \varepsilon_i, \ i = 1,2$$

$$C_3 = (4\rho p_o R_p^3/\mu I_x) A_3 \varepsilon_3 \qquad (3.14)$$

3.1.3 Control strategy

The generalized forces Q_i are controlled in a velocity and position sensitive manner according to the relations:

$$Q_\gamma = -\mu_\gamma \gamma' - \nu_\gamma(\gamma-\gamma_c) \qquad (3.15a)$$

$$Q_\beta = -\mu_\beta \beta' - \nu_\beta(\beta-\beta_c) \qquad (3.15b)$$

$$Q_\lambda = -\mu_\lambda \lambda' - \nu_\lambda(\lambda-\lambda_c) \qquad (3.15c)$$

where the system gains μ_i, ν_i are chosen according to some suitable criterion, such as, the least time of damping or the maximum permissible displacement during a nutation cycle. The position control parameters γ_c, β_c, and λ_c, however, are functions of the desired final orientation γ_f, β_f, and λ_f and are obtained from the equilibrium consideration of the controlled system (Equations 3.8). For nutation damping in a circular orbit, this results in

$$\gamma_c = \beta_c = 0, \quad \lambda_c = -(1/\nu_\lambda)K\sigma/JI \tag{3.16}$$

In principle, the plate rotations can be obtained by substituting Equations (3.15) into Equations (3.12) and solving for δ_i. This, of course, implies specification of the signs of U_1 and U_2, i.e., a combination of the plate-sets to be operated. However, there are still several mathematical problems as the system of Equations (3.12) may not possess a real solution. A trial with different sign combinations of U_1 and U_2 is thus necessary. Fortunately, for many applications, $|u_i| << |u_j|$, $|u_k|$ and λ executes small oscillations in the neighbourhood of nominal pitch attitudes $\lambda_f = 0, \pi/2, \pi$ or $3\pi/2$. In such situations, the required signs of U_1 and U_2 may be determined analytically.

Furthermore, the controller may be unable to provide the corrective moments demanded by the system

(Equations 3.15) at all times due to its physical limitations. It is, therefore, necessary to introduce saturation constraints on the control moments Q_i. Hence the real solution for δ_i has to be determined consistent with this constraint.

Q_λ being a function of δ_3 only, its maximum attainable value can easily be found,

$$|Q_\lambda|_{max} = E(\theta)(C_3/J)(u_j^2+u_k^2) \tag{3.17}$$

But Q_γ, Q_β are functions of both δ_1 and δ_2, hence it is necessary to specify a rational criterion for the controller operation. In the present analysis, based on physical considerations, it is taken to be the maximum of the total transverse torque, $(Q_\gamma^2\cos^2\beta+Q_\beta^2)^{1/2}$. This occurs at

$$\delta_1 = \pi/2+\tan^{-1}[(3/2)(u_j\sin\lambda-u_k\cos\lambda)/u_i \pm\{(9/4)(u_j\sin\lambda -u_k\cos\lambda)^2/u_i^2+2\}^{1/2}] \tag{3.18a}$$

$$\pm \text{ for}\{(u_j\sin\lambda-u_k\cos\lambda)/u_i\} \lesseqgtr 0,$$

and $$\delta_2 = \pi/2+\tan^{-1}[(3/2)(u_j\cos\lambda+u_k\sin\lambda)/u_i \pm\{(9/4)(u_j\cos\lambda +u_k\sin\lambda)^2/u_i^2+2\}^{1/2}] \tag{3.18b}$$

$$\pm \text{ for } \{(u_j\cos\lambda+u_k\sin\lambda)/u_i\} \lesseqgtr 0.$$

Substitution for $\delta_i (i = 1,2)$ from Equations (3.18) into Equations (3.12) yields the desired maximum values of Q_γ and Q_β. Appropriate signs of U_1 and U_2 are to be introduced which yield signs of $Q_{\gamma max}$ and $Q_{\beta max}$ consistent with those governed by Equations (3.15).

The control procedure may now be summarized as follows:

(i) sense the roll, yaw and pitch angles and rates, orbital position and the apparent position of the sun;

(ii) compute the control moments demanded by the system using Equations (3.15);

(iii) evaluate the maximum attainable moments using Equations (3.17, 3.18, 3.12a and b);

(iv) compare the moment demand with the attainable values. If the demand exceeds the maximum available, set it equal to the latter;

(v) determine the plates to be operated for roll-yaw control (through U_1 and U_2) and the rotations δ_1, δ_2 and δ_3 from Equations (3.12).

3.1.4 Results and discussion

The response of the system was studied by numerically integrating the equations of motion (3.8) along with the control relations (3.15). Again the Adams-Bashforth

predictor-corrector quadrature with the Runge-Kutta starter was used in conjunction with a step size of 3°. The important system parameters were varied gradually over the range of interest and the controller performance evaluated both in circular and elliptic orbits. In general, the system is exposed to extremely severe disturbances, much higher than it is likely to encounter in the normal operation, to evaluate the controller's performance under adverse conditions.

(a) Nutation damping

Figure 3.4 summarizes the influence of the controller gains μ_i, ν_i on the response. In general, an increase in μ_i provides an overdamped character to the system (Figures 3.4a and b) while a corresponding increase in ν_i for a given μ_i results in oscillations suggesting a reduction in damping (Figures 3.4a and c). The existence of an optimum choice of controller gains for a set of given system parameters is thus apparent. This is indicated in Figure 3.4d.

The effects of the satellite inertia parameter I and the spin parameter σ, presented in Figure 3.5 suggest that short, disc-like satellites (I = 1.5) withstand and damp a given disturbance relatively better than long, slender satellites (I = 0.5). It is of interest to point out that here the value of J, representing the ratio of the axial inertias of the platform and the satellite, is taken as 0.5. The analyses with J varying from 0.25 to 0.75 showed the system response to remain virtually unaffected. This is

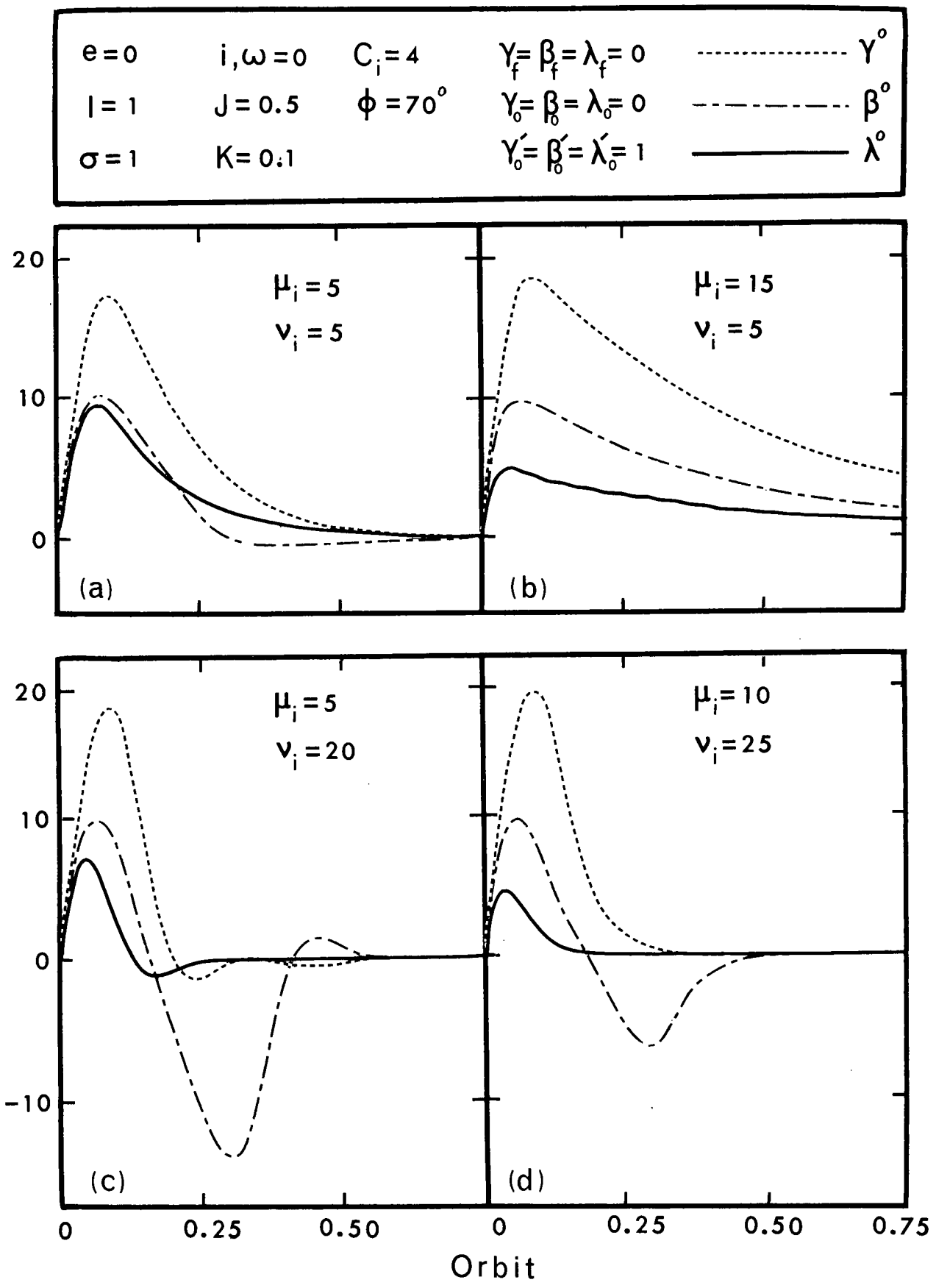

Figure 3.4 Influence of the solar controller gains μ_i, ν_i on the response

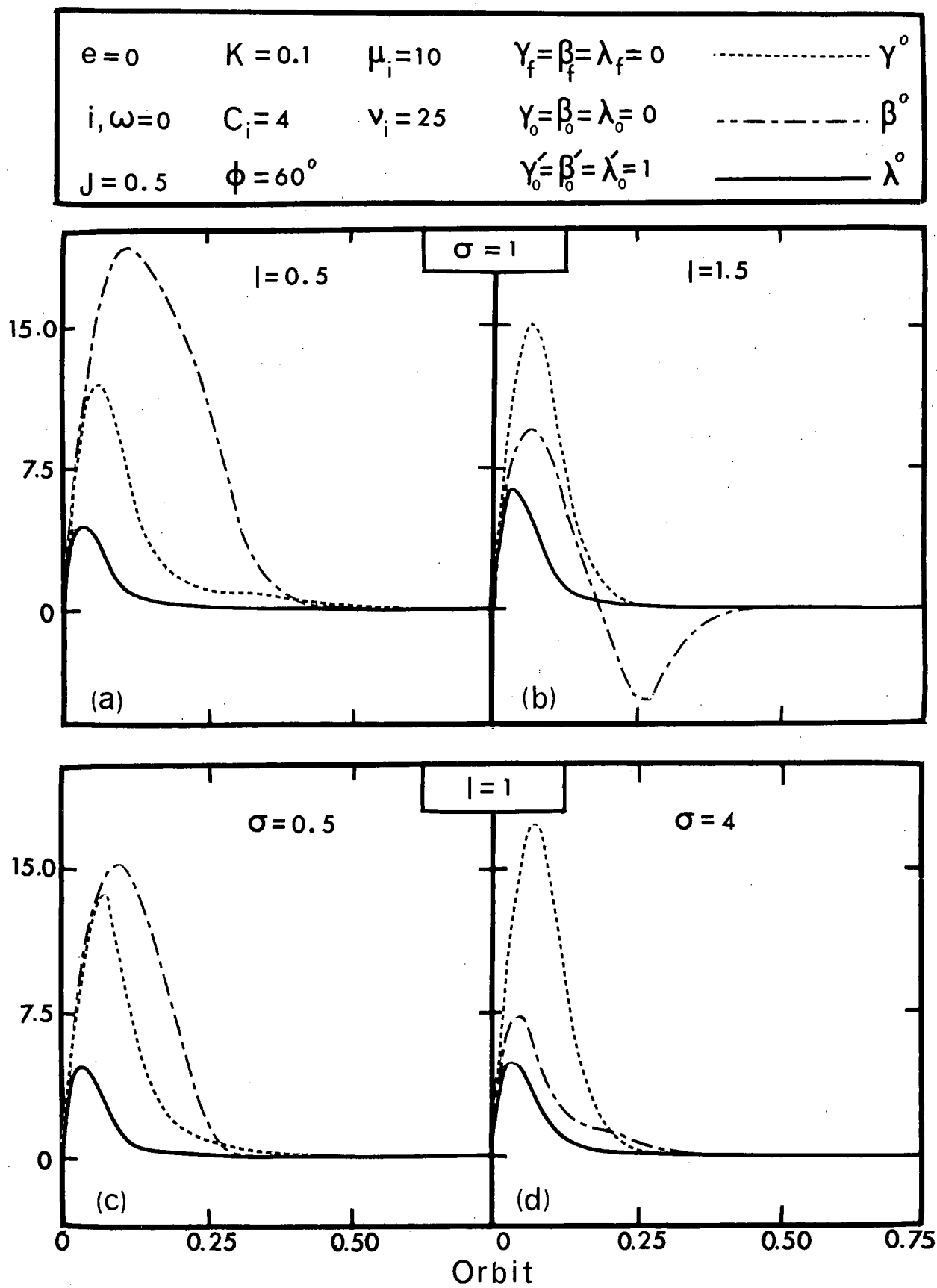

Figure 3.5 Damped response as affected by satellite inertia and spin parameters

understandable as large J makes it more amenable to controller corrections. The effect of the spin parameter σ was also found to be relatively insignificant. This is to be expected as the natural stiffness of the system, to which the spin parameter contributes, is largely provided by the controller gain ν_i (Figures 3.5c and d).

Figure 3.6 shows the influence of the solar parameters C_i and aspect angle ϕ on the controller performance. The limitation imposed by C_i on the maximum allowable control moments is clearly reflected in the response plots (Figures 3.6a and b). Note that an increase in C_i results in an overall improvement of the transient performance of the system. However, there is a restriction as to the maximum attainable values for C_i as imposed by the control plate areas and their moment arms.

The relative position of the sun (ϕ) affects the response in the γ and β degrees of freedom through the corresponding change in the available control moment. Thus roll and yaw attain different relative amplitudes in an orbit, however, their damping time remains essentially unaffected (Figures 3.6c and d).

The performance of the controller in an eccentric orbit remains essentially the same except for a steady state limit cycle appearing in the λ degree of freedom due to the periodic forcing function dependent on e (Equation 3.8c). This is indicated in Figures 3.7a and b, where the

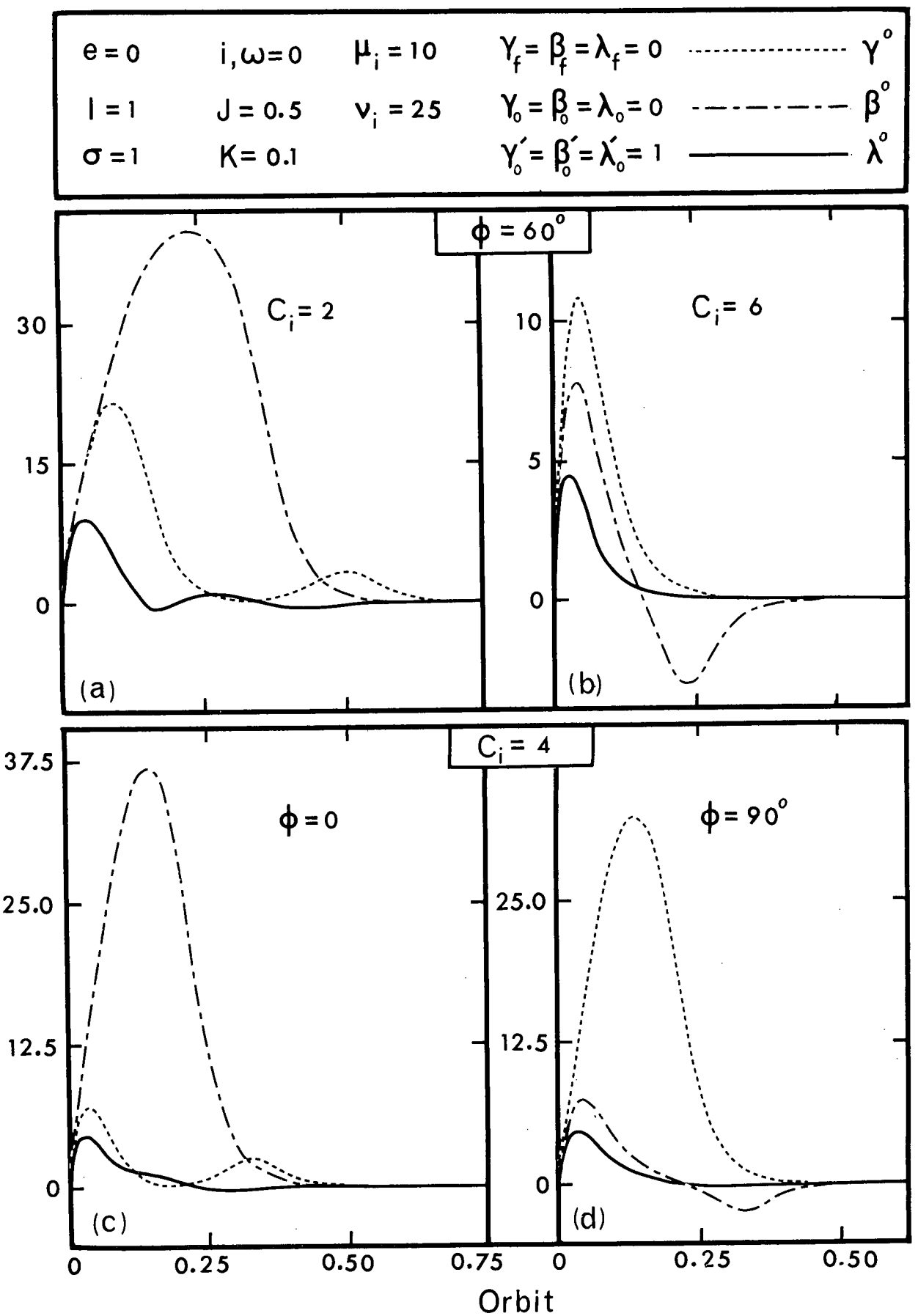

Figure 3.6 Effect of solar parameters and solar aspect angle on the damped response

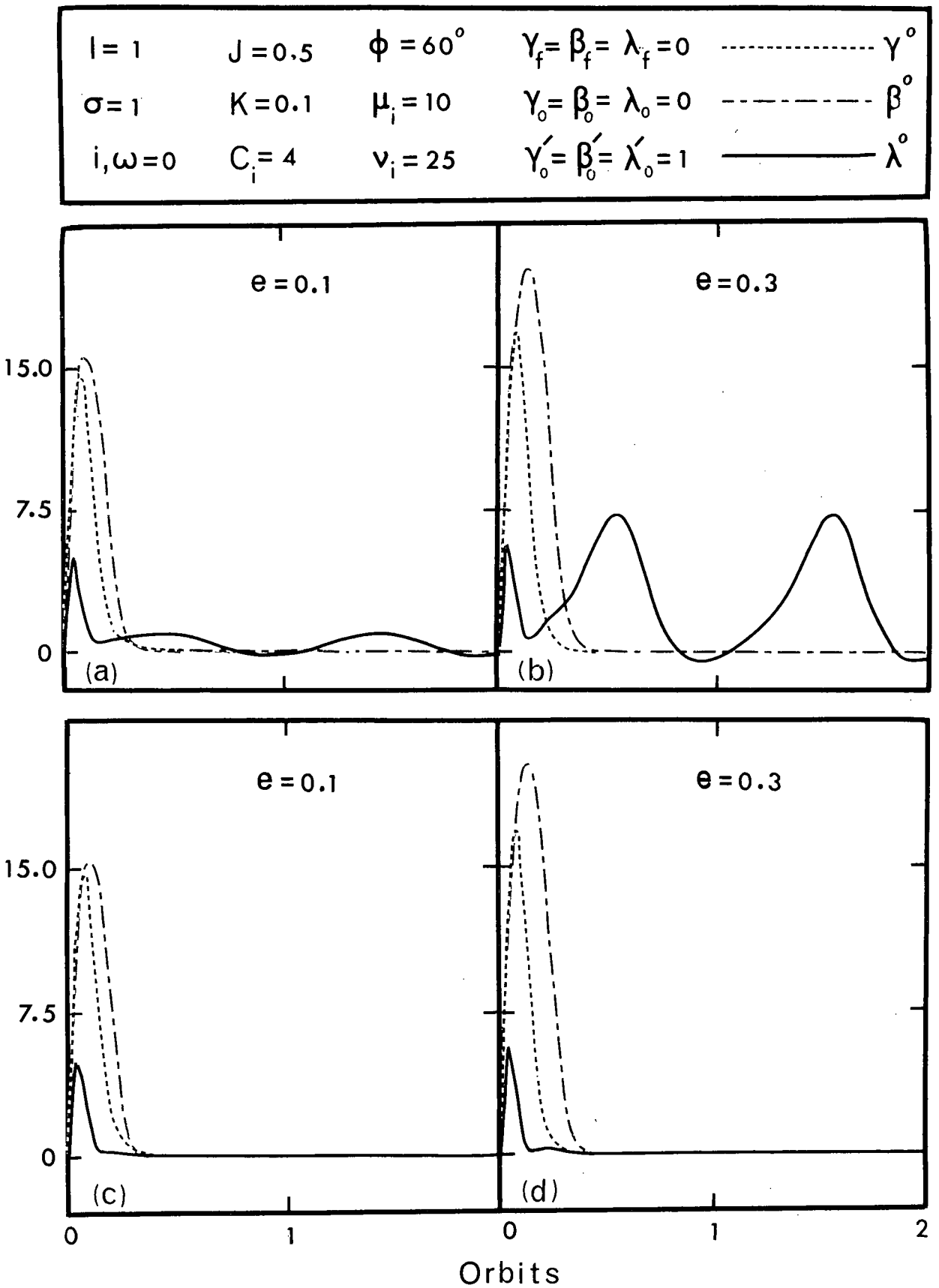

Figure 3.7 Response plot showing limit cycle oscillations in eccentric orbits and their removal through the modified control function

roll and yaw motions damp out quite quickly but the platform pitch persists as a limit cycle. The sustained oscillation of the platform would, in general, be highly undesirable. Fortunately, it can be eliminated using a modified control relation for Q_λ sensitive to the eccentricity induced disturbance,

$$\lambda_c = (1/\nu_\lambda)[-2e\sin\theta/(1+e\cos\theta)+\{(K/JI)(1+e)^{3/2}/(1+e\cos\theta)^2\}\times \{1-(\sigma+1)(1+e)^2/(1+e\cos\theta)^2\}] \qquad (3.15c)'$$

Figures 3.7c and d illustrate the effectiveness of the modified control relation in eliminating the limit cycle.

The information presented so far pertains to orbital motion in the plane of the ecliptic (i = 0). Of course, depending upon the mission, the orbital plane would be at an angle to the ecliptic. A systematic study showed the effect of i to be confined to local changes in response character without significantly altering the overall control performance. The plots in Figures 3.8a and b substantiate this conclusion.

(b) Rotor spin decay

The present analysis considers the rotor (body I) to have a constant average spin rate. Apparently, this would be achieved through some active energy source. However, the influence of possible rotor spin decay on the librational

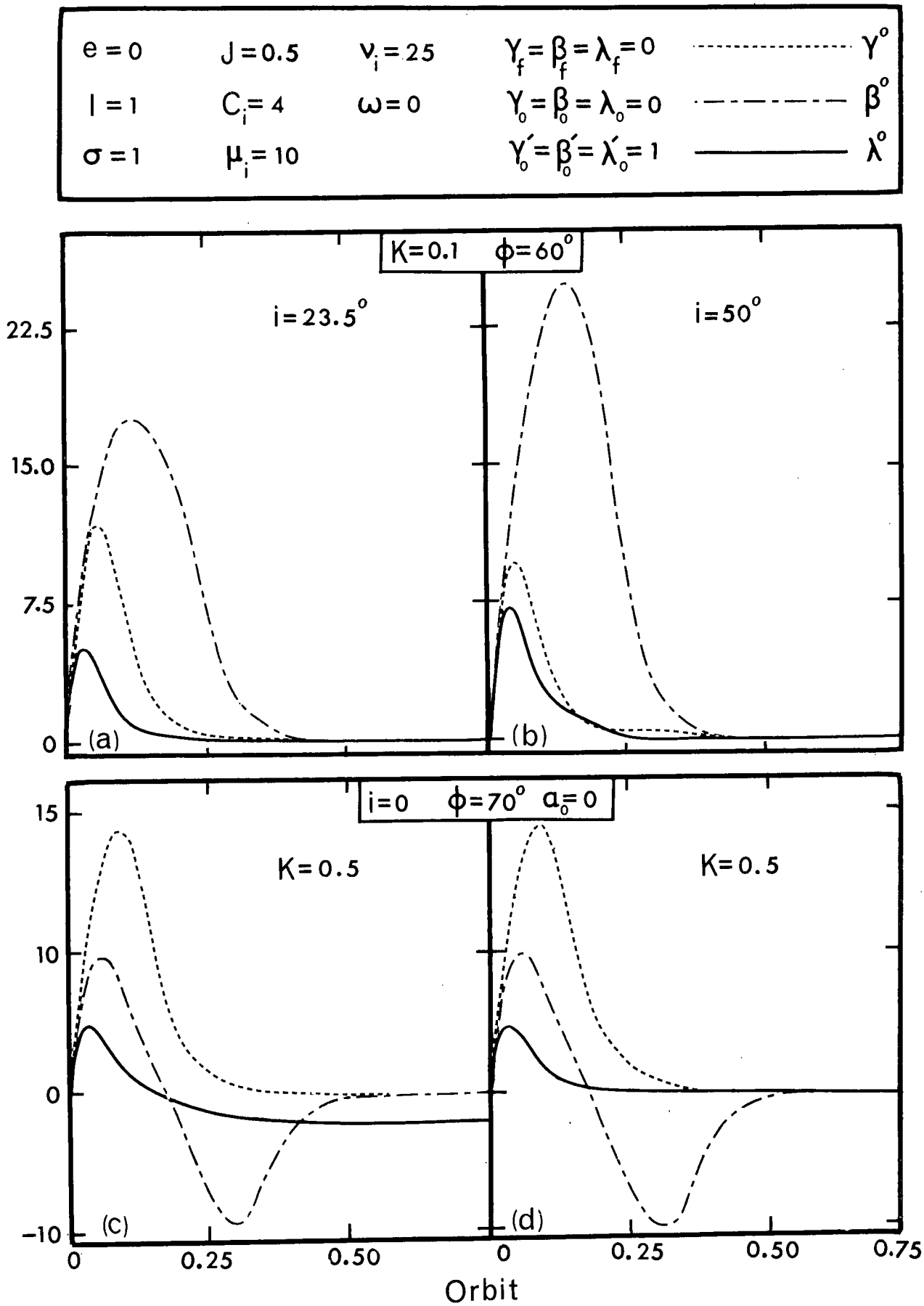

Figure 3.8 Response as affected by: (a,b) orbital inclination from the ecliptic; (c) rotor spin decay (d) modified control function

response of the system would be appropriate to explore. Although α still remains a cyclic coordinate, and hence the first integral is available, it is not possible to eliminate the rotor spin degree of freedom from the rest of the equations of motion. Thus one is faced with the solution of a 7th order system (as against the 6th order in the previous case). As can be anticipated, the roll and yaw motions damp out as before, coupling with the α degree of freedom being weak. However, the platform pitch angle λ tends to drift away from its preferred orientation λ_f (Figure 3.8c).

This does not reflect in any way a limitation on the capability of the controller but failure on our part to exploit it fully. The validity of this observation becomes quite apparent when one examines the modified pitch equation in the presence of dissipation,

$$\lambda'' - \gamma'' \sin\beta - \{2e\sin\theta/(1+e\cos\theta)\}(\lambda' - \gamma'\sin\beta + \cos\beta\cos\gamma)$$

$$-\beta'\gamma'\cos\beta - \gamma'\cos\beta\sin\gamma - \beta'\cos\gamma\sin\beta + (K/JI)\times$$

$$\{(1+e)^{3/2}/(1+e\cos\theta)^2\}(\lambda' - \alpha') = Q_\lambda \qquad (3.8c)'$$

Note the dynamic coupling between the rotor and the platform. On the other hand, the control relation for Q_λ (Equation 3.15c) does not involve α' explicitly. Thus the controller's potential to account for the rotor spin decay is not utilized. The situation can easily be

corrected by modifying the control function as indicated,

$$Q_\lambda = -\mu_\lambda \lambda' - a(\theta)\alpha' - \nu_\lambda(\lambda - \lambda_c) \qquad (3.15c)''$$

where

$$a(\theta) = (K/JI)(1+e)^{3/2}/(1+e\cos\theta)^2$$

$$\lambda_c = -(1/\nu_\lambda)(2e\sin\theta)/(1+e\cos\theta)$$

A typical system response using this modified control function is presented in Figure 3.8d.

Implication of this analysis is rather far reaching. It is no longer necessary to maintain the rotor spin rate from attitude dynamics considerations as the controller is able to provide sufficient torque irrespective of the spin rate. The system thus has a truly semi-passive character promising an increased satellite life-span.

(c) Attitude control

The controller provides an interesting possibility of changing the satellite's preferred orientation in orbit. This is accomplished by using the position control parameters γ_c, β_c and λ_c in accordance with the desired equilibrium configuration γ_f, β_f, and λ_f. As an illustration, for a static equilibrium of the satellite in a circular orbit, Equations (3.8) in conjunction with Equations (3.15) lead to

$$\gamma_c = (1/\nu_\gamma)[(\sin\gamma_f/\cos\beta_f)\{(1-J)I(\sigma+1) + JI\cos\beta_f\cos\gamma_f\}+(3I-4)\sin\gamma_f\cos\gamma_f] + \gamma_f \quad (3.19a)$$

$$\beta_c = (1/\nu_\beta)[\cos\gamma_f\sin\beta_f\{(1-J)I(\sigma+1)+(JI-1)\cos\beta_f\cos\gamma_f\} -3(I-1)\sin^2\gamma_f\sin\beta_f\cos\beta_f] + \beta_f \quad (3.19b)$$

$$\lambda_c = (1/\nu_\lambda)[(K/JI)\{\cos\beta_f\cos\gamma_f-\sigma-1\}] + \lambda_f \quad (3.19c)$$

Note that in this particular case of e = 0, the position control parameters are fixed once the final orientation is specified. On the other hand, for the case of an eccentric orbit, the parameters depend, in addition, on the satellite position in the orbit. Figure 3.9 illustrates the versatility of the semi-passive controller in achieving arbitrary orientations in space, for both circular and elliptic orbits. This suggests an exciting possibility for a space vehicle to extend its range of applicability and undertake diverse missions.

(d) Illustrative example

It was decided to demonstrate the effectiveness of the concept through a preliminary attitude dynamics study of the two well-known satellites, INTELSAT IV and Anik, when provided with the proposed controller. Appropriate

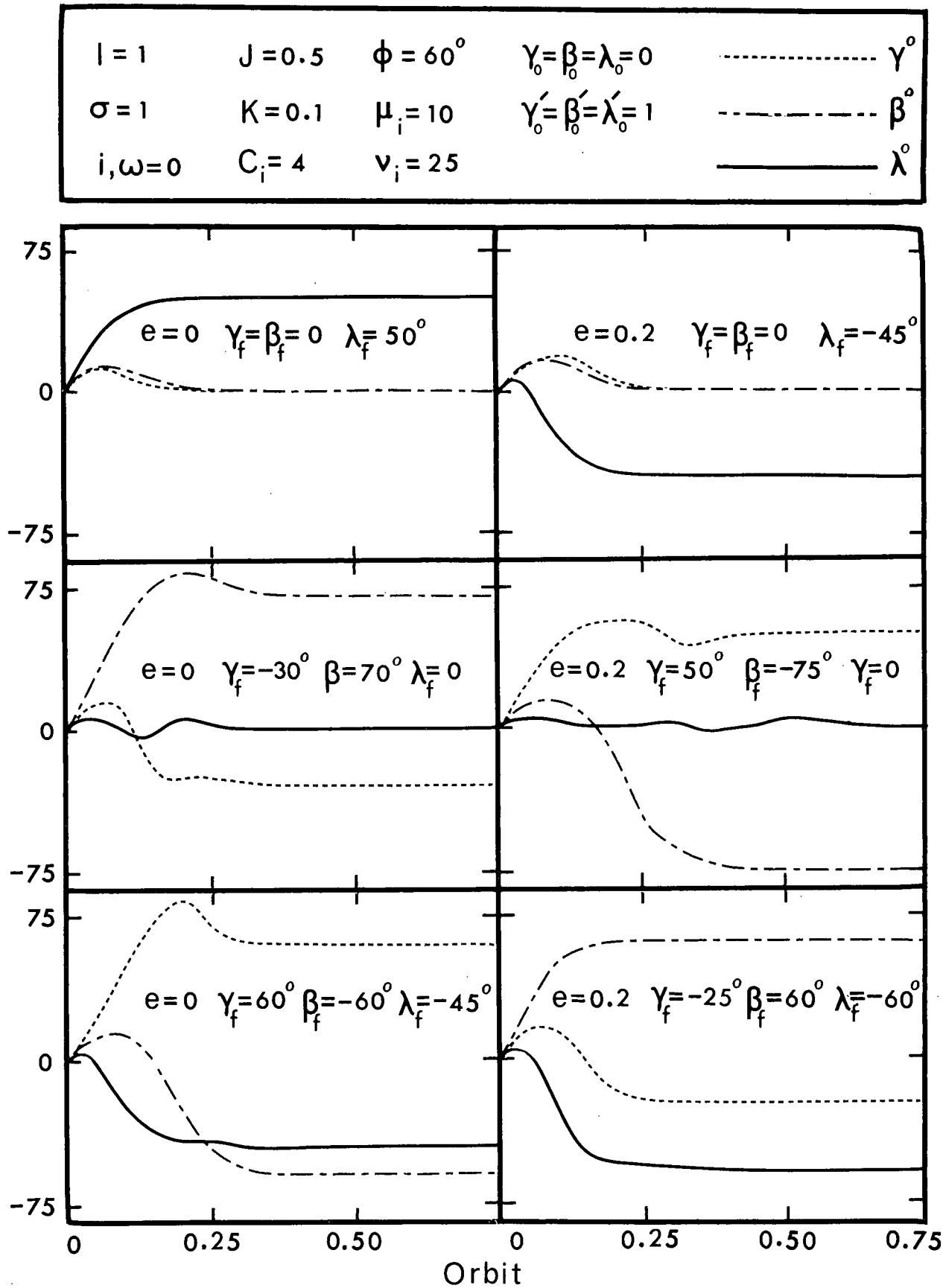

Figure 3.9 Effectiveness of the solar controller in achieving arbitrary orientations of the satellite

geometrical and inertia properties were assigned. As seen before, it is no longer necessary to spin a satellite for attitude control. However, nominal value of $\sigma = 1$ was taken to account for possible spin introduced from other considerations, e.g., temperature control. The solar parameter value of $C_i \simeq 2$ for INTELSAT IV can be obtained with control plate areas $A_i = 3$ ft^2 and moment arms $\varepsilon_i = 5$ ft. Similarly, $C_i \simeq 5$ for Anik may be achieved with plate areas $A_i = 1.2$ ft^2 and moment arms $\varepsilon_i = 5$ ft. Subjecting the satellites to a disturbance equivalent to that imparted by micrometeorite impacts over 24 hrs, which represents an enormous magnification of the real situation, gives[80] $-0.05 \leq \gamma_o', \beta_o', \lambda_o' \leq 0.05$. It is apparent (Figure 3.10) that the controller is able to damp such a severe disturbance quite effectively with the maximum deviation from the preferred orientation of less than 0.25°. The figure also shows the controller's effectiveness in achieving specified spatial orientations.

3.2 Improvement of Controller Design

Potential of the concept having been established, attention is next directed at rendering it more efficient and structurally more attractive. As the solar controller was found to be quite effective even in the absence of any spin, the case of a nonspinning satellite is now considered.

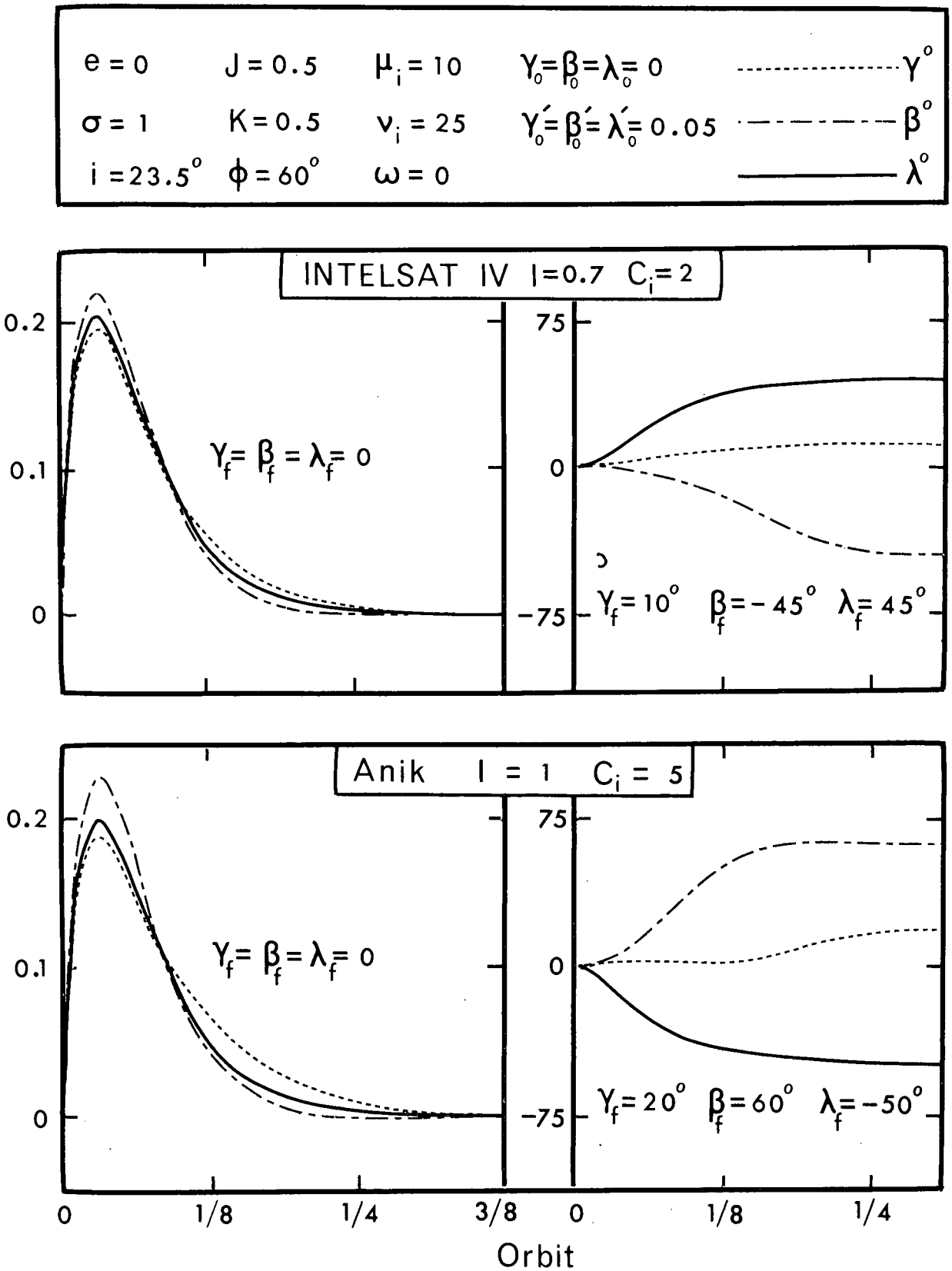

Figure 3.10 Projected controller performance in achieving nutation damping and attitude control of INTELSAT IV and Anik satellites

3.2.1 Equations of motion

The governing equations of motion follow directly from Equations (3.8) on substituting J = 1, K = 0:

$$\gamma'' - 2\beta'(\gamma'\tan\beta - \cos\gamma) - I(\lambda' - \gamma'\sin\beta + \cos\beta\cos\gamma)(\beta' - \sin\gamma)\sec\beta + \{3(I-1)/(1+e\cos\theta) - 1\}\sin\gamma\cos\gamma - \{2e\sin\theta/(1+e\cos\theta)\} \times (\gamma' + \cos\gamma\tan\beta) = Q_\gamma \qquad (3.20a)$$

$$\beta'' - \gamma'\cos\gamma - \{2e\sin\theta/(1+e\cos\theta)\}(\beta' - \sin\gamma) + \{I(\lambda' - \gamma'\sin\beta + \cos\beta\cos\gamma) + (\gamma'\sin\beta - \cos\beta\cos\gamma)\}(\gamma'\cos\beta + \cos\gamma\sin\beta) - 3\{(I-1)/(1+e\cos\theta)\}\sin^2\gamma\sin\beta\cos\beta = Q_\beta \qquad (3.20b)$$

$$\lambda'' - \gamma''\sin\beta - \{2e\sin\theta/(1+e\cos\theta)\}(\lambda' - \gamma'\sin\beta + \cos\beta\cos\gamma) - \beta'\gamma'\cos\beta - \gamma'\cos\beta\sin\gamma - \beta'\cos\gamma\sin\beta = Q_\lambda \qquad (3.20c)$$

3.2.2 Development of controller models

Controllers capable of providing general librational damping and three-axis attitude control require the three degrees of freedom of the system (γ, β and λ) to be controlled independently. A versatile solar controller configuration would thus result in generalized forces Q_i as functions of at least three control variables, δ_i. Of various configurations satisfying this requirement, only those permitting relatively easier solution for the control variables with a given set of Q_i would be practically feasible.

At the outset, it appears instructive to study the control moments generated by a single plate P with its support arm gimballed at the point T on the axis of symmetry of the satellite (Figure 3.11a). The arm supporting the plate is allowed rotations α_1 and α_2 while the plate can turn about it through an angle δ measured from the plane TSW. Following the procedure discussed earlier in detail, the generalized forces Q_i due to solar radiation pressure can be written as:

$$Q_\gamma = -\bar{C}E(\theta)|\cos\xi|\cos\xi\{(h/\varepsilon+\sin\alpha_2)(\sin\alpha_1\cos\delta+\cos\alpha_1\sin\alpha_2\sin\delta) +\cos\alpha_1\cos^2\alpha_2\sin\delta\}/(I_y\cos\beta) \quad (3.21a)$$

$$Q_\beta = -\bar{C}E(\theta)|\cos\xi|\cos\xi\{(h/\varepsilon)(\cos\alpha_1\cos\delta-\sin\alpha_1\sin\alpha_2\sin\delta) +\cos\alpha_1\sin\alpha_2\cos\delta-\sin\alpha_2\sin\delta\}/I_y \quad (3.21b)$$

$$Q_\lambda = \bar{C}E(\theta)|\cos\xi|\cos\xi\cos\alpha_2\cos\delta/I_x \quad (3.21c)$$

where

$$\cos\xi = -u_i\cos\alpha_2\sin\delta+u_j(\sin\alpha_1\cos\delta+\cos\alpha_1\sin\alpha_2\sin\delta) -u_k(\cos\alpha_1\cos\delta-\sin\alpha_1\sin\alpha_2\sin\delta) \quad (3.22)$$

As is evident, each of the Q_i depends on the variables α_1, α_2 and δ. The transcendental nature of these functions makes it difficult to establish the bounds

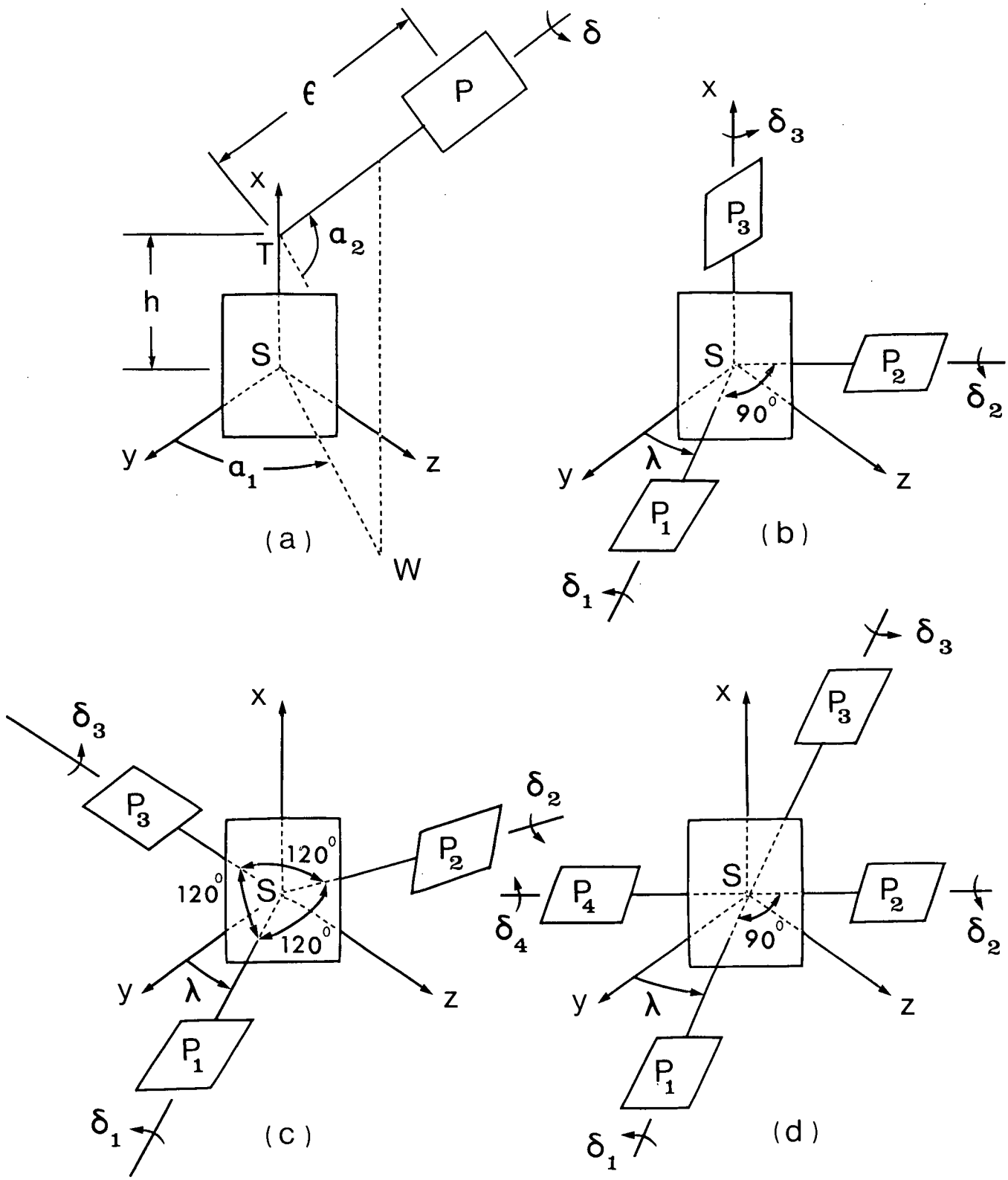

Figure 3.11 Development of solar controller configurations

$|Q_\gamma|_{max}$, $|Q_\beta|_{max}$ and $|Q_\lambda|_{max}$ within which Equations (3.21) possess real solutions for α_1, α_2 and δ. It is, therefore, necessary to consider modifications which would reduce these equations to a more amenable form.

A logical approach seems to lie in devising configurations where some of the three variables become constants. The best choice, from a practical viewpoint, would be to remove the gimbal and fix the axis of the plate to the satellite body, thereby rendering α_1 and α_2 constants. This reduction in the number of control variables, of course, would have to be compensated by a corresponding increase in the number of plates rotating about body-fixed axes. Numerous controller configurations were considered to this end, however, for conciseness, only a few are discussed here.

Figure 3.11b shows an arrangement of three plates $P_i (i = 1,2,3)$ rotatable about three mutually perpendicular body-fixed axes. The rotations $\delta_i (i = 1,2)$ are measured from the yz-plane while δ_3 is measured from the xy-plane. The evaluation of the generalized forces Q_i resulting from this configuration may be carried out either from the first principles, or, by appropriate substitutions for α_1, α_2 and δ for each plate into Equations (3.21). These are found to be:

$$Q_\gamma = E(\theta)\{\bar{C}_1|\cos\xi_1|\cos\xi_1\cos\delta_1\cos\lambda-\bar{C}_2|\cos\xi_2|\cos\xi_2\cos\delta_2\sin\lambda$$
$$+\bar{C}_3|\cos\xi_3|\cos\xi_3\sin\delta_3\}/(I_y\cos\beta) \qquad (3.23a)$$

$$Q_\beta = E(\theta)\{-\bar{C}_1|\cos\xi_1|\cos\xi_1\cos\delta_1\sin\lambda-\bar{C}_2|\cos\xi_2|\cos\xi_2\cos\delta_2\cos\lambda$$
$$+\bar{C}_3|\cos\xi_3|\cos\xi_3\cos\delta_3\}/I_y \qquad (3.23b)$$

$$Q_\lambda = E(\theta)\{\bar{C}_1|\cos\xi_1|\cos\xi_1\sin\delta_1+\bar{C}_2|\cos\xi_2|\cos\xi_2\sin\delta_2\}/I_x \qquad (3.23c)$$

where

$$\cos\xi_1 = u_i\cos\delta_1+(u_j\sin\lambda-u_k\cos\lambda)\sin\delta_1$$

$$\cos\xi_2 = u_i\cos\delta_2+(u_j\cos\lambda+u_k\sin\lambda)\sin\delta_2$$

$$\cos\xi_3 =-u_j\sin\delta_3+u_k\cos\delta_3 \qquad (3.24)$$

It may be observed that the dependence of the generalized forces $Q_i(i = \gamma,\beta,\lambda)$ on the control variables $\delta_i(i = 1,2,3)$ is quite involved and the system of Equations (3.23) does not appear to lend itself to an analytical treatment. Figures 3.11c and d show alternative arrangements. An analysis of the generalized force expressions, which are essentially of the same nature as Equations (3.23), showed them to present similar difficulties.

Following the approach discussed in preceding sections, the controller configuration shown in Figure 3.12 is finally arrived at. The performance of this model is investigated in detail as both the hardware and software requirements are relatively simple to implement. It consists of four plates $P_i (i = 1,2,3,4)$ with their support arms forming a crisscross. The plates P_1 and P_2 rotate about the axis of symmetry of the satellite, the rotations δ_1 and δ_2 being measured from the xy-plane. The plates P_3 and P_4 rotate about arms, lying in the plane perpendicular to the axis of symmetry, with the rotations δ_3 and δ_4 measured from the yz-plane. The moments generated by this arrangement are found to be:

$$Q_\gamma = E(\theta)[C_1|\cos\xi_1|\cos\xi_1\sin\delta_1 - C_2|\cos\xi_2|\cos\xi_2\sin\delta_2 + I\{C_3|\cos\xi_3|\cos\xi_3\cos\delta_3 - C_4|\cos\xi_4|\cos\xi_4\cos\delta_4\}\cos\lambda]\sec\beta \quad (3.25a)$$

$$Q_\beta = E(\theta)[C_1|\cos\xi_1|\cos\xi_1\cos\delta_1 - C_2|\cos\xi_2|\cos\xi_2\cos\delta_2 + I\{-C_3|\cos\xi_3|\cos\xi_3\cos\delta_3 + C_4|\cos\xi_4|\cos\xi_4\cos\delta_4\}\sin\lambda] \quad (3.25b)$$

$$Q_\lambda = E(\theta)\{C_3|\cos\xi_3|\cos\xi_3\sin\delta_3 + C_4|\cos\xi_4|\cos\xi_4\sin\delta_4\} \quad (3.25c)$$

where

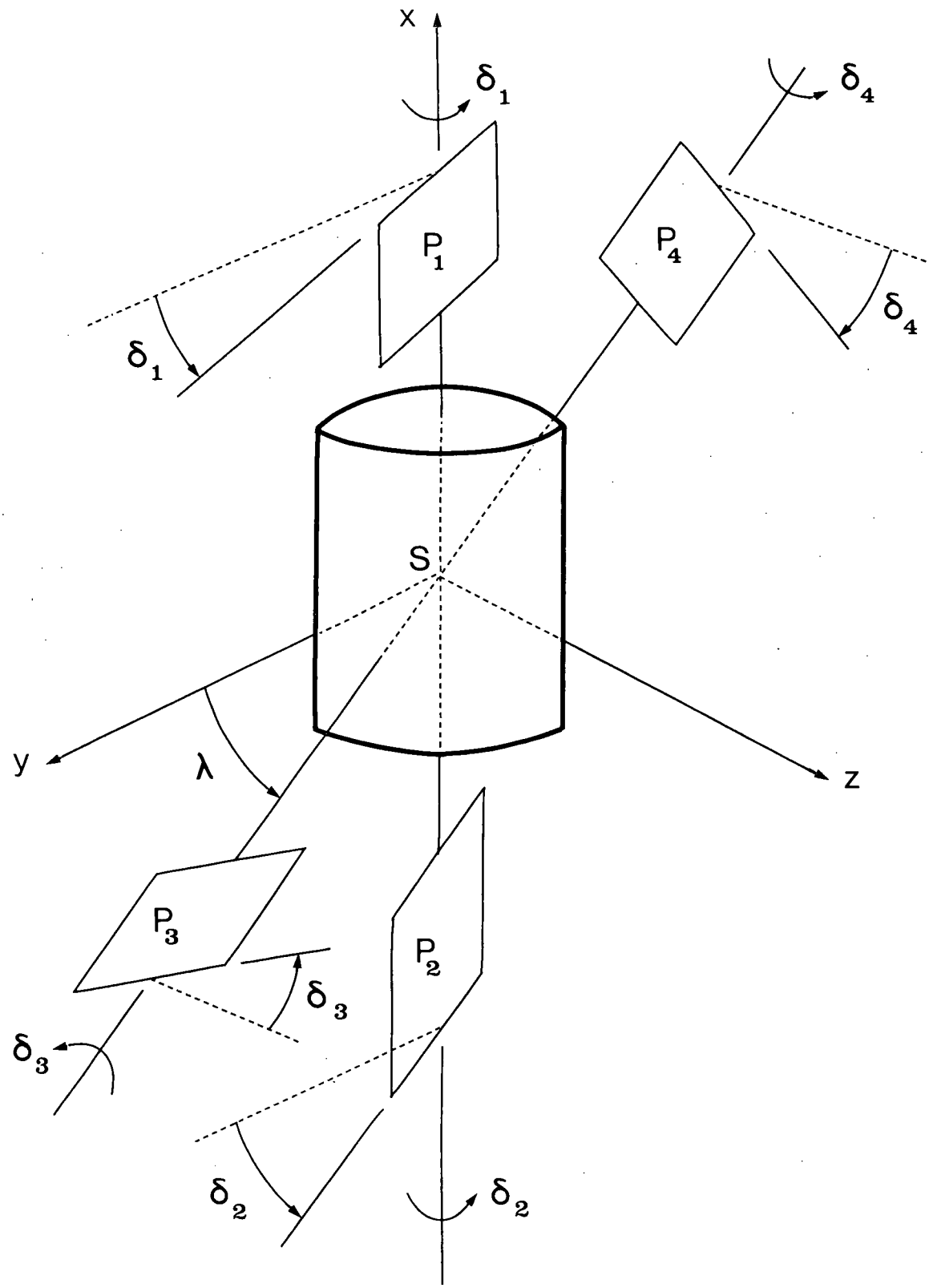

Figure 3.12 Proposed four-plate solar controller model

$$\cos\xi_i = -u_j\sin\delta_i + u_k\cos\delta_i, \quad i = 1,2$$

$$\cos\xi_3 = u_i\cos\delta_3 + (u_j\sin\lambda - u_k\cos\lambda)\sin\delta_3$$

$$\cos\xi_4 = u_i\cos\delta_4 - (u_j\sin\lambda - u_k\cos\lambda)\sin\delta_4 \qquad (3.26)$$

and the solar parameters are defined as,

$$C_i = (2\rho p_o R_p^3/\mu I_y)A_i\varepsilon_i, \quad i = 1,2$$

$$= (2\rho p_o R_p^3/\mu I_x)A_i\varepsilon_i, \quad i = 3,4 \qquad (3.27)$$

Although Equations (3.25) indicate a rather complex dependence of Q_i on the control variables, it is possible to obtain relatively simple analytical solutions for δ_i (i = 1,2,3,4) through a judicious control strategy.

3.2.3 Control strategy

An inspection of Equations (3.25) indicates that the plates P_1 and P_2 do not produce any moment in the pitch (λ) degree of freedom, hence this control will have to be accomplished through plates P_3, P_4. Ideally, one would like their operation to be free of coupling roll-yaw moments. Fortunately, this can be achieved through a simple control law:

$$\delta_3 = \pi/2, \quad \delta_4 = \text{'off'}$$

or

$$\delta_3 = \text{'off'}, \quad \delta_4 = \pi/2, \tag{3.28}$$

the option being dicated by the sign required of Q_λ. δ_i = 'off' implies its rendering the corresponding $\cos\xi_i = 0$, i.e., physically, the sun-line would lie in the plane of the plate. A pure pitch moment thus produced has the magnitude

$$\bar{Q}_\lambda = E(\theta)C_{3,4}(u_j\sin\lambda - u_k\cos\lambda)^2 \tag{3.29}$$

where $C_3 = C_4 = C_{3,4}$ is assumed for convenience.

In order to provide the roll-yaw moments controlling the orientation of the axis of symmetry of the satellite, plates P_1 and P_2 may be operated simultaneously or one at a time with the other 'off'. The latter mode of operation, resulting in greater transverse torques, is considered here. The generalized forces in the roll and yaw degrees of freedom now take the form:

$$Q_\gamma = \pm E(\theta)C_i\left|-u_j\sin\delta_i + u_k\cos\delta_i\right|(-u_j\sin\delta_i + u_k\cos\delta_i)\sin\delta_i\sec\beta \tag{3.30a}$$

$$Q_\beta = \pm E(\theta)C_i\left|-u_j\sin\delta_i + u_k\cos\delta_i\right|(-u_j\sin\delta_i + u_k\cos\delta_i)\cos\delta_i \tag{3.30b}$$

where the plus and minus signs correspond to plates P_1 and P_2, respectively. Note that the moments Q_γ and Q_β are coupled through the plate rotation angle δ_i.

The next step would be to maximize the available moments consistent with the control requirements of appropriate sign. There are several aspects to this problem. One approach is to maximize the total transverse torque, $(Q_\gamma^2\cos^2\beta+Q_\beta^2)^{1/2}$. Unfortunately, the resulting critical δ_i (orienting the control plate so as to maximize $\cos\xi_i$) yields only two of the four possible combinations of the roll and yaw moment directions:

$$Q_\gamma,\ Q_\beta\colon\ +\ +,\ +\ -,\ -\ +,\ -\ -$$

An alternate procedure would be to maximize $|Q_\gamma|$ and $|Q_\beta|$, in turn, with respect to δ_i. the maximum value of $|Q_\gamma| = Q_\gamma^m$ is found to occur at

$$\delta_{im} = \pi/2+\tan^{-1}[\{-3u_j\pm(9u_j^2+8u_k^2)^{1/2}\}/2u_k] \qquad (3.31a)$$

with the corresponding $|Q_\beta| = Q_\beta^c$ being given by Equation (3.30b) with $\delta_i = \delta_{im}$. Similarly, the maximum of $|Q_\beta| = Q_\beta^m$ occurs at

$$\delta_{im} = \tan^{-1}[\{3u_k\pm(9u_k^2+8u_j^2)^{1/2}\}/2u_j] \qquad (3.31b)$$

with the corresponding $|Q_\gamma| = Q_\gamma^c$ given by Equation (3.30a). The proper sign of the quantity within the square-root is determined from the coupling constraint imposed by Equations (3.30), i.e.,

$$\tan\delta_i = Q_\gamma \cos\beta / Q_\beta \tag{3.32}$$

A consideration of Equations (3.31a and b) indicates that in each case, the two values of δ_{im}, corresponding to the plus and the minus signs, lie in adjacent quadrants. Hence, one of them always satisfies the constraint relation (3.32). Thus use of the proper sign in the evaluation of δ_{im} (Equations 3.31) in conjunction with an appropriate choice of the plate P_1 or P_2 (Equations 3.30) enables the controller to provide all possible sign combinations of Q_γ and Q_β. Of the two admissible sets of moments, (Q_γ^m, Q_β^c) and (Q_γ^c, Q_β^m), the one resulting in a greater magnitude of the total torque to control the axis of symmetry of the satellite, i.e., $(Q_\gamma^2 \cos^2\beta + Q_\beta^2)^{1/2}$, is used.

For example, let the required control moments be $Q_\gamma > 0$ and $Q_\beta < 0$. As $\cos\beta$ is positive, $\tan\delta_i < 0$. Thus δ_i must lie either in the second or the fourth quadrant (Figure 3.13). Let the two values of δ_{im} as given by Equation (3.31a) be $(\delta_{im})_{a_1}$ and $(\delta_{im})_{a_2}$ as shown. Note that they have to be in adjacent quadrants as pointed out before. Let the δ_{im} corresponding to Equation (3.31b) be in the third and the fourth quadrants. Consistent with our require-

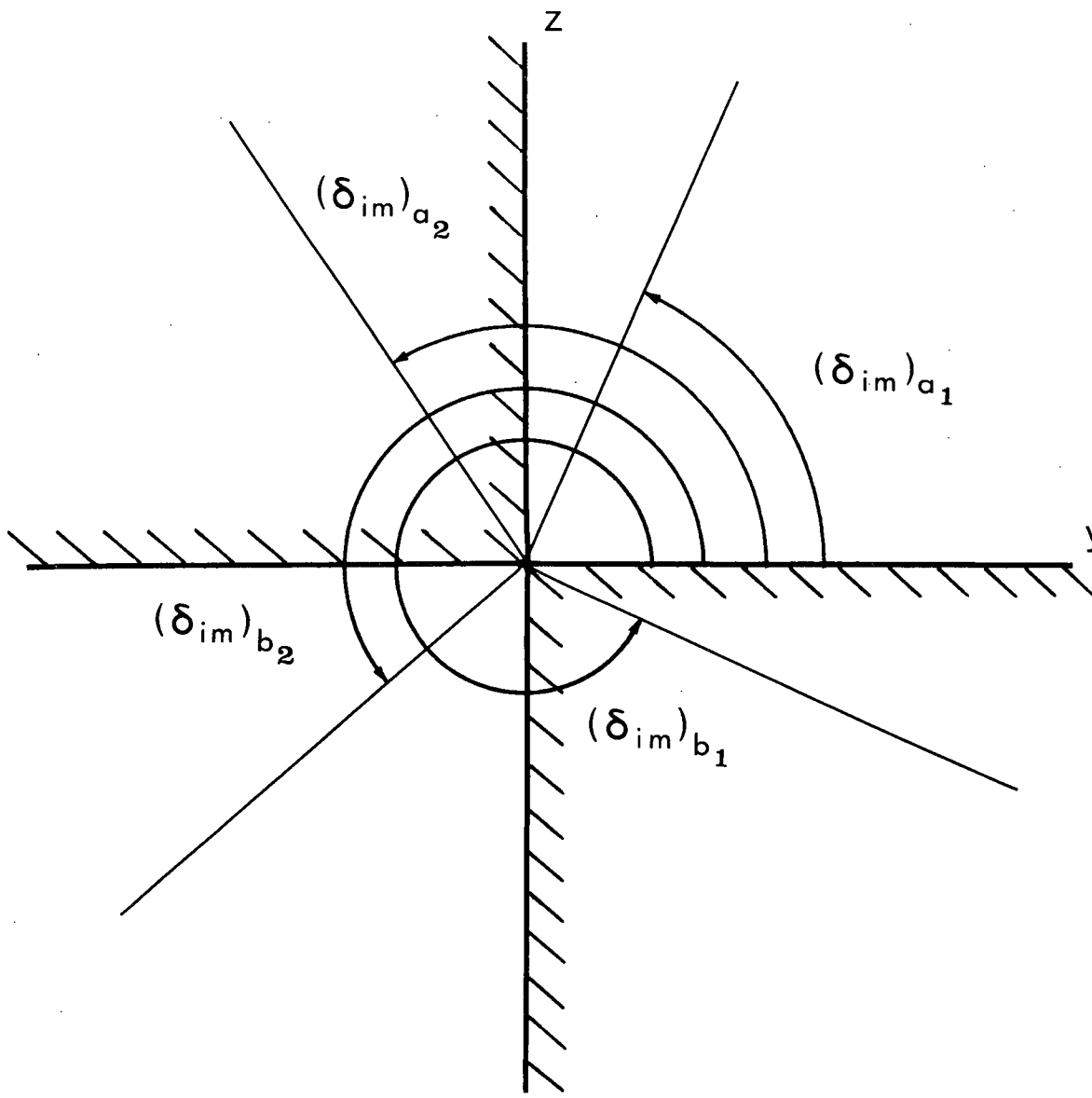

Figure 3.13 Quadrant constraint for plate rotation δ_i

ments, the admissible values are $(\delta_{im})_{a_2}$ and $(\delta_{im})_{b_1}$. Of these, the one resulting in a higher value of the total transverse torque is used in the analysis.

The control moments thus determined are applied in a bang-bang fashion in conjunction with linear displacement and velocity sensitive switching functions,

$$Q_i = -\bar{Q}_i \operatorname{sgn} S_i \tag{3.33}$$

where

$$S_i = i' + m(i-i_f), \quad i = \gamma,\beta,\lambda \tag{3.34}$$

$$\bar{Q}_\gamma = Q_\gamma^m,\ \bar{Q}_\beta = Q_\beta^c \text{ for } (Q_\gamma^{m^2}\cos^2\beta+Q_\beta^{c^2}) \geq (Q_\gamma^{c^2}\cos^2\beta+Q_\beta^{m^2})$$

$$\bar{Q}_\gamma = Q_\gamma^c,\ \bar{Q}_\beta = Q_\beta^m \text{ for } (Q_\gamma^{m^2}\cos^2\beta+Q_\beta^{c^2}) < (Q_\gamma^{c^2}\cos^2\beta+Q_\beta^{m^2})$$

and m represents the system gain, chosen according to some suitable criterion.

The control procedure may now be summarized as follows:

(i) sense the roll, yaw and pitch angles and rates, orbital position and the solar aspect angle;

(ii) determine the signs required of Q_i according to the switching criterion (Equations 3.33);

(iii) during pitch control, use ($\delta_3 = \pi/2$, δ_4 = 'off' or (δ_3 = 'off', $\delta_4 = \pi/2$) for $Q_\lambda/(u_j\sin\lambda - u_k\cos\lambda) \gtrless 0$, respectively (Equations 3.25c and 3.26).

(iv) for roll-yaw control, compute the four values of $\delta_i = \delta_{im}$ from Equations (3.31a and b) and of the two satisfying the quadrant constraint (3.32), choose the δ_i producing the greater resultant transverse torque. Substitute into Equation (3.30a or b) and select the plate to be operated through the sign required in the right hand side.

3.2.4 Results and discussion

As before, the response of the system is studied by numerically integrating the equations of motion (3.20) along with the control relations (3.33). Much smaller integration steps were required due to the bang-bang nature of the control law. A step size of 0.1° gave results of sufficient accuracy for the solar parameters $C_i \leq 5$. For cases with larger values of C_i, the step size had to be correspondingly decreased. The controller performance was evaluated in both circular and elliptic orbits and the influence of important system parameters investigated.

(a) Libration damping in circular orbits

Figure 3.14 summarizes the performance of the controller in damping the librational motion in circular orbits in the form of optimization plots for the controller gain m. It shows the variation of the damping time τ_d,

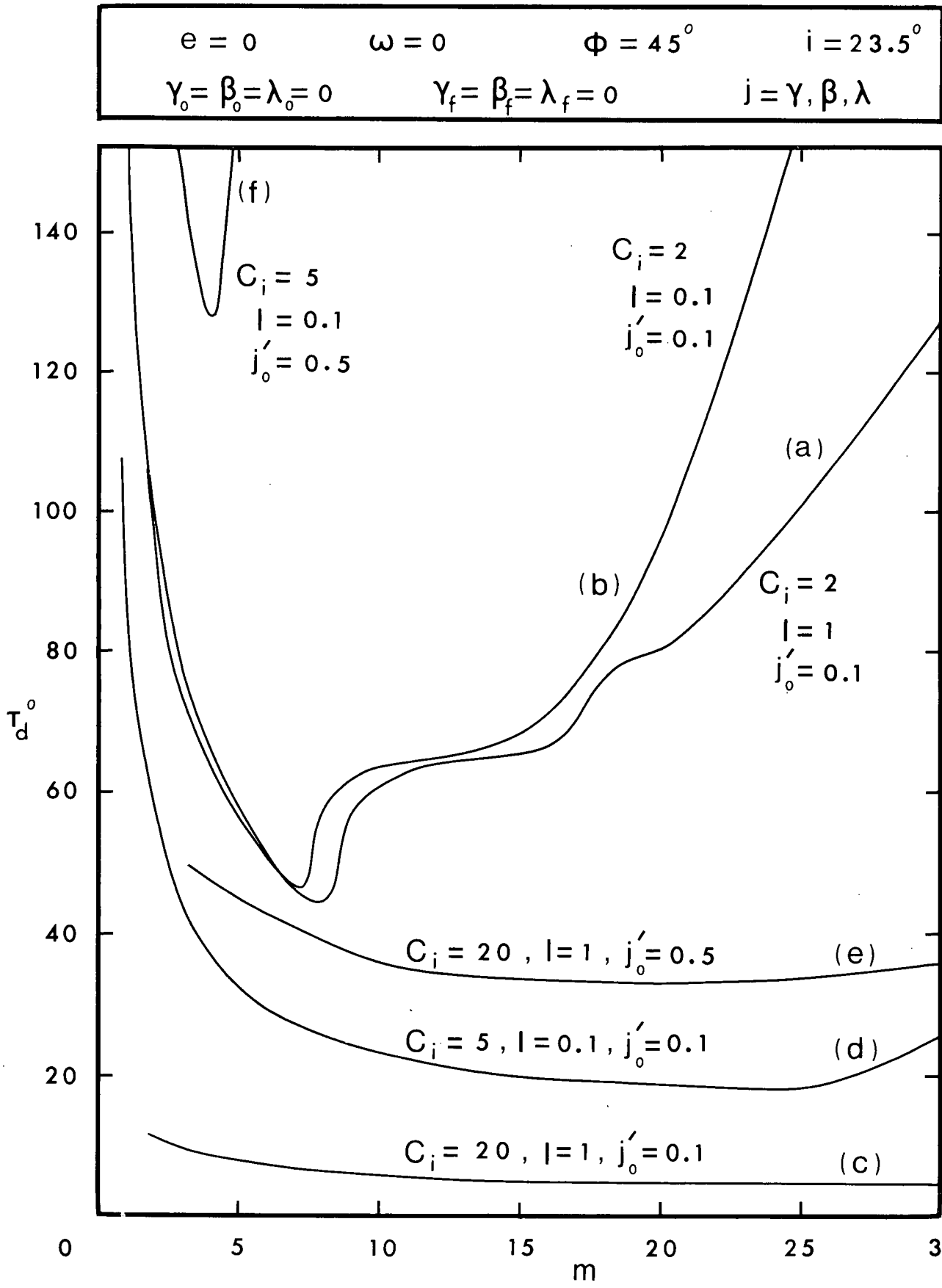

Figure 3.14 Optimization plots for the solar controller gain m

defined here as the time taken for all the three libration angles to settle within 0.1° of the final orientation, with the gain m for different combinations of system parameters and initial conditions. The plots, in general, indicate the existence of an optimum value of the system gain resulting in the least time of damping.

The influence of the satellite inertia parameter I on the performance of the controller is indicated by a comparison of curves (a) and (b). Despite the drastic change in the satellite mass distribution from pencil-like (I = 0.1) to spherical (I = 1), only a small variation in the optimum value of m and the general damping behaviour is observed. It may be pointed out here that curves (a) and (b) were obtained using a relatively small value of the solar parameters $C_i = 2$. For larger values of C_i, the effect of I was hardly perceivable. The effectiveness of the control system in libration damping of satellites with a wide variety of mass distributions is thus apparent.

The effect of the solar parameters C_i, characterizing the magnitude of the solar torques, is observed by comparing curves (a and c) and (b and d). An increase in C_i not only results in a substantial reduction in the damping time but renders the controller performance relatively insensitive to the system gain m as well.

A comparison of curves (d and f) and (c and e) shows the effect of the initial disturbances. An increase

in the initial conditions results in longer damping times as anticipated. In addition, for smaller values of C_i, the system performance shows a strong dependence on the controller gain m (curves d and f).

The influence of the apparent position of the sun, indicated by the solar aspect angle ϕ, and the perigee argument ω on the system behaviour was also studied. The results, however, showed local changes in the response character only, leaving the damping performance essentially unaffected.

Typical optimal responses for a satellite in an equatorial orbit are presented in Figure 3.15a. Even when subjected to severe impulsive disturbances in the roll, yaw and pitch degrees of freedom simultaneously, the controller is able to damp the satellite librations in a few degrees of orbital travel with the amplitudes remaining quite small.

(b) Libration damping in elliptic orbits

The effectiveness of the controller in damping the roll-yaw (γ, β) oscillations of the axis of symmetry of the satellite remained virtually unchanged in eccentric orbits. The pitch (λ) degree of freedom, however, executes a steady-state limit cycle (Figure 3.15b). These oscillations result due to the presence of the periodic forcing function dependent on e (Equation 3.20c) and the inability of the controller to generate sufficient torque to counter it at all times.

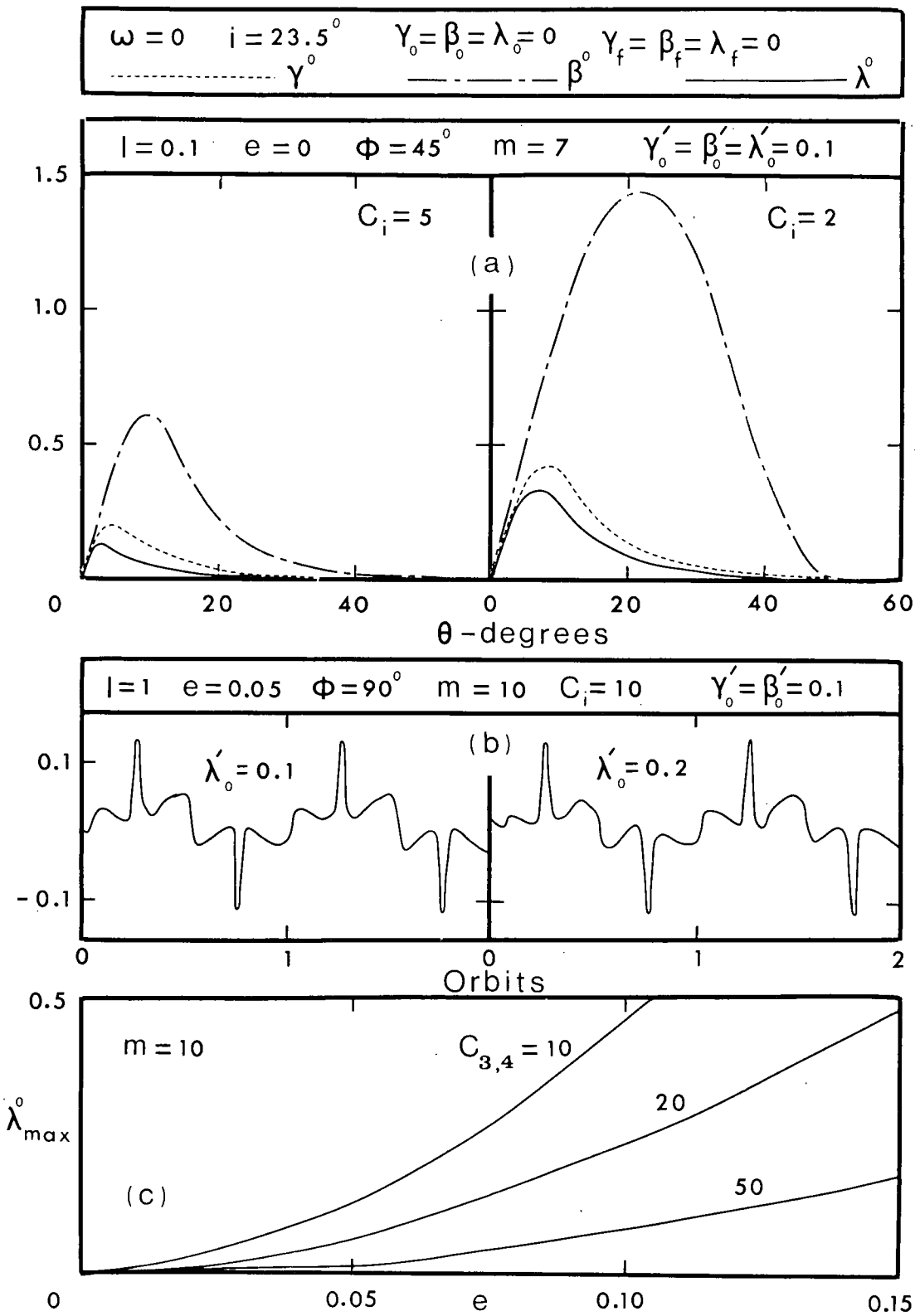

Figure 3.15 (a) Typical optimum response in circular orbits; (b) Limit cycle oscillation in elliptic orbits; (c) Variation of limit cycle amplitude with system parameters

From design considerations, it is of interest to investigate the limit cycle amplitude as a function of system parameters. Once the roll-yaw oscillations are completely damped, Equations (3.20a and b) are identically satisfied. Letting $\gamma = \gamma' = \beta = \beta' = 0$ and substituting from Equations (3.29 and 3.33) into Equation (3.20c), the governing equation for the pitch oscillations reduces to

$$\lambda'' - \{2e\sin\theta/(1+e\cos\theta)\}\lambda' = -C_{3,4}E(\theta) \times$$

$$(u_j\sin\lambda - u_k\cos\lambda)^2 \operatorname{sgn} S_\lambda + 2e\sin\theta/(1+e\cos\theta) \qquad (3.20c)'$$

The limit cycle oscillation being the steady-state solution of this equation, its amplitude may be expressed as

$$\lambda_{max} = f(C_{3,4}, e, m, \lambda_f, i, \omega, \phi) \qquad (3.36)$$

The largest amplitudes would result when the maximum magnitude of the eccentricity induced disturbance and the minimum (zero) magnitude of the pitch control torque occur simultaneously. The latter would physically correspond to the projection of the sun-line on the yz-plane becoming coincident with the axis about which plates P_3 and P_4 rotate. Note that such a situation would arise only twice a year for an earth satellite. Considering small e, the condition for worst limit cycle is given by

$$\tan\phi = (\tan\lambda_f \sin\omega - \cos\omega)\sec i/(\tan\lambda_f \cos\omega + \sin\omega) \qquad (3.37)$$

Figure 3.15c shows the variation of the pitch limit cycle amplitude with the orbital eccentricity for a range of values of the solar parameter $C_{3,4}$ under the most adverse situation. Even here, only moderate values of $C_{3,4}$ are required to limit the amplitude to a generally acceptable value.

(c) Attitude control

The ability of the controller in imparting arbitrary orientations to the satellite and thus enabling it to undertake diverse missions appears interesting to explore. Figure 3.16a shows, for both circular and elliptic orbits, the effectiveness of the control system in providing an arbitrary pitch attitude to the satellite while the axis of symmetry remains normal to the orbital plane. The ability to align the symmetry axis with the local vertical direction and simultaneously attain a desired pitch attitude is indicated in Figures 3.16b and c. Note the excessive overshoots with a larger value of the system gain which suggest the use of small m for a smooth transition between widely differing attitudes.

Thus with the present control system, an antenna aboard the spacecraft is able to scan substantial regions of the sky as arbitrary pitch attitudes are attainable

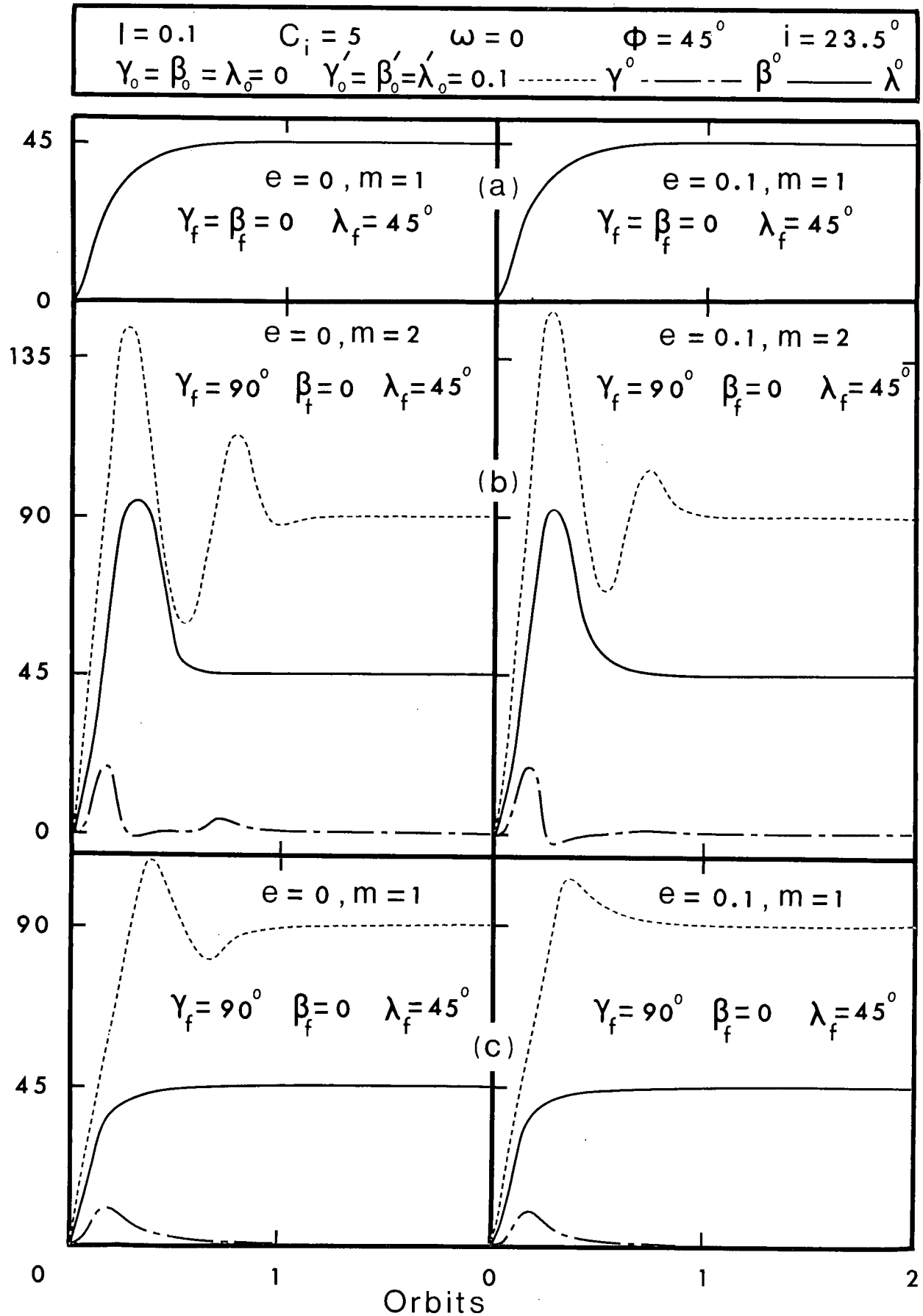

Figure 3.16 Effectiveness of the four-plate model in achieving arbitrary orientations of the satellite

with the axis of symmetry either along the orbit normal or the local vertical. The possibility of stabilizing the satellite axis of symmetry at other orientations was also investigated. The analysis suggests that the controller is able to achieve this but only at the cost of higher values of C_i.

(d) Illustrative example

In order to obtain preliminary estimates of the control plate areas and moment arms required, the proposed Canadian Communications Technology Satellite (CTS) and Anik, are considered. The latter is assumed to be non-spinning which represents an adverse situation. An impulsive disturbance of 0.1 is applied in all the three degrees of freedom which is in excess of that imparted by micrometeorite impacts over 24 hours. As the inertia parameter ($I \simeq 0.1$ for CTS, 1 for Anik) did not affect the performance significantly, most curves in Figure 3.14 (especially curves c, d and e) are representative of the librational behaviour of both satellites considered here. The solar parameter value of $C_i \simeq 5$ can be obtained for CTS using plate areas $A_{1,2} = 12$ ft^2, $A_{3,4} = 1.2$ ft^2 with the moment arms $\varepsilon_i = 10$ ft. Similarly, $C_i \simeq 20$ for Anik may be achieved with each of the plates having an area of 5 ft^2 and moment arm 10 ft. As indicated by curves (d and c) in Figure 3.14 these moderate control plate areas are sufficient to damp the satellite

librations within a few degrees of orbital travel. The librational amplitudes also remained within a fraction of a degree. The plots presented in Figure 3.16 indicate the effectiveness of the controller in providing attitude control to the CTS.

Finally, a comment concerning earth shadow, which would render the solar controllers ineffective, is appropriate here. For a geostationary orbit, the influence of shadow is confined to quarter of the satellite's lifespan, and even here, only during 5% of the orbital period. The results showed the controller performance to remain virtually unaffected.

3.3 Concluding Remarks

The significant conclusions based on the analysis may be summarized as follows:

(i) The feasibility of a semi-passive controller using solar radiation pressure for three-axis nutation damping and attitude control of spinning satellites is clearly demonstrated.

(ii) The system is capable of damping extremely severe disturbances in a fraction of an orbit. The time of damping can be further reduced by an optimum choice of the system gains.

(iii) With the use of the general controller configuration a directional device aboard the stabilized platform may be earth-oriented, space-oriented

or made to track a specified celestial object through a proper choice of the position control parameters. Even with the simplified model, scanning of a substantial region of the sky is possible. The solar pressure controllers thus impart versatility to a space vehicle in undertaking diverse missions.

(iv) The effectiveness of the system remains unaffected, even during a spin decay, with a proper choice of the modified control function. Thus it is no longer necessary to maintain a constant spin rate by compensating for the dissipated energy.

(v) A logical approach for evolving a three-axis solar controller model suitable for practical implementation is presented. The proposed four-plate controller model appears to be quite attractive due to its simplicity of design and the associated software.

(vi) The use of bang-bang control relations substantially improves the system performance. For solar parameter values attainable in practice, a wide range of controller gain yield near optimum performance. Satellites with different mass distributions exhibit essentially the same damping characteristics.

(vii) As the controllers do not require any mass expulsion scheme or active gyros involving large power consumption, the solar pressure control system is essentially semi-active. This promises as increased lifespan.

4. MAGNETIC-SOLAR HYBRID ATTITUDE CONTROL

The earth's magnetic field presents an interesting possibility of generating control moments by interaction with onboard dipoles. Magnetic torquing appears to be particularly attractive as it offers increased reliability through the elimination of moving parts. The shortcoming of the method, as pointed out by Bainum and Mackison[59] and others, lies in its inability to produce sufficient pitch control torques in equatorial orbits where the geomagnetic field is nearly parallel to the orbit normal. On the other hand, the usefulness of placing satellites in equatorial orbits cannot be overemphasized, e.g., the communications satellites in the geostationary orbit.

A need for evolving a system which retains the simplicity of the magnetic concept and yet able to provide pitch control, is thus apparent. Having established the effectiveness of the solar pressure controller, it is proposed here to utilize it for damping pitch oscillations.

This chapter explores the feasibility of the three-axis nutation damping and attitude control of a dual-spin satellite using a magnetic-solar hybrid control system. Two magnetic controller models are considered. A bang-bang control law with linear displacement and velocity sensitive switching functions is employed and analytical

solutions for the control variables are obtained. The performance of the control system is evaluated numerically and the results are presented as functions of system parameters. An illustrative example towards the end establishes the effectiveness of the system.

4.1 Formulation of the Problem

4.1.1 Equations of motion

The geometry of motion (Figure 4.1) of the satellite being the same as the dual-spin spacecraft considered in Chapter 3, Equations (3.8) apply where $Q_i (i = \gamma,\beta,\lambda)$ now represent the total generalized forces due to the magnetic and solar controllers. For convenience, the governing equations of motion are cited again:

$$\gamma'' - 2\beta'(\gamma'\tan\beta - \cos\gamma) - (\beta' - \sin\gamma)\sec\beta\,[(1-J)I(\sigma+1)\times \{(1+e)/(1+e\cos\theta)\}^2 + JI(\lambda' - \gamma'\sin\beta + \cos\beta\cos\gamma)] + \{3(I-1)/(1+e\cos\theta) - 1\}\sin\gamma\cos\gamma - \{2e\sin\theta/(1+e\cos\theta)\}\times(\gamma' + \cos\gamma\tan\beta) = Q_\gamma \qquad (4.1a)$$

$$\beta'' - \gamma'\cos\gamma - \{2e\sin\theta/(1+e\cos\theta)\}(\beta' - \sin\gamma) + (\gamma'\cos\beta + \cos\gamma\sin\beta)\times[(1-J)I(\sigma+1)\{(1+e)/(1+e\cos\theta)\}^2 + JI(\lambda' - \gamma'\sin\beta + \cos\beta\cos\gamma)$$

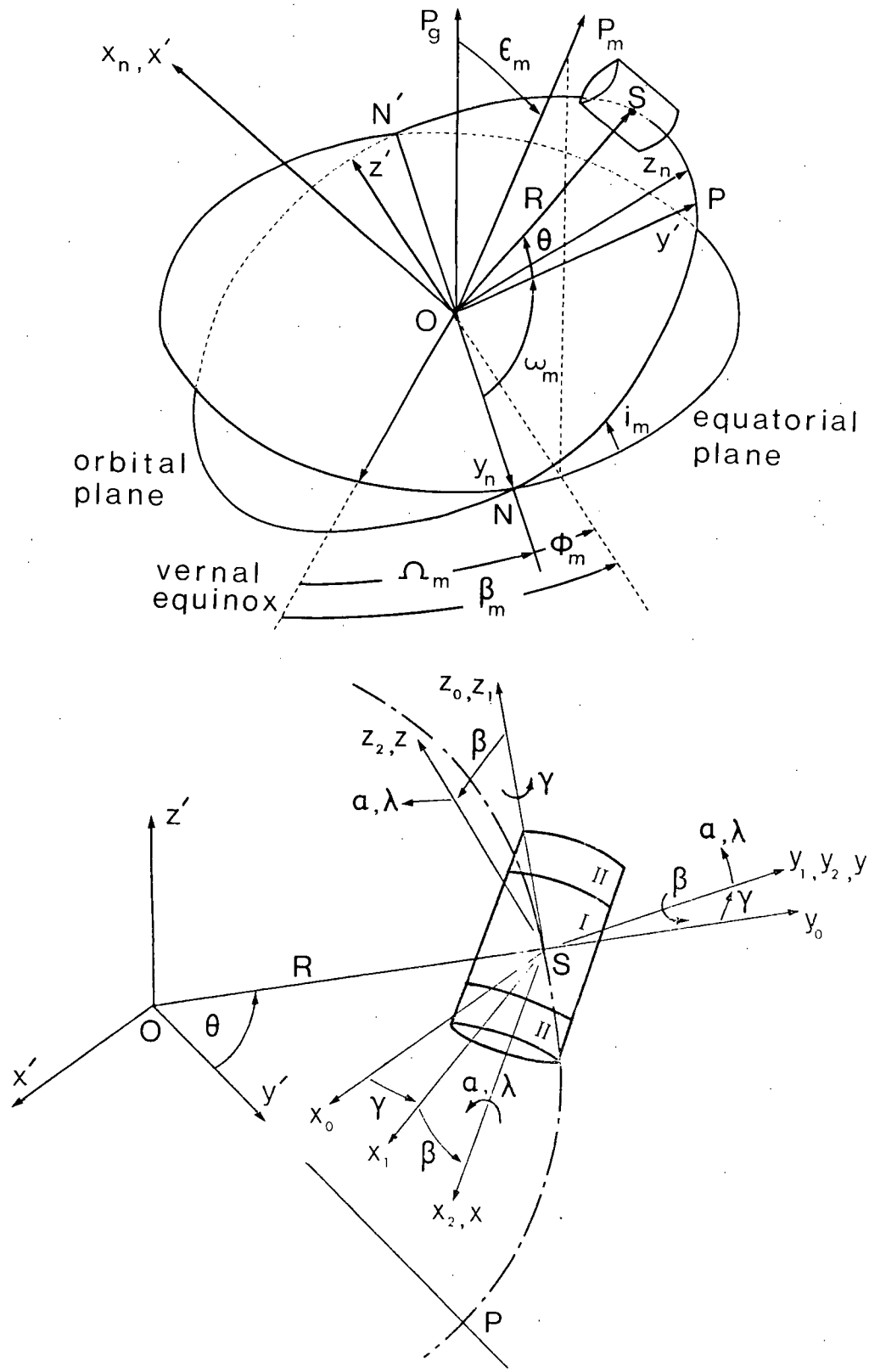

Figure 4.1 Geometry of motion of dual-spin satellite in the earth's magnetic field

$$+(\gamma'\sin\beta-\cos\beta\cos\gamma)]-3\{(I-1)/(1+e\cos\theta)\}\sin^2\gamma\sin\beta\cos\beta = Q_\beta \tag{4.1b}$$

$$\lambda''-\gamma''\sin\beta-\{2e\sin\theta/(1+e\cos\theta)\}(\lambda'-\gamma'\sin\beta+\cos\beta\cos\gamma)-\beta'\gamma'\cos\beta$$
$$-\gamma'\cos\beta\sin\gamma-\beta'\cos\gamma\sin\beta+(K/JI)\{(1+e)^{3/2}/(1+e\cos\theta)^2\}\times$$
$$[\lambda'-\gamma'\sin\beta+\cos\beta\cos\gamma-(\sigma+1)\{(1+e)/(1+e\cos\theta)\}^2] = Q_\lambda \tag{4.1c}$$

4.1.2 Magnetic roll-yaw control

Consider a single dipole onboard the platform with an arbitrary orientation $\bar{p}$, strength h_m^2 and polarity U. The moment generated by interaction with the earth's magnetic field is then given by,

$$\bar{M} = \bar{P} \times \bar{B} = Uh_m^2\bar{p} \times \bar{B} \tag{4.2}$$

Expressing the unit vector $\bar{p}$ and the geomagnetic induction vector $\bar{B}$ in terms of their components along the xyz-axes and using the principle of virtual work, the generalized forces in the roll, yaw and pitch degrees of freedom can be written as:

$$Q_\gamma = UC_m(p_iB_j-p_jB_i)\sec\beta/(1+e\cos\theta) \tag{4.3a}$$

$$Q_{\beta} = UC_m(p_k B_i - p_i B_k)/(1+e\cos\theta) \qquad (4.3b)$$

$$Q_{\lambda m} = U(C_m/JI)(p_j B_k - p_k B_j)/(1+e\cos\theta) \qquad (4.3c)$$

where the magnetic parameter C_m, characterizing the magnitude of the magnetically generated moments, is defined as

$$C_m = h_m^2 M_e/\mu I_y \qquad (4.4)$$

The body components of $\bar{B}/D_m$ are given by the relations

$$\begin{bmatrix} B_i \\ B_j \\ B_k \end{bmatrix} = \begin{bmatrix} \cos\beta\cos\gamma & \cos\beta\sin\gamma\cos\eta_m + \sin\beta\sin\eta_m & \cos\beta\sin\gamma\sin\eta_m - \sin\beta\cos\eta_m \\ -\sin\gamma & \cos\gamma\cos\eta_m & \cos\gamma\sin\eta_m \\ \sin\beta\cos\gamma & \sin\beta\sin\gamma\cos\eta_m - \cos\beta\sin\eta_m & \sin\beta\sin\gamma\sin\eta_m + \cos\beta\cos\eta_m \end{bmatrix} \begin{bmatrix} B_{xn} \\ B_{yn} \\ B_{zn} \end{bmatrix} \qquad (4.5)$$

The geomagnetic induction components along the orbit normal, ascending node and perpendicular to the line of nodes in the orbital plane are well established[81]. For an earth-centered canted dipole model, they are:

$$B_{xn} = -\cos i_m \cos\varepsilon_m + \sin i_m \sin\phi_m \sin\varepsilon_m \qquad (4.6a)$$

$$B_{yn} = (3/2)\sin i_m \sin 2\eta_m \cos\varepsilon_m + (1/2)[\cos\phi_m + (3/2)\times \{(1+\cos i_m)\cos(2\eta_m-\phi_m)+(1-\cos i_m)\cos(2\eta_m+\phi_m)\}]\sin\varepsilon_m \quad (4.6b)$$

$$B_{zn} = (1/2)\sin i_m (1-3\cos 2\eta_m)\cos\varepsilon_m + (1/2)[\cos i_m \sin\phi_m + (3/2)\{(1+\cos i_m)\sin(2\eta_m-\phi_m)+(1-\cos i_m)\times \sin(2\eta_m+\phi_m)\}]\sin\varepsilon_m \quad (4.6c)$$

It may be pointed out here that the angle ϕ_m varies due to the earth's rotation and the regression of the line of nodes, according to $\dot{\phi}_m = (n_e+n_r)$. Its governing equation with the orbital angle as the independent variable is,

$$\phi_m' = (n_e+n_r)(R_p^3/\mu)^{1/2}(1+e)^{3/2}/(1+e\cos\theta)^2 \quad (4.7)$$

which has the solution (for $e < 1$)

$$\phi_m = \phi_{mo} + \{(n_e+n_r)(R_p^3/\mu)^{1/2}(1+e)^{3/2}/(1-e^2)\}\times [-e\sin\theta/(1+e\cos\theta)+\{2/(1-e^2)^{1/2}\}\tan^{-1} \{(1-e)^{1/2}\tan(\theta/2)/(1+e)^{1/2}\}] \quad (4.8)$$

where the appropriate quadrant for the arctan function is to be introduced. The present analysis ignores the nodal regression as a dynamic effect which is equivalent to assuming the earth to be gravitationally spherical.

For controlling satellite nutations in an equatorial orbit with the nominal position of the spin axis along the orbit normal, it can be easily shown that the maximum transverse torque, $(Q_\gamma^2\cos^2\beta+Q_\beta^2)^{1/2}$, results when $p_i = 0$. Accordingly, two magnetic controller models with dipoles in the satellite's transverse plane are considered here (Figure 4.2).

Model A consists of a single dipole rotatable about the x_p axis in the platform fixed reference x_p,y_p,z_p. Physically, it would correspond to a single electromagnet rotating about the axis of symmetry or two (or more) fixed electromagnets with variable currents. The moments generated are given by,

$$Q_\gamma = -UC_m p_j B_i \sec\beta/(1+e\cos\theta) \qquad (4.9a)$$

$$Q_\beta = UC_m p_k B_i/(1+e\cos\theta) \qquad (4.9b)$$

$$Q_{\lambda m} = U(C_m/JI)(p_j B_k - p_k B_j)/(1+e\cos\theta) \qquad (4.9c)$$

where

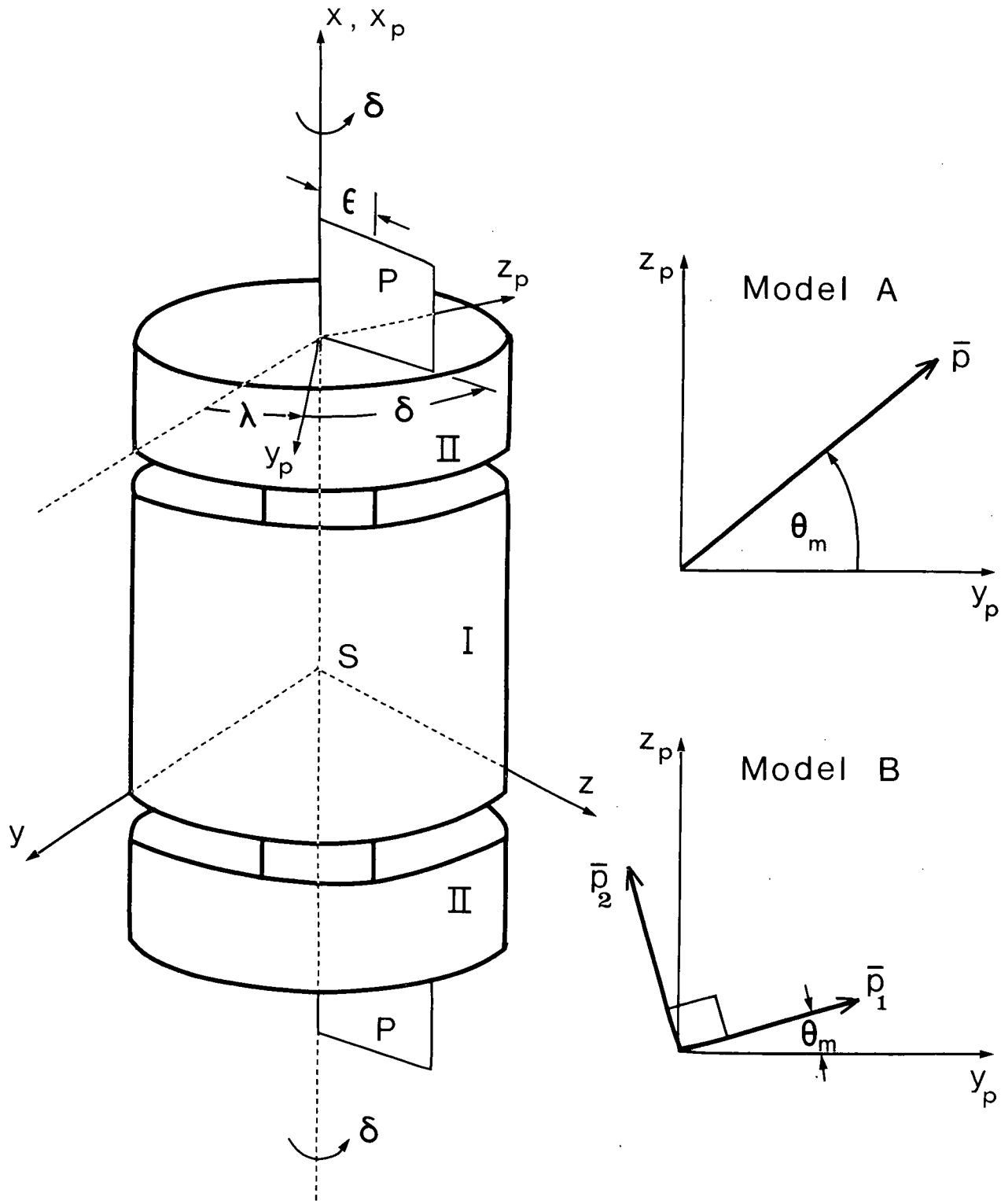

Figure 4.2 Magnetic-solar controller configurations

$$p_j = \cos(\theta_m+\lambda), \quad p_k = \sin(\theta_m+\lambda) \tag{4.9d}$$

A constant dipole level h_m^2, leading to a constant value of the magnetic parameter C_m, is assumed in the present analysis. The components of the total transverse torque are controlled according to the relations:

$$\text{sgn}(Q_\gamma \cos\beta) = -\text{sgn } S_\gamma \tag{4.10a}$$

$$\text{sgn } Q_\beta = -\text{sgn } S_\beta \tag{4.10b}$$

$$Q_\gamma \cos\beta / Q_\beta = S_\gamma / S_\beta \tag{4.10c}$$

where the switching functions $S_i (i = \gamma,\beta)$ are defined as

$$S_i = i' + m(i-i_f), \quad i = \gamma,\beta \tag{4.11}$$

and m represents the system gain.

This results in a simple control law for the dipole angle θ_m (Figure 4.2),

$$\theta_m = -\lambda - \tan^{-1}(S_\beta / S_\gamma) \tag{4.12}$$

Note that no polarity reversals are required if the angle θ_m is permitted any values in the range 0 to 2π. However, it would be desirable to restrict θ_m to the range $-\pi/2$ to $\pi/2$ (for the gimballed electromagnet) and permit

polarity reversals, which leads to the controls:

$$\theta_m = -\tan^{-1}\{(S_\beta+S_\gamma\tan\lambda)/(S_\gamma-S_\beta\tan\lambda)\} \qquad (4.13a)$$

$$U = \text{sgn}\{(S_\gamma\cos\lambda-S_\beta\sin\lambda)/B_i\} \qquad (4.13b)$$

where the principal value of the arctan function is to be admitted.

Model B consists of two mutually perpendicular dipoles with orientations $\bar{p}_1$ and $\bar{p}_2$ fixed in the platform and allowed polarity reversals (Figure 4.2). Substituting for the unit vectors $\bar{p}_1$ and $\bar{p}_2$ in Equations (4.3), the magnetic control moments become,

$$Q_\gamma = -(U_1p_{1j}+U_2p_{2j})C_mB_i\sec\beta/(1+e\cos\theta) \qquad (4.14a)$$

$$Q_\beta = (U_1p_{1k}+U_2p_{2k})C_mB_i/(1+e\cos\theta) \qquad (4.14b)$$

$$Q_{\lambda m} = \{U_1(p_{1j}B_k-p_{1k}B_j)+U_2(p_{2j}B_k-p_{2k}B_j)\}\times (C_m/JI)/(1+e\cos\theta) \qquad (4.14c)$$

where

$$p_{1j} = p_{2k} = \cos(\theta_m+\lambda), \quad p_{1k} = -p_{2j} = \sin(\theta_m+\lambda) \qquad (4.14d)$$

Although the bang-bang controller can no longer distribute the total transverse moment between the roll and yaw degrees of freedom in proportion to the demands governed by the switching functions, appropriate signs of Q_γ and Q_β (Equations 4.10a and b) may be achieved with the polarity controls:

$$\text{for} \left|\tan(\theta_m+\lambda)\right|<1, \quad U_1 = \text{sgn}\{S_\gamma/B_i \cos(\theta_m+\lambda)\}$$

$$U_2 = -\text{sgn}\{S_\beta/B_i \cos(\theta_m+\lambda)\} \qquad (4.15a)$$

$$\text{for} \left|\tan(\theta_m+\lambda)\right|>1, \quad U_1 = -\text{sgn}\{S_\beta/B_i \sin(\theta_m+\lambda)\}$$

$$U_2 = \text{sgn}\{S_\gamma/B_i \sin(\theta_m+\lambda)\} \qquad (4.15b)$$

Note that θ_m defining the locations of the dipoles with respect to the platform-fixed axes is a constant in this case. For the final pitch orientation $\lambda_f = 0$ (the axis y_p pointing towards the earth), minimum cancellation of the torques due to the two dipoles occurs when $\theta_m = 0$. Furthermore, for most applications requiring $-\pi/4 < \lambda < \pi/4$, the controls reduce to:

$$U_1 = \text{sgn}(S_\gamma/B_i), \quad U_2 = -\text{sgn}(S_\beta/B_i) \qquad (4.16)$$

4.1.3 Solar pitch control

The platform pitch control is accomplished using a solar pressure controller consisting of plates PP which are allowed a rotation δ about the axis of symmetry of the satellite (Figure 4.2). For highly reflective plates, the pure pitch moment resulting from solar radiation pressure is (Equation 3.12c),

$$Q_{\lambda s} = -C\{(1+e)^3/(1+e\cos\theta)^4\}|-u_j\sin(\delta+\lambda) + u_k\cos(\delta+\lambda)|\{-u_j\sin(\delta+\lambda)+u_k\cos(\delta+\lambda)\} \quad (4.17)$$

where

$$C = (4\rho p_o R_p^3/\mu I_{xp})A\varepsilon \quad (4.18)$$

Using the control relation

$$Q_{\lambda s} = -|Q_{\lambda s}|_{max}\,\mathrm{sgn}\; S_\lambda \quad (4.19)$$

with

$$S_\lambda = \lambda' + m(\lambda-\lambda_f), \quad (4.20)$$

the control law for the plate rotation δ becomes,

$$\text{for } u_j>0,\ \delta = \tan^{-1}(u_k/u_j)-\lambda-(\pi/2)\,\mathrm{sgn}\; S_\lambda$$

$$\text{for } u_j<0,\ \delta = \pi+\tan^{-1}(u_k/u_j)-\lambda-(\pi/2)\,\mathrm{sgn}\; S_\lambda$$

$$\text{for } u_j = 0,\ \delta = \cos^{-1}\{-\text{sgn}(u_k S_\lambda)\} \tag{4.21}$$

where the principal value of the arctan function is to be introduced.

The total generalized force in the pitch degree of freedom is then given by,

$$Q_\lambda = Q_{\lambda m} + Q_{\lambda s} \tag{4.22}$$

It may be pointed out here that the components of the unit vector in the direction of the sun involve orbital parameters Ω, i and ω referred to the ecliptic plane while the formulation of the magnetic controller requires the same angles referred to the earth's equatorial plane. The relations governing these parameters for an arbitrary orbital plane are readily obtained as:

$$\sin\Omega_m \sin i_m = \sin\Omega \sin i \tag{4.23a}$$

$$\cos\Omega_m \cos\omega_m - \sin\Omega_m \sin\omega_m \cos i_m = \cos\Omega\cos\omega - \sin\Omega\sin\omega\cos i \tag{4.23b}$$

$$\cos\Omega_m \sin\omega_m + \sin\Omega_m \cos\omega_m \cos i_m = \cos\Omega\sin\omega + \sin\Omega\cos\omega\cos i \tag{4.23c}$$

4.2 Results and discussion

The response of the system was studied by numerically integrating the equations of motion (4.1) along with the control relations governing the magnetic and solar moments, i.e., Equations (4.9, 4.13, 4.21 and 4.22) and Equations (4.14, 4.15, 4.21 and 4.22) for models A and B, respectively. The Adams-Bashforth predictor-corrector quadrature with the Runge-Kutta starter was used with a step size of 0.1°. The important system parameters were varied gradually over the range of interest and the controller performance evaluated both in circular and elliptic orbits. The amount of information thus generated is rather extensive; however, for conciseness, only the typical results sufficient to establish trends are presented here.

4.2.1 Nutation damping

Figure 4.3 summarizes the performance of the proposed magnetic-solar hybrid controller in damping the nutational motion of the satellite spin axis and the pitch oscillation of the platform. It shows the variation of the damping time τ_d with the controller gain m for a variety of combinations of the system parameters and initial conditions. Here the damping time is defined as the time required for all the three degrees of freedom; namely, the roll γ, yaw β and the platform pitch λ, to settle within

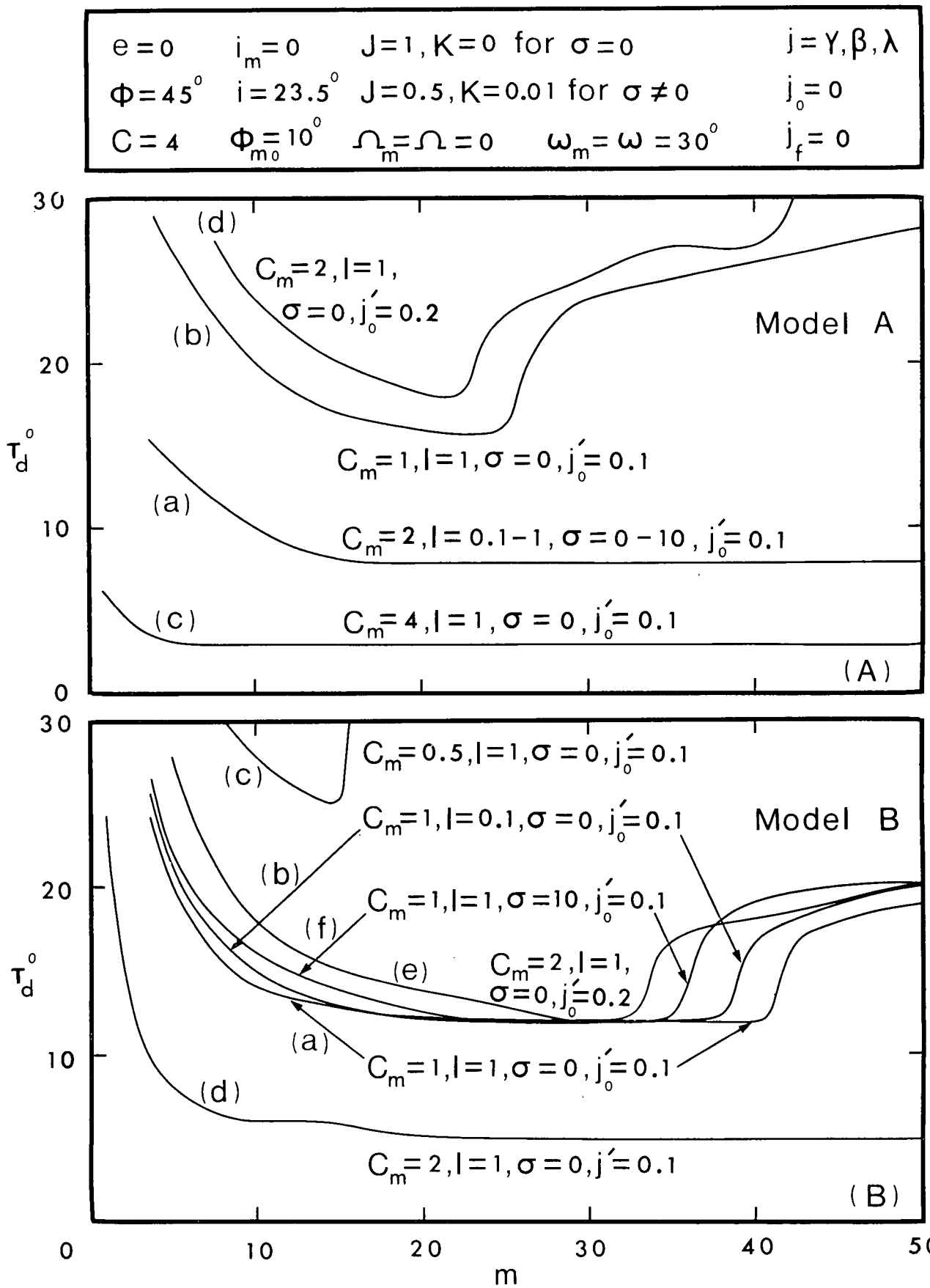

Figure 4.3 Optimization plots for the magnetic-solar controller gain m

0.1° of the desired final orientation. The responses of both magnetic controller models A and B are presented, which, in general, indicate the existence of an optimum value of the system gain m leading to the minimum time of damping, and the sensitivity of the optimum to the system parameters and initial conditions.

The influence of the satellite inertia and spin parameters on the attitude dynamics of passively stabilized satellites is well recognized. Their effect on the nutation damping performance of the present controlled system, however, appears to be negligible. This is indicated by curve (a) in Figure 4.3A where the results for pencil-like to spherical mass distributions (I = 0.1 to 1) and non-spinning to moderate spin rates (σ = 0 to 10) were virtually indistinguishable. The banding together of curves (a,b and f) in Figure 4.3B reflects similar system behaviour. The insensitivity of the transient response to I and moderate values of σ is understandable as these parameters, contributing restoring forces to the system, are now largely provided for by the controller gain m. The performance under high spin rates is investigated in a later section.

The effect of the magnetic parameter C_m, characterizing the magnitude of the magnetic control torques, is indicated by a comparison of curves (b,a and c) in Figure 4.3A for the case of the single rotatable dipole. As anticipated, increasing the value of C_m leads to a corres-

ponding reduction in the damping time τ_d. Larger values of the magnetic parameter (curves a and c) show a response pattern that is relatively insensitive to the controller gain m, thus indicating a large range of values of the latter to provide near-optimum damping. It may, however, be pointed out that the maximum attainable value of C_m is subject to constraints imposed by the electromagnet weight and power requirement. Curves (c,a and d) indicate similar effect of the magnetic parameter for the model with two fixed transverse dipoles (Figure 4.3B).

A comment concerning the influence of the solar parameter would be appropriate here. An increased value of C led to a reduced damping time for the pitch (λ) degree of freedom. However, even with a value of C = 2, the pitch motion, in general, damped out faster than the roll-yaw motion, except for the case of large viscous drags on the platform (large K, σ).

A comparison of curves (a and d) in Figure 4.3A and curves (d and e) in Figure 4.3B shows the effect of initial conditions on the performance of controller models A and B, respectively. In both cases, an increased impulsive disturbance not only leads to an anticipated increase in the damping time but also renders the response quite sensitive to the system gain m. With larger values of C_m, however, the latter effect was found to be less pronounced.

It is of interest to compare the performance of the two magnetic controller models in damping the attitude motion. A suitable criterion for the comparison is the same total electromagnet weight and power consumption which requires the value of the magnetic parameter C_m for model A to be twice the value for model B. Comparisons may be made of curves (b, a and c) in Figure 4.3A with curves (c, a and d) in Figure 4.3B, respectively, towards this end. The results clearly indicate a better performance of the single rotatable dipole model A. This is explained by the ability of this model to distribute the total magnetic torque between the roll and yaw degrees of freedom in proportion to their demands, determined here by the switching functions S_γ and S_β, respectively.

The single rotating dipole model A may be obtained by using a rotating electromagnet, which, however, would involve additional weight and power requirement for the turning mechanism and a reduction in the system reliability due to physical movement of the electromagnet. Alternately, two fixed electromagnets with variable currents may be employed. Unfortunately, this would require each electromagnet to be the same size as the single rotating one in order to maintain the same resultant dipole strength as the latter, thus doubling the total weight. The choice between the physical arrangements leading to model A or B would be governed by such mission oriented factors as the system

reliability, associated hardware and software, and performance requirements.

Typical damped responses of a satellite subjected to an extremely severe impulsive disturbance are shown in Figure 4.4 for both controller models. The time history of the controls is also included. Figure 4.4a shows the response in a circular orbit with a nominal value of $\sigma = 1$, which may be required from such considerations as temperature control. The damped attitude motion of a nonspinning satellite in an eccentric orbit is shown in Figure 4.4b, which indicates a slight increase in the maximum amplitude and the damping time. The effectiveness of the controllers in damping such a severe impulsive disturbance in a few degrees of the satellite's orbital travel is thus apparent. The amplitudes are also limited to a few degrees. The controls, in general, require rather infrequent switching until the corresponding amplitudes become very small and chatter initiates. This may, however, be prevented by the inclusion of suitable deadbands in the control relations which would depend on the pointing accuracies required.

The effectiveness of the control system in capturing a satellite from initial roll, yaw and pitch errors is presented in Figure 4.5. Both circular and eccentric orbit as well as nonspinning and moderate spin rate cases are considered. The initial error of 20° in

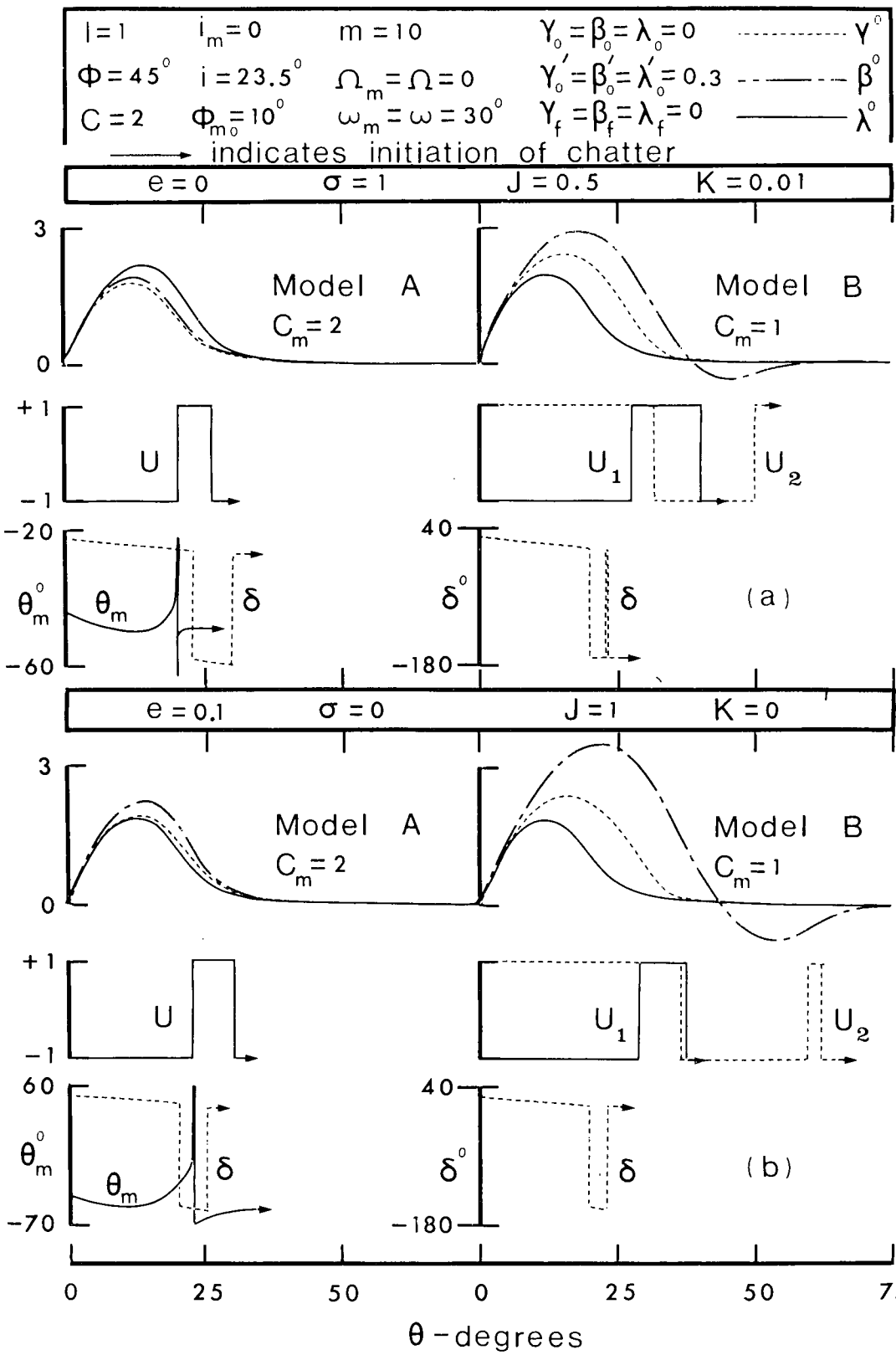

Figure 4.4 Damped response and time history of controls subsequent to initial impulsive disturbance

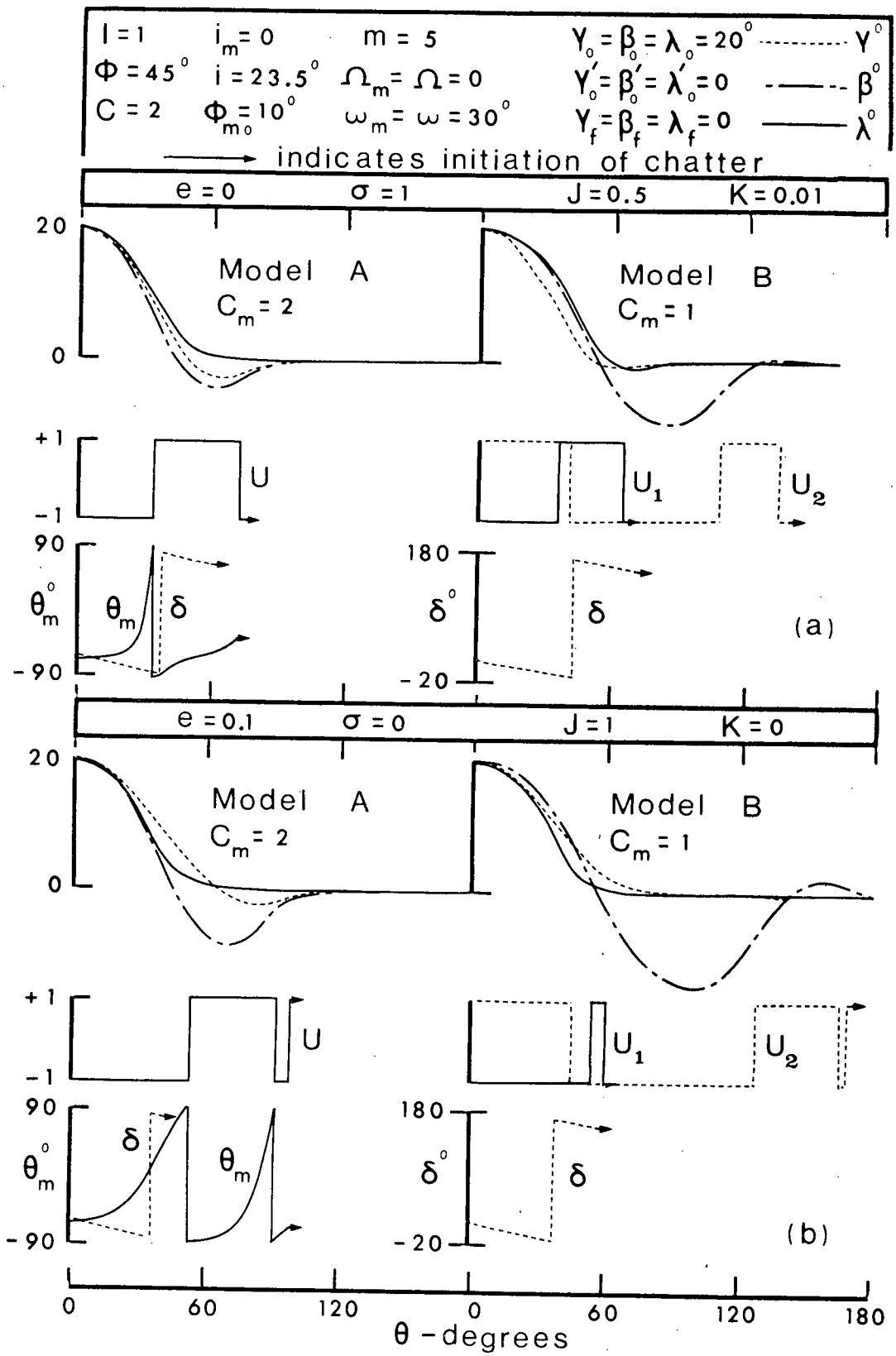

Figure 4.5 Damped response and time history of controls subsequent to initial position disturbance

each degree of freedom is corrected in approximately one-third of an orbit with model A and half an orbit with model B. The performance may be improved further through an optimum choice of the controller gain.

4.2.2 High spin rates and spin decay

The discussion so far pertains to satellites which are either nonspinning or have moderate spin rates. The effectiveness of the control system (model B) for satellites with high spin rates is indicated by the response data presented in Table 1, which shows the coning amplitude of the spin axis, Φ_{max}, and the damping time τ_d. The coning amplitude Φ_{max} reached in the absence of the controller is also presented. For low spin rates, the control system, in addition to providing quick nutation damping, helps keep the amplitudes low. However, for high spin rates, it essentially acts as a damper. A comparison of the controller performance with m = 10 and m = 30 shows its effect on the amplitude to be slight but the damping time is affected appreciably, up to spin parameter values as high as $\sigma = 200$. These observations substantiate the earlier conclusion regarding the controller gain lending stiffness to the system. For still higher spin rates ($\sigma > 200$), however, the influence of m is negligible indicating the dominance of the gyroscopic restoring forces.

TABLE 4.1

Response With High Spin Rates

$e = 0$ $I = 1.2$ $i_m = 0$ $\Omega_m = \Omega = 0$ $\gamma_o = \beta_o = \lambda_o = 0$

$J = 0.5$ $\phi = 45°$ $i = 23.5°$ $\omega_m = \omega = 30°$ $\gamma'_o = \beta'_o = 0.3$

$K = 0$ $C = 4$ $\phi_{mo} = 10°$ $\lambda'_o = 0$ $\gamma_f = \beta_f = \lambda_f = 0$

σ	$C_m = 2$, $m = 10$		$C_m = 2$, $m = 30$		$C_m = 0$
	$\Phi°_{max}$	$\tau°_d$	$\Phi°_{max}$	$\tau°_d$	$\Phi°_{max}$
0	1.86	28.20	1.86	29.50	39.88
10	1.78	28.26	1.77	30.86	6.61
25	1.61	26.04	1.53	34.56	2.99
35	1.39	30.96	1.34	43.56	2.19
50	1.12	24.22	1.10	25.50	1.56
75	0.84	21.84	0.84	35.56	1.05
100	0.67	19.44	0.67	33.88	0.79
200	0.37	15.54	0.37	22.26	0.40
300	0.25	11.82	0.25	13.20	0.27
400	0.19	9.70	0.19	9.78	0.20
500	0.16	6.68	0.16	6.66	0.16
600	0.13	4.50	0.13	4.52	0.13

The analysis so far considered the rotor (body I) to have a constant average spin rate. Apparently this would be achieved through some active energy source compensating for rotor spin decay due to bearing losses. Even in the absence of such energy supply, the analysis continues to be valid provided the spin parameter σ remains sensibly invariant over a time interval of the order of the damping times attained here. This is of considerable value as any spin decay is likely to occur very slowly indeed. Thus the data presented in Table 1 can also be used to predict the long range performance of a spinning satellite. The controller's effectiveness in achieving quick nutation damping even in the absence of any spin promises an increased satellite life-span.

4.2.3 Attitude control

The control system offers the exciting possibility of stabilizing the satellite along any arbitrary orientation in space, thus enabling it to undertake diverse missions. This may be achieved through the parameters γ_f, β_f and λ_f, defining the final desired orientation, which are incorporated in the switching functions S_γ, S_β and s_λ, respectively. Figure 4.6 shows the ability of the controller in achieving a variety of spatial orientations, the time taken being well within an orbit. Note that a fairly small value of the gain m used here leads to a smooth transition between widely

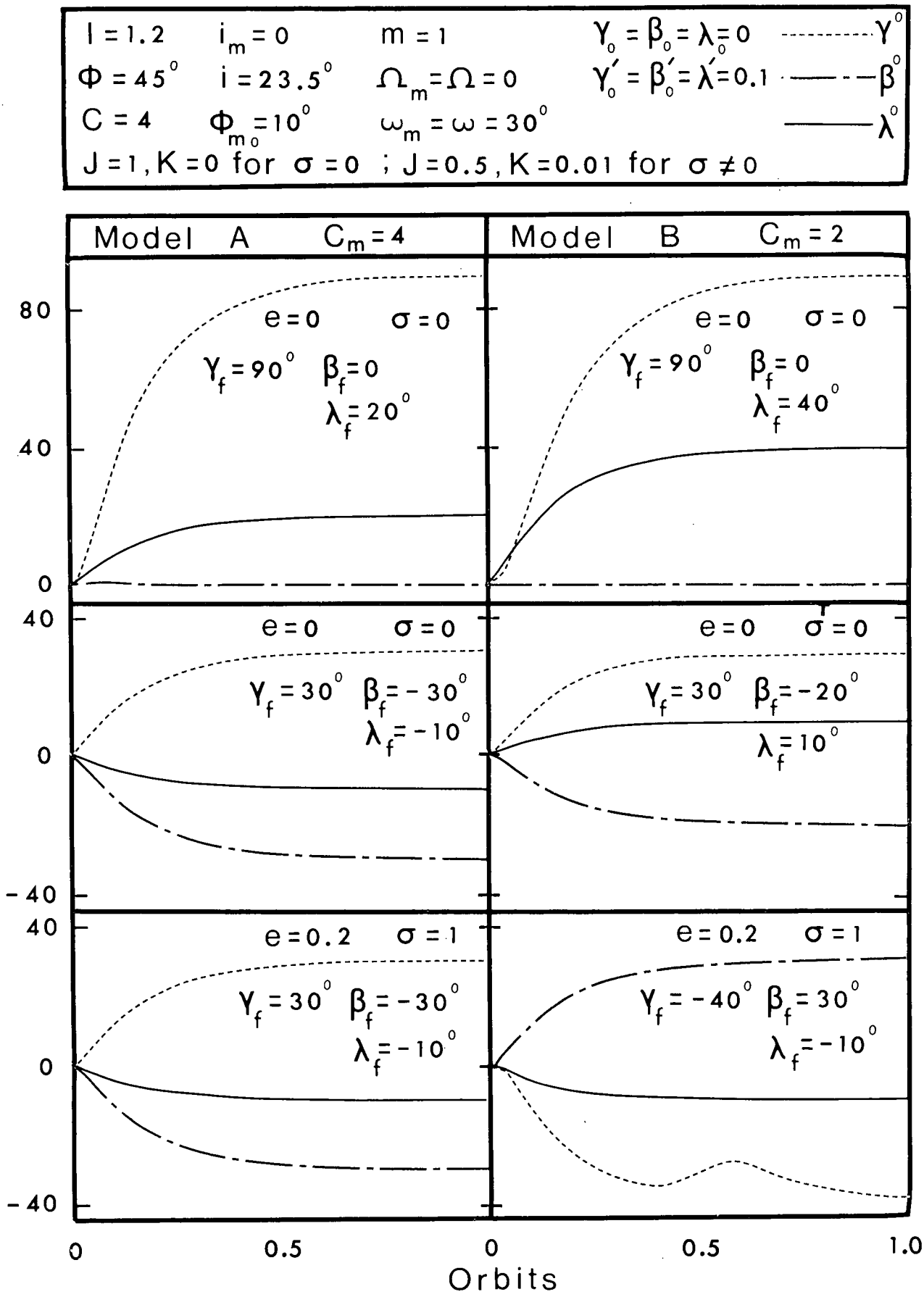

Figure 4.6 Effectiveness of the magnetic-solar controller in imparting arbitrary orientations to the satellite

different attitudes. On the other hand, larger values of m were found to result in an undesirable overshoot of the final orientation. It may be pointed out further that except for final orientations along equilibrium points of the system, the controller must at all times provide corrective torques to counter the gravity gradient and gyroscopic moments. Moderate values of the magnetic parameter taken here, $C_m = 4$ for model A and $C_m = 2$ for model B, are found to be sufficient for both nonspinning and a nominal spin rate in circular as well as eccentric orbits (Figure 4.6).

4.2.4 Illustrative example

It appears interesting to evaluate the performance of the magnetic-solar controller through a preliminary attitude dynamics study of two well-known satellites, the proposed Canadian Communications Technology Satellite (CTS) and Anik, when provided with the proposed control system. For convenience the latter may be considered as nonspinning which only represents an adverse situation. Values of the magnetic parameter $C_m = 4$ for model A and 2 for model B are attainable with total dipole levels of approximately 200 and 20 ampere-meter^2 for the CTS and Anik, respectively. A control plate area $A \simeq 0.5$ ft^2 and moment arm $\varepsilon = 5$ ft yield a solar parameter value of $C \simeq 2$. On the other hand, pitch control may be achieved using a reaction wheel of

capacity ≃ 0.1 lb-ft-sec/day which is equivalent to C = 2. An impulsive disturbance of 0.1 is applied in all the three degrees of freedom simultaneously which is in excess of that imparted by micrometeorite impacts over 24 hrs, and thus represents an enormous magnification of the real situation. As the inertia parameter (I ≃ 0.1 for CTS, 1 for Anik) did not affect the performance significantly, most of the results presented in this chapter are representative of these satellites. It is apparent (Figure 4.3) that the controllers are able to damp out such a severe disturbance in about 3° and 5° of the orbit with models A and B, respectively. The maximum deviation from the orbit normal attitude also remained less than 0.2°. Any arbitrary orientations may be imparted to the satellites in well within an orbital period (Figure 4.6).

Finally, it may be mentioned that the comment concerning the earth shadow made earlier also applies here. The results showed the controller performance to remain virtually unaffected. Furthermore, the analysis ignores dynamics due to relative motion of the gimballed electromagnet (model A) and the solar control plates as well as the shadowing of the latter by the satellite.

4.3 Concluding Remarks

The conclusions based on the analysis may be summarized as follows:

(i) The analysis clearly establishes the potential of a magnetic-solar hybrid system for nutation damping and attitude control of satellites.

(ii) The concept permits interchangeability of the solar controller and a variable speed pitch momentum wheel, thus effectively providing a gyromagnetic control system.

(iii) The ability of the system in damping extremely severe disturbances in a few degrees of the orbit makes it quite suitable for applications, such as, communications satellites.

(iv) Even with rotor spin decay, the system continues to function effectively which promises an increased satellite life-span.

(v) It is possible for a satellite to attain any arbitrary orientation in space, both in circular and elliptic orbits, thus widening the scope of its mission.

5. AERODYNAMIC-SOLAR HYBRID ATTITUDE CONTROL

The analyses in the earlier chapters apply primarily to satellites in high altitude orbits since the influence of the earth's atmosphere was ignored. However, several space applications, such as, weather forecasting, earth resources exploration, military scouting, etc., depend on high resolution photography and hence necessarily negotiate near-earth trajectories. Unfortunately, interaction with free molecular reaction forces reduces their effective life-span leading to expensive periodic replacement. One possible solution would be to employ an elliptic trajectory making a space vehicle to spend major portion of its orbital period above the atmosphere and dip into it only when actively engaged in its mission. This presents an interesting situation where aerodynamic forces may be used to advantage for attitude control, possibly in conjunction with solar radiation pressure.

The present chapter explores the feasibility of such a hybrid control system. The governing equations of motion, together with a bang-bang control law, are analyzed numerically and the influence of the important system parameters on the performance is evaluated.

5.1 Formulation of the Problem

5.1.1 Equations of motion

The case of a nonspinning satellite is considered here, which, in view of the analysis in Chapter 4, represents an adverse situation. Equations (3.20) therefore apply where $Q_i (i = \gamma,\beta,\lambda)$ now represent the total generalized forces due to the solar pressure and the aerodynamic forces:

$$\gamma'' - 2\beta'(\gamma'\tan\beta - \cos\gamma) - I(\lambda' - \gamma'\sin\beta + \cos\beta\cos\gamma)(\beta' - \sin\gamma)\sec\beta + \{3(I-1)/(1+e\cos\theta) - 1\}\sin\gamma\cos\gamma - \{2e\sin\theta/(1+e\cos\theta)\} \times (\gamma' + \cos\gamma\tan\beta) = Q_\gamma \qquad (5.1a)$$

$$\beta'' - \gamma'\cos\gamma - \{2e\sin\theta/(1+e\cos\theta)\}(\beta' - \sin\gamma) + \{I(\lambda' - \gamma'\sin\beta + \cos\beta\cos\gamma) + (\gamma'\sin\beta - \cos\beta\cos\gamma)\}(\gamma'\cos\beta + \cos\gamma\sin\beta) - 3\{(I-1)/(1+e\cos\theta)\} \times \sin^2\gamma\sin\beta\cos\beta = Q_\beta \qquad (5.1b)$$

$$\lambda'' - \gamma''\sin\beta - \{2e\sin\theta/(1+e\cos\theta)\}(\lambda' - \gamma'\sin\beta + \cos\beta\cos\gamma) - \beta'\gamma'\cos\beta - \gamma'\cos\beta\sin\gamma - \beta'\cos\gamma\sin\beta = Q_\lambda \qquad (5.1c)$$

5.1.2 Controller configuration and generalized forces

The controller configuration studied for establishing the feasibility of solar pressure control is considered

for the hybrid aerodynamic-solar control as well (Figure 5.1). The generalized forces due to solar radiation pressure were found earlier (Equations 3.12) as:

$$Q_{\gamma s} = -E(\theta)[U_1 C_1 |\cos\xi_1| \cos\xi_1 \sin\delta_1 \sin\lambda + U_2 C_2 |\cos\xi_2| \cos\xi_2 \sin\delta_2 \cos\lambda] \sec\beta \tag{5.2a}$$

$$Q_{\beta s} = -E(\theta)[U_1 C_1 |\cos\xi_1| \cos\xi_1 \sin\delta_1 \cos\lambda - U_2 C_2 |\cos\xi_2| \cos\xi_2 \sin\delta_2 \sin\lambda] \tag{5.2b}$$

$$Q_{\lambda s} = -E(\theta) C_3 |\cos\xi_3| \cos\xi_3 \tag{5.2c}$$

where

$$U_i = +1 \text{ for } P_i, \; -1 \text{ for } P_i'; \quad i = 1,2$$

$$\cos\xi_1 = u_i \cos\delta_1 + (u_j \sin\lambda - u_k \cos\lambda)\sin\delta_1$$

$$\cos\xi_2 = u_i \cos\delta_2 + (u_j \cos\lambda + u_k \sin\lambda)\sin\delta_2$$

$$\cos\xi_3 = -u_j \sin(\delta_3+\lambda) + u_k \cos(\delta_3+\lambda) \tag{5.3}$$

The solar parameters, C_i, are given by,

$$C_i = (4\rho p_o R_p^3/\mu I_y) A_i \varepsilon_i, \quad i = 1,2$$

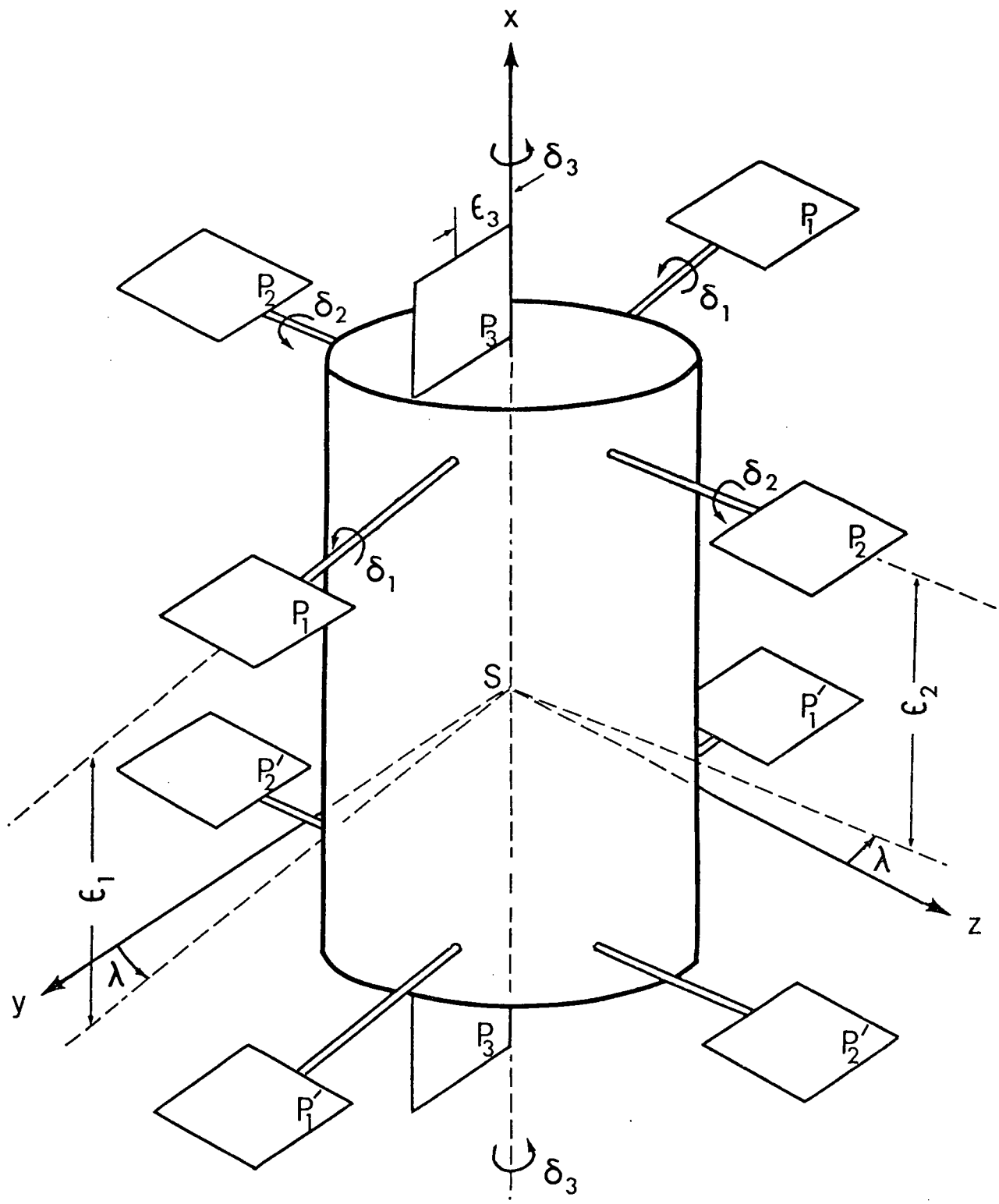

Figure 5.1 Aerodynamic-solar hybrid controller configuration

$$C_3 = (4\rho p_o R_p^3/\mu I_x) A_3 \varepsilon_3 \tag{5.4}$$

The resultant free molecular force on an elemental area, considering specular reflection, may be expressed as[82],

$$d\bar{F}_a = (1/2)\rho_a V^2 dA|\cos\xi_a|\{(C_D - C_L \operatorname{cosec}\xi_a|\cos\xi_a|)\bar{v} + (C_L \operatorname{cosec}\xi_a \operatorname{sgncos}\xi_a)\bar{n}\} \tag{5.5}$$

Evaluating the total moment about the satellite center of mass due to the aerodynamic forces and using the principle of virtual work leads to:

$$Q_{\gamma a} = J(\theta)[U_1 C_{a1}|\cos\xi_{a1}|\{v_j - (C_L/C_D)\operatorname{cosec}\xi_{a1}(v_j|\cos\xi_{a1}| - \sin\delta_1 \sin\lambda \operatorname{sgncos}\xi_{a1})\} + U_2 C_{a2}|\cos\xi_{a2}|\{v_j - (C_L/C_D)\operatorname{cosec}\xi_{a2} \times (v_j|\cos\xi_{a2}| - \sin\delta_2 \cos\lambda \operatorname{sgncos}\xi_{a2})\} - C_{a3}|\cos\xi_{a3}|\{1 - (C_L/C_D) \times \operatorname{cosec}\xi_{a3}|\cos\xi_{a3}|\} v_i \cos(\delta_3 + \lambda)]\sec\beta \tag{5.6a}$$

$$Q_{\beta a} = -J(\theta)[U_1 C_{a1}|\cos\xi_{a1}|\{v_k - (C_L/C_D)\operatorname{cosec}\xi_{a1}(v_k|\cos\xi_{a1}| + \sin\delta_1 \cos\lambda \operatorname{sgncos}\xi_{a1})\} + U_2 C_{a2}|\cos\xi_{a2}|\{v_k - (C_L/C_D)\operatorname{cosec}\xi_{a2} \times (v_k|\cos\xi_{a2}| - \sin\delta_2 \sin\lambda \operatorname{sgncos}\xi_{a2})\} - C_{a3}|\cos\xi_{a3}|\{1 - (C_L/C_D) \times \operatorname{cosec}\xi_{a3}|\cos\xi_{a3}|\} v_i \sin(\delta_3 + \lambda)] \tag{5.6b}$$

$$Q_{\lambda a} = J(\theta)C_{a3}[|\cos\xi_{a3}|+(C_L/C_D)\sin\xi_{a3}]\cos\xi_{a3} \qquad (5.6c)$$

where

$$U_i = +1 \text{ for } P_i, \ -1 \text{ for } P_i'; \quad i = 1,2$$

$$\cos\xi_{a1} = v_i\cos\delta_1+(v_j\sin\lambda-v_k\cos\lambda)\sin\delta_1$$

$$\cos\xi_{a2} = v_i\cos\delta_2+(v_j\cos\lambda+v_k\sin\lambda)\sin\delta_2$$

$$\cos\xi_{a3} = -v_j\sin(\delta_3+\lambda)+v_k\cos(\delta_3+\lambda) \qquad (5.7)$$

The aerodynamic parameters, C_{ai}, are defined as

$$C_{ai} = (C_D\rho_{ap}R_p^2/I_y)A_i\varepsilon_i, \quad i = 1,2$$

$$C_{a3} = (C_D\rho_{ap}R_p^2/I_x)A_3\varepsilon_3 \qquad (5.8)$$

The variation of the atmospheric density with altitude, incorporated in the definition of the function $J(\theta)$, is modelled according to the relation

$$\rho_a = \rho_{ap}\{(R-R_e)/(R_p-R_e)\}^n \qquad (5.9)$$

where n varies in the range -5 to -7 depending on the altitude[83].

The total generalized forces due to the radiation pressure and the aerodynamic forces may be expressed as functions of the control variables U_i(i=1,2) and δ_i(i=1,2,3) in the form:

$$Q_\gamma = Q_{\gamma s}(U_1,U_2,\delta_1,\delta_2)+Q_{\gamma a}(U_1,U_2,\delta_1,\delta_2,\delta_3) \tag{5.10a}$$

$$Q_\beta = Q_{\beta s}(U_1,U_2,\delta_1,\delta_2)+Q_{\beta a}(U_1,U_2,\delta_1,\delta_2,\delta_3) \tag{5.10b}$$

$$Q_\lambda = Q_{\lambda s}(\delta_3)+Q_{\lambda a}(\delta_3) \tag{5.10c}$$

In view of Equations (5.2 and 5.6), the dependence of the moments Q_i on the control variables is quite complicated. However, it is possible to obtain relatively simple analytical solutions for the plate rotations δ_i through a judicious control strategy.

5.2 Control Strategy

The magnitudes of the control moments are constrained by the control surface areas and moment arms (through the solar parameters C_i and the aerodynamic parameters C_{ai}). In order to utilize the maximum moments available from the controller, the following bang-bang control law is employed here:

$$Q_i = -|Q_i|_{max} \operatorname{sgn} S_i \tag{5.11}$$

where the switching functions S_i are defined as

$$S_i = i'+m(i-i_f), \quad i = \gamma,\beta,\lambda \tag{5.12}$$

and m represents the system gain.

The determination of the simultaneous maxima, $|Q_i|_{max}$, that the controller can provide, is rather involved. The problem may be simplified considerably by recognizing that the solar pressure and the aerodynamic forces represent the respective dominant influences at high and low altitudes. Only over a small portion of an elliptic trajectory are the two effects comparable in magnitude. The plate rotations δ_i, producing the maximum moments, may thus be obtained in accordance with the solar pressure at high altitudes and aerodynamic forces at low altitudes. The switch-over point can be determined by comparing the magnitudes of the two forces.

5.2.1 High altitude

Maximization of the solar pitch moment, $Q_{\lambda s}$, leads to the following control law for δ_3:

$$\begin{aligned}
&\text{for } u_j > 0, \quad \delta_{3s} = \tan^{-1}(u_k/u_j) - \lambda - (\pi/2)\,\mathrm{sgn}\ S_\lambda \\
&\text{for } u_j < 0, \quad \delta_{3s} = \pi + \tan^{-1}(u_k/u_j) - \lambda - (\pi/2)\,\mathrm{sgn}\ S_\lambda \\
&\text{for } u_j = 0, \quad \delta_{3s} = \cos^{-1}\{\mathrm{sgn}(u_k S_\lambda)\} - \lambda
\end{aligned} \tag{5.13}$$

where the principal value of the arctan function is to be admitted.

The solar roll-yaw control moments $Q_{\gamma s}$ and $Q_{\beta s}$ being coupled through the rotations δ_1 and δ_2, the total

transverse torque, $(Q_{\gamma s}^2 \cos^2\beta + Q_{\beta s}^2)^{1/2}$, is maximized which occurs at:

$$\delta_{1s} = \pi/2 + \tan^{-1}[(3/2)(u_j \sin\lambda - u_k \cos\lambda)/u_i \pm \{(9/4) \times (u_j \sin\lambda - u_k \cos\lambda)^2/u_i^2 + 2\}^{1/2}] \qquad (5.14a)$$

$$\pm \text{ for } \{(u_j \sin\lambda - u_k \cos\lambda)/u_i\} \lesseqgtr 0,$$

and $$\delta_{2s} = \pi/2 + \tan^{-1}[(3/2)(u_j \cos\lambda + u_k \sin\lambda)/u_i \pm \{(9/4)(u_j \cos\lambda + u_k \sin\lambda)^2/u_i^2 + 2\}^{1/2}] \qquad (5.14b)$$

$$\pm \text{ for } \{(u_j \cos\lambda + u_k \sin\lambda)/u_i\} \lesseqgtr 0.$$

In general, all sign combinations of $Q_{\gamma s}$ and $Q_{\beta s}$ are available through an appropriate choice of the control plates to be operated. Occasionally, due to the time-varying nature of the components u_i, u_j, u_k, the desired signs of $Q_{\gamma s}$ and $Q_{\beta s}$ may not be available. In such situations, the roll-yaw control plates are to be turned 'off', which may be done either by making the corresponding $\delta_i = 0$ or, by aligning the plates parallel to the incident radiation, i.e., choosing δ_i so as to render the corresponding $\cos\xi_i = 0$.

The control moments at high altitude thus become,

$$Q_\gamma = Q_{\gamma s}(U_1,U_2,\delta_{1s},\delta_{2s})+Q_{\gamma a}(U_1,U_2,\delta_{1s},\delta_{2s},\delta_{3s}) \quad (5.15a)$$

$$Q_\beta = Q_{\beta s}(U_1,U_2,\delta_{1s},\delta_{2s})+Q_{\beta a}(U_1,U_2,\delta_{1s},\delta_{2s},\delta_{3s}) \quad (5.15b)$$

$$Q_\lambda = Q_{\lambda s}(\delta_{3s})+Q_{\lambda a}(\delta_{3s}) \quad (5.15c)$$

5.2.2 Low altitude

In a manner similar to the solar control at high altitude, the moments due to the aerodynamic forces may be maximized at low altitude. The exact determination of the critical δ_i being more complicated in this case, simplifying assumptions such as $|v_i|$, $|v_j| << |v_k|$ and $C_L/C_D << 1$ are employed. These approximations, however, extend only as to the determination of the maximizing δ_i, the subsequent evaluation of the moments being exact.

The control law for the rotation δ_3, maximizing the aerodynamic pitch control torque $Q_{\lambda a}$, is found to be:

$$\text{for } v_j > 0, \quad \delta_{3a} = \tan^{-1}(v_k/v_j)-\lambda+(\pi/2)\,\text{sgn}\, S_\lambda$$

$$\text{for } v_j < 0, \quad \delta_{3a} = \pi+\tan^{-1}(v_k/v_j)-\lambda+(\pi/2)\,\text{sgn}\, S_\lambda$$

$$\text{for } v_j = 0, \quad \delta_{3a} = \cos^{-1}\{-\text{sgn}(v_k S_\lambda)\}-\lambda \quad (5.16)$$

where the principal value of the arctan function is to be introduced.

The aerodynamic roll-yaw moment is maximized by the rotations δ_1 and δ_2 given by,

$$\delta_{1a} = \pi/2-\tan^{-1}\{v_i/(v_j\sin\lambda-v_k\cos\lambda)\} \tag{5.17a}$$

$$\delta_{2a} = \pi/2-\tan^{-1}\{v_i/(v_j\cos\lambda+v_k\sin\lambda)\} \tag{5.17b}$$

An investigation of Equations (5.6) indicates that, in highly eccentric orbits, the drag component of the aerodynamic force governs the directions of both the roll and the yaw moments. As a result, all sign combinations of $Q_{\gamma a}$ and $Q_{\beta a}$, in general, are not available. This presents an option as to controlling either the roll or the yaw moment and retaining the associated torques in the other degree of freedom. Recognizing that $|Q_{\beta a}| >> |Q_{\gamma a}|$ for small yaw angles β, a large proportion of the total transverse torque may be utilized by selecting the control plates according to the sign required of Q_β. A preliminary investigation of the system performance, however, revealed the effect of the coupled roll moment $Q_{\gamma a}$ to be generally adverse. The roll-yaw control law in the aerodynamic region is, therefore, modified to exercise control action only over those portions of the trajectory where the associated roll moment $Q_{\gamma a}$ is also of the correct sign, the controller being switched 'off' otherwise. The latter may be accomplished by making all the roll-yaw control plates parallel to each other or to the flow

direction (by choosing δ_i so as to render the corresponding $\cos\xi_{ai} = 0$).

The control moments at low altitude thus take the form:

$$Q_\gamma = Q_{\gamma s}(U_1, U_2, \delta_{1a}, \delta_{2a}) + Q_{\gamma a}(U_1, U_2, \delta_{1a}, \delta_{2a}, \delta_{3a}) \quad (5.18a)$$

$$Q_\beta = Q_{\beta s}(U_1, U_2, \delta_{1a}, \delta_{2a}) + Q_{\beta a}(U_1, U_2, \delta_{1a}, \delta_{2a}, \delta_{3a}) \quad (5.18b)$$

$$Q_\lambda = Q_{\lambda s}(\delta_{3a}) + Q_{\lambda a}(\delta_{3a}) \quad (5.18c)$$

The control procedure may be summarized as follows:

(i) sense the roll, yaw and pitch angles and rates, orbital position and the solar aspect angle. Estimate the atmospheric density.

(ii) determine the switch-over point by comparing the magnitudes of the solar and aerodynamic parameters. It may change due to variations in the atmospheric density.

(iii) for pitch control, provide rotation δ_3 determined from Equations (5.13) and (5.16) at high and low altitudes, respectively.

(iv) for roll-yaw control at high altitude, compute $\delta_i (i = 1,2)$ from Equations (5.14) and provide these rotations to the sets of plates resulting in the signs of $Q_{\gamma s}$ and $Q_{\beta s}$ governed by Equation

(5.11). If the proper signs are not available, turn the roll-yaw control plates 'off'. At low altitude, compute δ_i (i = 1,2) from Equations (5.17) and determine the plate sets yielding maximum $Q_{\beta a}$ of the proper sign. If the associated $Q_{\gamma a}$ is of the correct sign, provide these rotations; otherwise, turn the roll-yaw control plates 'off'.

5.3 Results and Discussion

The response of the proposed hybrid control system was studied by numerically integrating the equations of motion (5.1) along with the appropriate control relations (Equations 5.15 or 5.18). The Adams-Bashforth predictor-corrector quadrature with the Runge-Kutta starter was used. A step size of 0.1° at high altitudes and 0.02° at low altitudes gave results of sufficient accuracy. The important system parameters were varied gradually over the range of interest and the controller performance evaluated. For conservative estimate of the controller's performance, it was purposely subjected to severe disturbances.

It should be pointed out here that the atmospheric density depends, in addition to the altitude, on several classes of solar and geophysical phenomena. In the present analysis, density variations due to the latter over a few orbits of the satellite are ignored and a reference atmosphere corresponding to an exospheric temperature of 1250°K is

considered[84]. The value of $\rho_a = 0.74 \times 10^{-14}$ gm/cm^3 at the perigee altitude h_p = 250 miles and the drag coefficient $C_D = 2.2$ yield the ratio $C_{ai}/C_i \simeq 50$. The switch-over point is found to be at an altitude of approximately 500 miles.

5.3.1 Libration Damping

The performance of the controller in damping the librational motion of the satellite is summarized in Figure 5.2 in the form of optimization plots for the controller gain m. The damping time τ_d, defined as the time taken for all the three libration angles to settle within 1° of the desired orientation, is presented as a function of the system gain. Various combinations of the important system parameters and initial conditions are considered. The plots, in general, indicate the existence of an optimum value of the system gain resulting in the minimum settling time.

The influence of the satellite inertia parameter I on the controller performance is indicated by a comparison of curves (a) and (b). A reduction in the damping time with an increased value of I is apparent. Curves (f), (c) and (g) exhibit a similar trend for the case of a larger C_i(=1). The zero settling time in curve (g) simply implies that, with this set of parameters, none of the attitude angles exceeded 1° in amplitude. The advantage of disc-like satellite mass distribution (I > 1) is thus obvious.

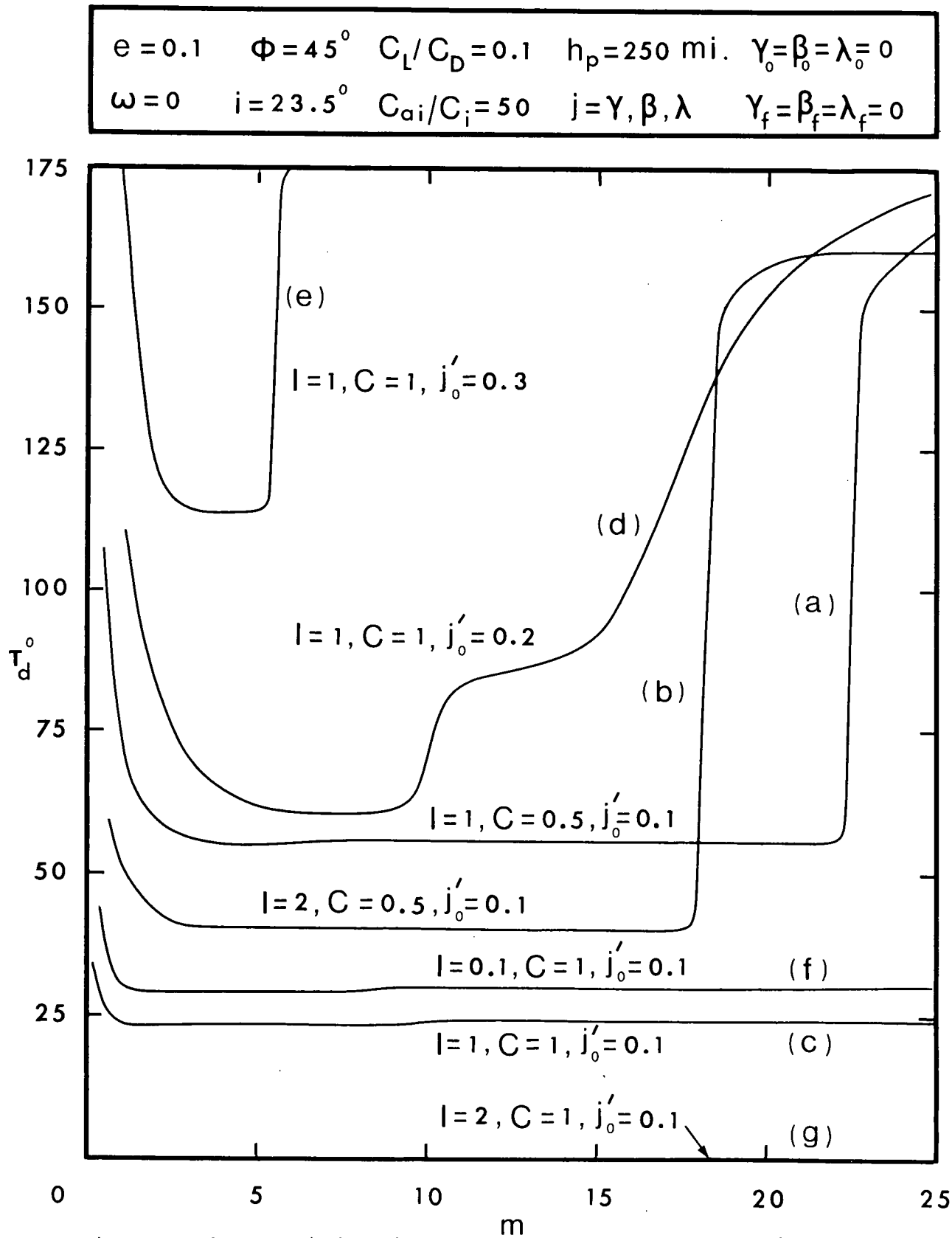

Figure 5.2 Optimization plots for the aerodynamic-solar controller gain m

The effect of the solar parameters C_i and the aerodynamic parameters C_{ai}, which are directly related for a given plate size and moment arm, is shown by curves (a) and (c), and (b) and (g). Increasing the value of C_i leads to a substantial reduction in the damping time. This, of course, can be anticipated as C_i characterize the magnitudes of the control moments available. Their maximum attainable values in practice, however, are constrained due to considerations such as launch, deployment and operation. It is interesting to determine the physical size of the controller yielding a given C_i (or C_{ai}). For example, consider a satellite with the mass properties of the Canadian communications satellite Anik ($I \simeq 1$). A value of $C_i = 1$ ($C_{ai} = 50$) is found to be attainable with plate sizes of about 5' × 5' and moment arms $\varepsilon_i = 10$ ft for a perigee altitude $h_p = 250$ miles.

A comparison of curves (c), (d) and (e) indicates the system performance as affected by the initial impulsive disturbance. As expected, an increased disturbance implies larger damping times. In addition, this results in a leftward shift of the optimum gain m, suggesting the use of a smaller system gain for quick damping of large impulsive disturbances. The optimum gain being dependent on initial conditions, a value of m would have to be selected that promises reasonably good libration damping rates for all initial conditions that the satellite is likely to encounter

in its normal operation. This does not appear to be difficult as for $\gamma'_o = \beta'_o = \lambda'_o \leq 0.2$, which represents an extremely severe disturbance, a large range of values of the system gain m yield near-optimum performance.

Typical damped responses of the satellite are presented in Figure 5.3, with severe initial disturbances applied at different positions of an elliptic trajectory. Figure 5.3a shows the damping of a disturbance encountered at the pericenter. The large aerodynamic yaw and pitch moments restrict the corresponding amplitudes to a negligible value. On the other hand, the satellite executes a small roll oscillation resulting from the relatively smaller roll control torques and occasional loss of roll-yaw control at low altitude. Note the small hump in yaw due to a reduction of control moments in the neighbourhood of the switch-over point ($\theta \simeq 67°$). Figure 5.3b shows the response to a disturbance occuring just before the switch-over point. The satellite traverses a short distance through the aerodynamic region and most of the damping occurs under the influence of solar pressure torques.

Figure 5.3c presents the response to a disturbance applied at the apocenter where solar radiation pressure has the greatest influence. As anticipated, quick libration damping results with the attitude errors settling within 1° in about 30° of the satellite's orbital travel. The same disturbance, applied shortly before the satellite is

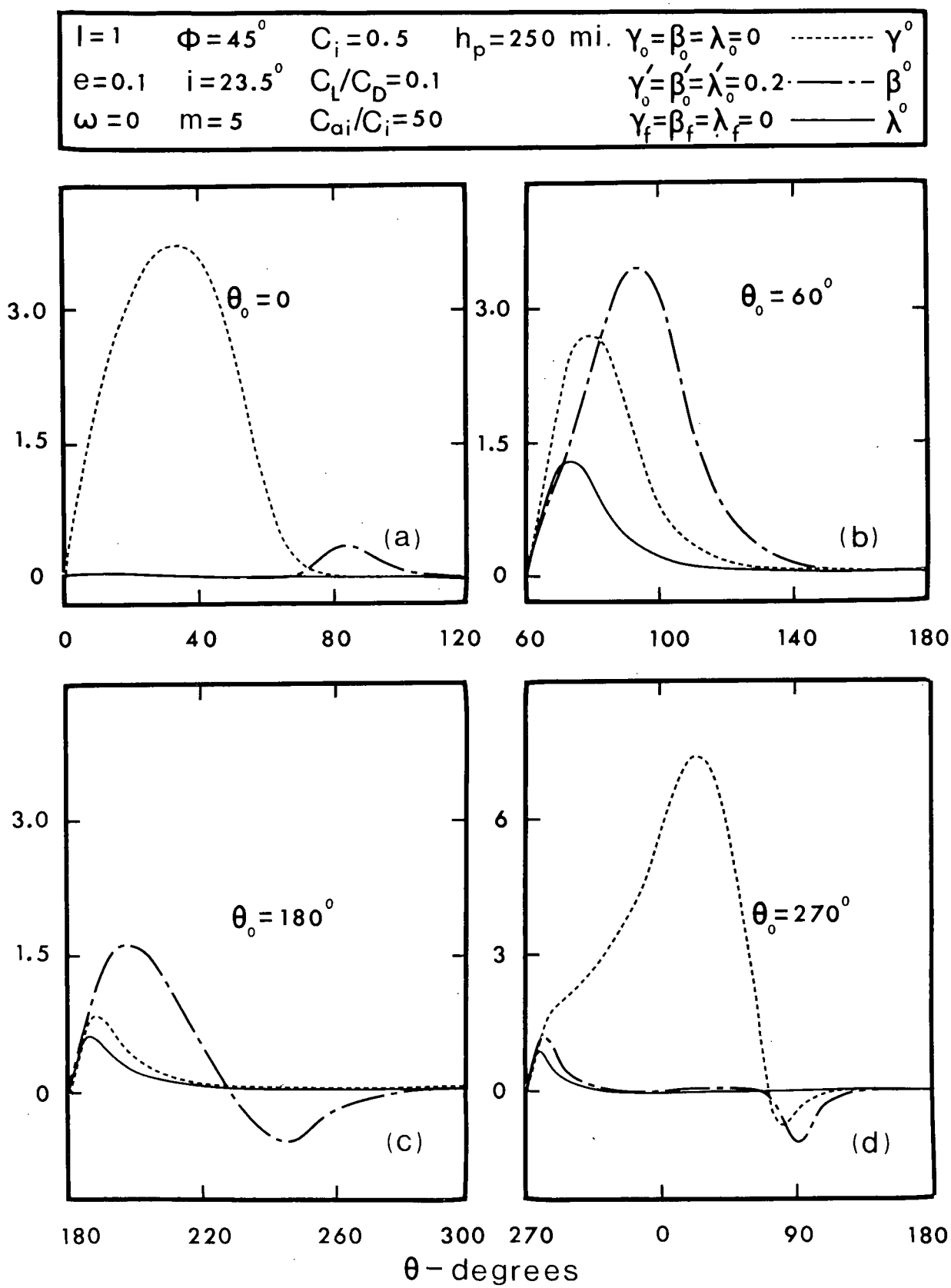

Figure 5.3 Typical responses showing the effectiveness of the aerodynamic-solar controller at different orbital positions

about to re-enter the aerodynamic region, leads to the response indicated in Figure 5.3d. The loss of continuous roll-yaw control in the aerodynamic region is reflected by the relatively larger (≃7°) roll amplitude and the longer damping time.

5.3.2 Attitude control

At times, missions involving diverse objectives may require a satellite to change its preferred orientation in orbit. The controller's ability to impart any desired orientation to the satellite is explored here. Figure 5.4a shows the effectiveness of the control system in providing arbitrary pitch attitudes with the axis of symmetry of the satellite along the orbit normal.

The ability to align the symmetry axis with the local vertical direction and simultaneously attain a desired pitch attitude is indicated in Figure 5.4b for a slender satellite (I = 0.1). For satellites with large I, the controller was able to accomplish the same, but only at the cost of higher values of C_i as it must now overcome the gravity torques in addition to the inertia of the satellite. Note that the attitude angle β represents the planar oscillation in the local vertical configuration. The steady state motion noticeable for the case of e = 0.2, resulting from the eccentricity induced disturbance (Equation 5.1b), indicates the need of a larger value of C_i for its elimination.

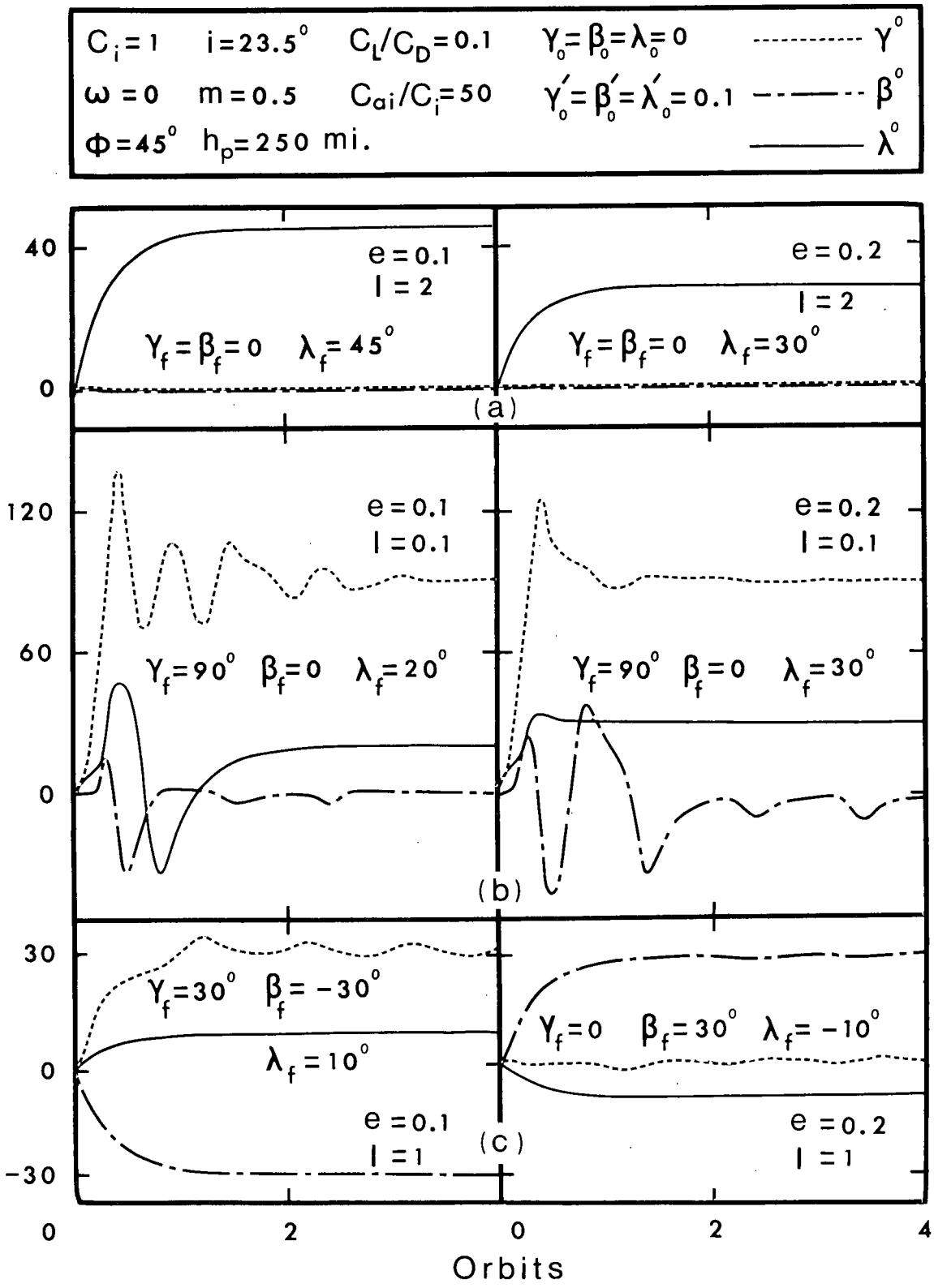

Figure 5.4 Effectiveness of the aerodynamic-solar controller in imparting arbitrary orientations to the satellite

Figure 5.4c presents results for stabilization along arbitrarily chosen values for all the three degrees of freedom.

Finally, a comment concerning the earth's shadow, which would render the controller ineffective in the solar pressure mode, is appropriate here. It is apparent that its effect would be negligible in near-polar orbits. On the other hand, the influence would be maximum for orbits in the plane of the ecliptic. Even in the latter case, the effect of shadow would be of little consequence if the apparent position of the sun is in the neighbourhood of the apocenter as now the control in the shadow region is primarily accomplished aerodynamically. Hence, depending upon the mission, a judicious selection of the location of the line of nodes, orbital inclination from the ecliptic and the perigee argument could effectively minimize the influence of the earth's shadow.

5.4 Concluding Remarks

The significant conclusions based on the analysis may be summarized as follows:

(i) The feasibility of aerodynamic-solar hybrid control of near-earth satellites in elliptical orbits is established.

(ii) The control system is capable of damping extremely severe disturbances in a fraction of an orbit

with the maximum amplitudes during the process limited to a few degrees.

(iii) The controller permits the spacecraft to undertake diverse missions through stabilization along arbitrary attitudes. The pointing accuracies appear to be sufficient for many applications of near-earth satellites.

(iv) The system is essentially semi-active which promises an increased satellite life-span.

6. TIME-OPTIMAL PITCH CONTROL USING SOLAR RADIATION PRESSURE

The investigations presented in the preceding chapters clearly establish the possibility of utilizing the environmental forces to achieve general three-axis librational damping and attitude control. With the control systems offering increased satellite life-times through their semi-passive character, it seems logical to direct efforts at improving their performance. This involves two aspects, namely, physical controller design and efficient control laws. The former having been stressed in the earlier chapters, attention here is directed at the possibility of using optimal control laws.

As the energy required to turn the control plates is low and could be generated easily through the use of solar cells, the performance index need only include the damping time which is of prime concern. Time-optimal control of multi-degree of freedom systems, such as the coupled roll-yaw-pitch motions of a satellite, can generally be achieved only through enormous software complexities since the solution of a two point boundary value problem is involved. This is why switching criteria that are simple functions of the state variables were considered in the earlier analyses. On the other hand, a single degree of freedom system may lend itself to an analytical synthesis of the time-optimal

switching criterion. This is significant as, if successful, it not only could be applied to several situations of practical importance (platform pitch control of a spinning satellite or pure pitch control of a gravity gradient system as in the case of COSMOS-149[70]) but may also suggest switching laws that are likely to be efficient in controlling the general motion.

This chapter investigates the development of the time-optimal control law for the planar pitch motion of a satellite. The utilization of solar radiation pressure for attitude control in a circular orbit is considered. The analysis leads to a useful relationship between the magnitude of the disturbance, control plate areas and moment arms, and the corresponding minimum damping time.

6.1 Formulation of the Problem

Figure 6.1 shows an unsymmetrical satellite executing planar pitch libration ψ, with the center of mass S moving in a circular orbit about the center of force O. The governing equation of motion is well-known,

$$\psi'' + 3K_i \sin\psi\cos\psi = Q_\psi \qquad (6.1)$$

where Q_ψ represents the generalized force due to solar radiation pressure.

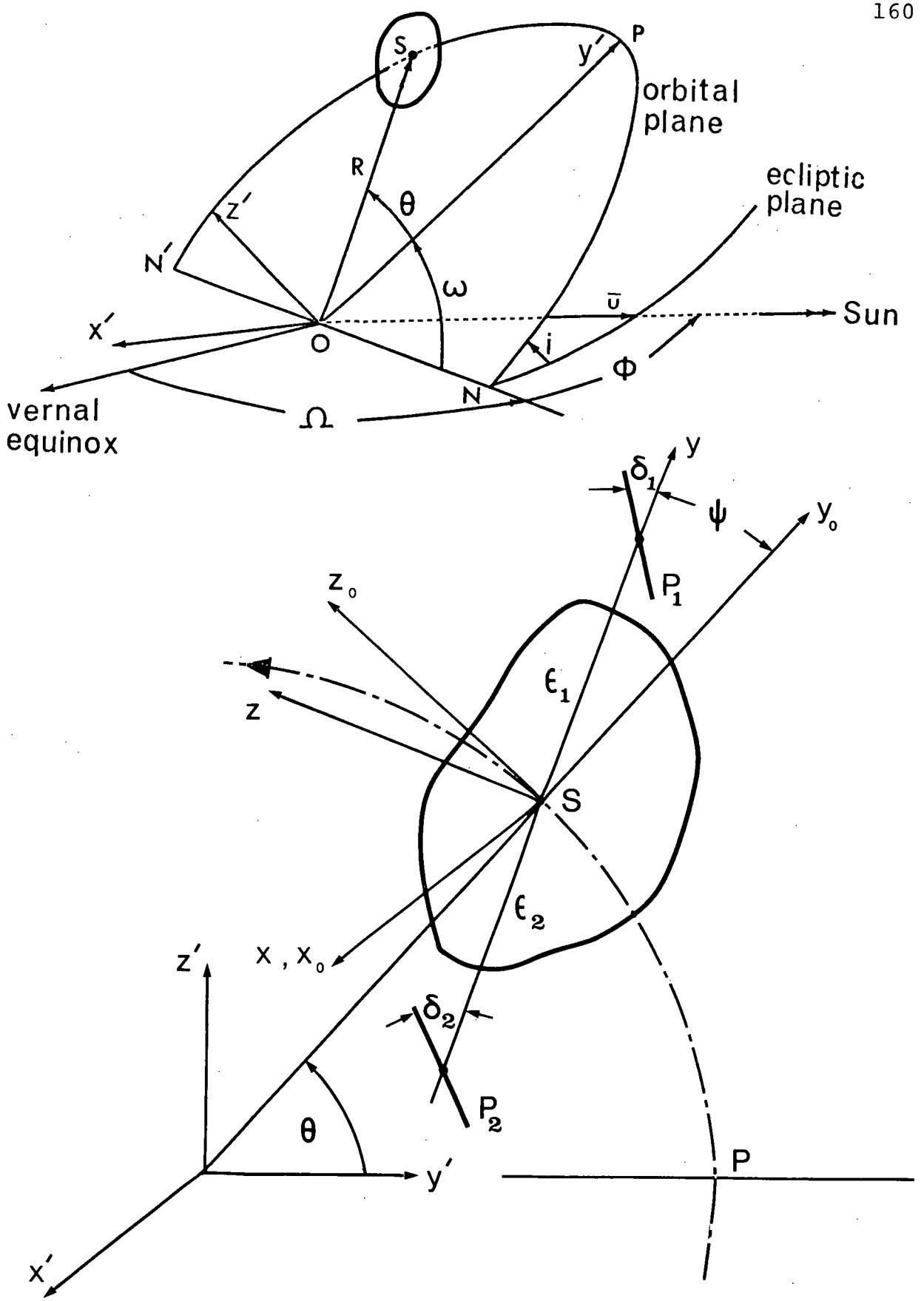

Figure 6.1 Geometry of motion of unsymmetrical satellite in the solar pressure environment

The solar pressure controller consists of two highly reflective control plates P_1 and P_2 which are permitted rotations δ_1 and δ_2, respectively, in the orbital plane. The center of pressure of each plate is taken to lie on the satellite y axis (could be anywhere on the yz-plane) so as to yield a pure pitch moment. The moment generated by the controller is

$$Q_\psi = \pm C_i |\sin(\delta_i+\zeta)| \sin(\delta_i+\zeta)\cos\delta_i, \quad i = 1,2 \qquad (6.2)$$

(+ for P_1, - for P_2)

where the solar parameter is defined as

$$C_i = (2\rho p_o R_p^3/\mu I_x) A_i \varepsilon_i (1-\sin^2\phi \sin^2 i) \qquad (6.3)$$

Through a judicious choice of the plate to be operated (P_1 or P_2), in accordance with the angle $(\delta_i+\zeta)$, Q_ψ may be controlled in sign. The magnitude of the control moment, $|Q_\psi|$, varies with both the angle ζ and the control variable δ_i. Its maximum with respect to δ_i occurs at

$$\delta_{im} = \tan^{-1}[(-3/2)\tan\zeta \pm \{(9/4)\tan^2\zeta+2\}^{1/2}] \qquad (6.4)$$

where the $\pm$ signs apply for $\tan\zeta \gtrless 0$, respectively. The variation of $|Q_\psi|_{max}$ with ζ is shown in Figure 6.2a where

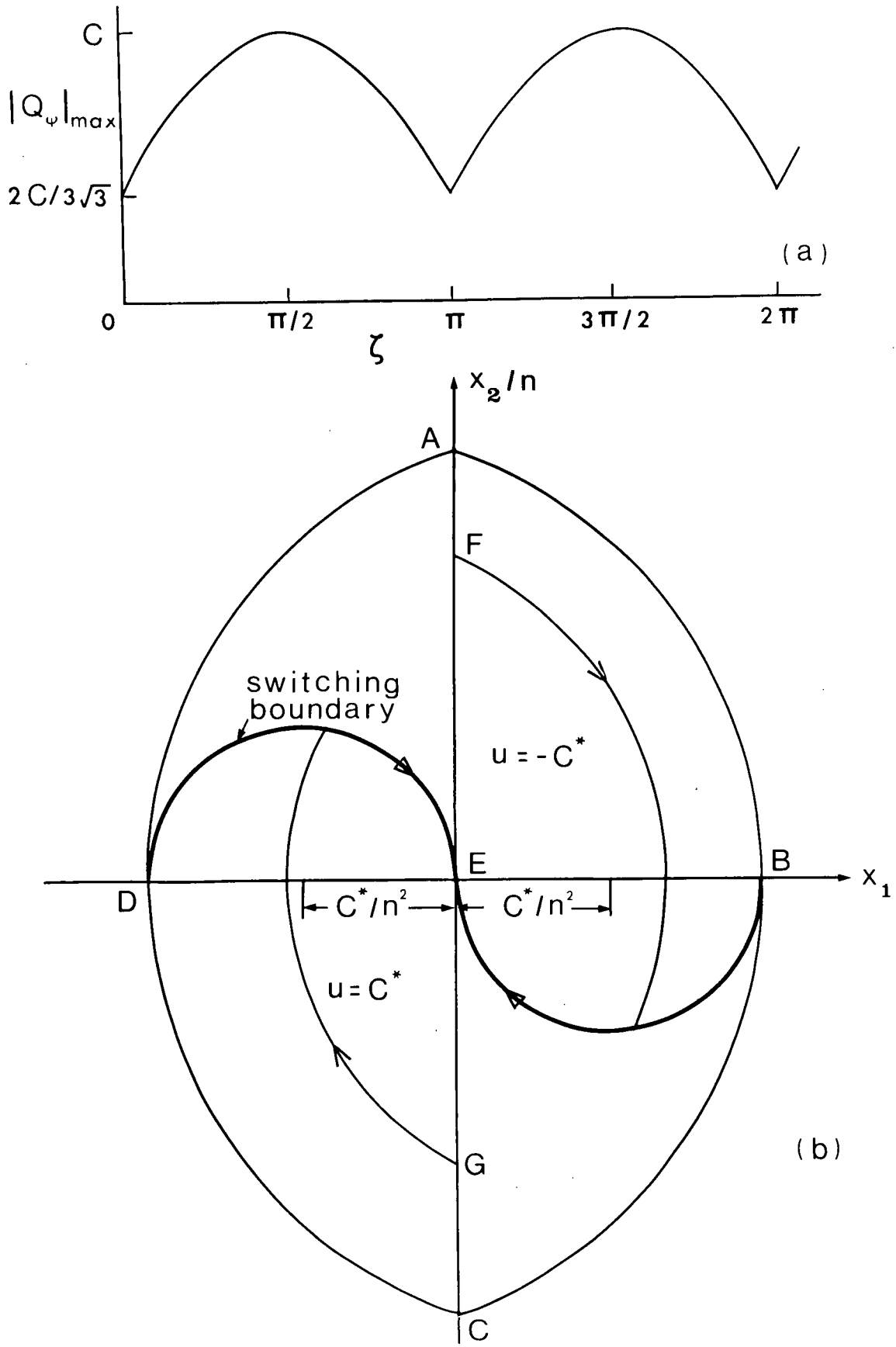

Figure 6.2 (a) Variation of $|Q_\psi|_{max}$ with ζ; (b) Phase plane portrait of the system

$C_1 = C_2 = C$ is assumed for convenience. The system is able to provide a value $|Q_\psi|_{max} = (2/3\sqrt{3})C$ at all times. The governing equation of motion (6.1) may thus be presented as

$$\psi'' + 3K_i \sin\psi\cos\psi = u(\theta) \tag{6.5}$$

with

$$-(2/3\sqrt{3})C - 3K_i \sin\psi_e\cos\psi_e \leq u(\theta) \leq (2/3\sqrt{3})C - 3K_i \sin\psi_e\cos\psi_e$$

A symmetrical band on the control,

$$|u(\theta)| \leq C^* = (2/3\sqrt{3})C - |3K_i \sin\psi_e\cos\psi_e|, \tag{6.6}$$

is considered here for convenience. Its effect is only to yield a slightly conservative bound on the control either on the plus or the minus side depending on the nominal attitude ψ_e.

6.2 Time-Optimal Synthesis

Using the state variables $x_1 = \psi$ and $x_2 = \psi'$, and linearizing about the nominal attitude $\psi = \psi_e$, the system (6.5) can be expressed in the form,

$$\underline{x}' = A\underline{x} + B\underline{u} \tag{6.7}$$

where

$$A = \begin{bmatrix} 0 & 1 \\ -n^2 & 0 \end{bmatrix} \qquad B = \begin{bmatrix} 0 \\ 1 \end{bmatrix} \quad \text{and} \quad |u(\theta)| \leq C^*$$

Taking the initial time $\theta_o = 0$, the state-transition matrix $\Phi(\theta)$ is obtained as

$$\Phi(\theta) = \begin{bmatrix} \cos n\theta & (1/n)\sin n\theta \\ -n\sin n\theta & \cos n\theta \end{bmatrix} \tag{6.8}$$

The solution for the system of Equation (6.7) then becomes,

$$\underline{x}(\theta) = \Phi(\theta)\underline{x}(0) + \int_0^{\theta} \Phi(\theta-\tau)B\underline{u}(\tau)d\tau \tag{6.9}$$

A control $\underline{u}(\tau)$ is sought which will bring the system state from $\underline{x}(0)$ to $\underline{x}(\theta_f) = \underline{0}$ in minimum θ_f. Substituting the initial and the final states in Equation (6.9) results in

$$\int_0^{\theta_f} \Phi(-\tau)B\underline{u}(\tau)d\tau = -\underline{x}(0) \tag{6.10}$$

The solution for $\underline{u}(\theta)$ bringing the system state to rest in minimum θ_f is well-known to be $u(\theta) = \pm C^*$, with the number of switches depending upon the initial state of the system[85]. Considering initial states that can be driven to rest in a single switch, the control takes the form

$$u(\theta) = K_1, \quad 0 \leq \theta < \theta_s$$
$$u(\theta) = K_2, \quad \theta_s \leq \theta \leq \theta_f \tag{6.11}$$

where

$$|K_1| = |K_2| = C^*.$$

Substituting for $u(\theta)$ in Equation (6.10) leads to:

$$K_1 = n\{-nx_1(0)(\sin n\theta_f - \sin n\theta_s) + x_2(0)(\cos n\theta_f - \cos n\theta_s)\}/\Delta \tag{6.12a}$$

$$K_2 = n\{nx_1(0)\sin n\theta_s + x_2(0)(1-\cos n\theta_s)\}/\Delta \tag{6.12b}$$

where

$$\Delta = \sin(n\theta_f - n\theta_s) - \sin n\theta_f + \sin n\theta_s$$

The proper signs of K_1 and K_2 are best obtained from the phase plane portrait of the optimally controlled system (Figure 6.2b). The trajectories are circular arcs with centers at $x_1 = \pm C^*/n^2$, $x_2 = 0$ for $u = \pm C^*$, respectively. The switching boundary is composed of semi-circles passing through the origin. For any initial condition $\underline{x}(0)$, the

system state moves on the switching boundary for $\theta_s \leq \theta \leq \theta_f$ as shown in the figure. It is apparent that all initial states lying within the region ABCDA of the phase diagram can be driven to the origin with a single switch of the control. For optimal response, the control $u(\theta)$ assumes the value $u = -C^*$ if the system state lies above the switching boundary and $u = +C^*$ if it is below the switching boundary.

Equations (6.12) may now be solved to obtain the switching time θ_s and the final time θ_f for a given initial condition. This yields the open-loop realization of the control in the form $u = u(\theta)$. On the other hand, use of the switching boundary yields the feedback realization $u = u(\underline{x})$, which makes the system self-correcting to slight deviations of the state vector.

Of particular interest are impulsive disturbances which a satellite is likely to encounter through, say, micrometeorite impacts. The phase portrait immediately yields the maximum impulsive disturbance from which the satellite can be brought to rest in a single switch of the control and the error amplitude during the process as:

$$|\tilde{x}_2(0)|_{max} = 2\sqrt{2} \tag{6.13a}$$

$$|\tilde{x}_1(\theta)|_{max} = \{1+\tilde{x}_2^2(0)\}^{1/2}-1 \tag{6.13b}$$

where the normalized state variables $\tilde{x}_1$ and $\tilde{x}_2$ are defined as

$$\tilde{x}_1(\theta) = n^2 x_1(\theta)/C^* \tag{6.13c}$$

$$\tilde{x}_2(\theta) = n\, x_2(\theta)/C^* \tag{6.13d}$$

The variation of the normalized error amplitude with the initial impulsive disturbance is shown in Figure 6.3a. The switching and the final times obtained by solving Equations (6.12) are also presented as functions of the impulsive disturbance (Figure 6.3b).

6.3 Results and Discussion

In order to ascertain the applicability of the optimal control law synthesized from linear theory to the actual nonlinear system, the response of both the linearized and nonlinear equations governing the motion was evaluated. The two systems were subjected to the same disturbance and control.

Figures (6.4a and b) show response plots indicating the effect of the inertia parameter to be negligible for the pitch attitude nominally along the local vertical. As anticipated, the open-loop and the feedback response of the linear system are identical. On the other hand, the open-loop control system is unable to bring the nonlinear system to rest exactly. The feedback system, however, accomplishes

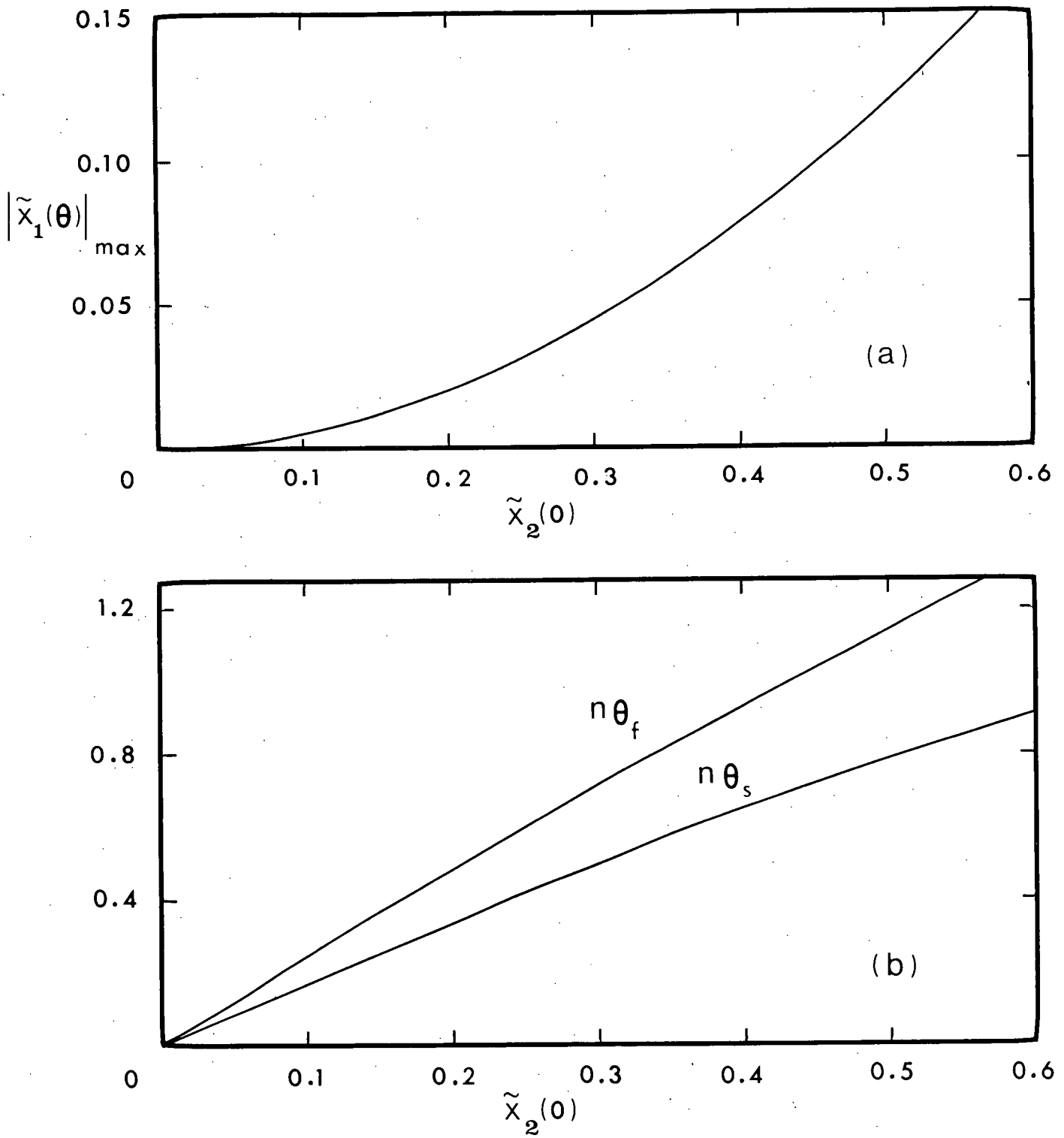

Figure 6.3 (a) Variation of transient amplitude $|\tilde{x}_1(\theta)|_{max}$ with initial condition $\tilde{x}_2(0)$; (b) Variation of switching time θ_s and final time θ_f with initial condition $\tilde{x}_2(0)$

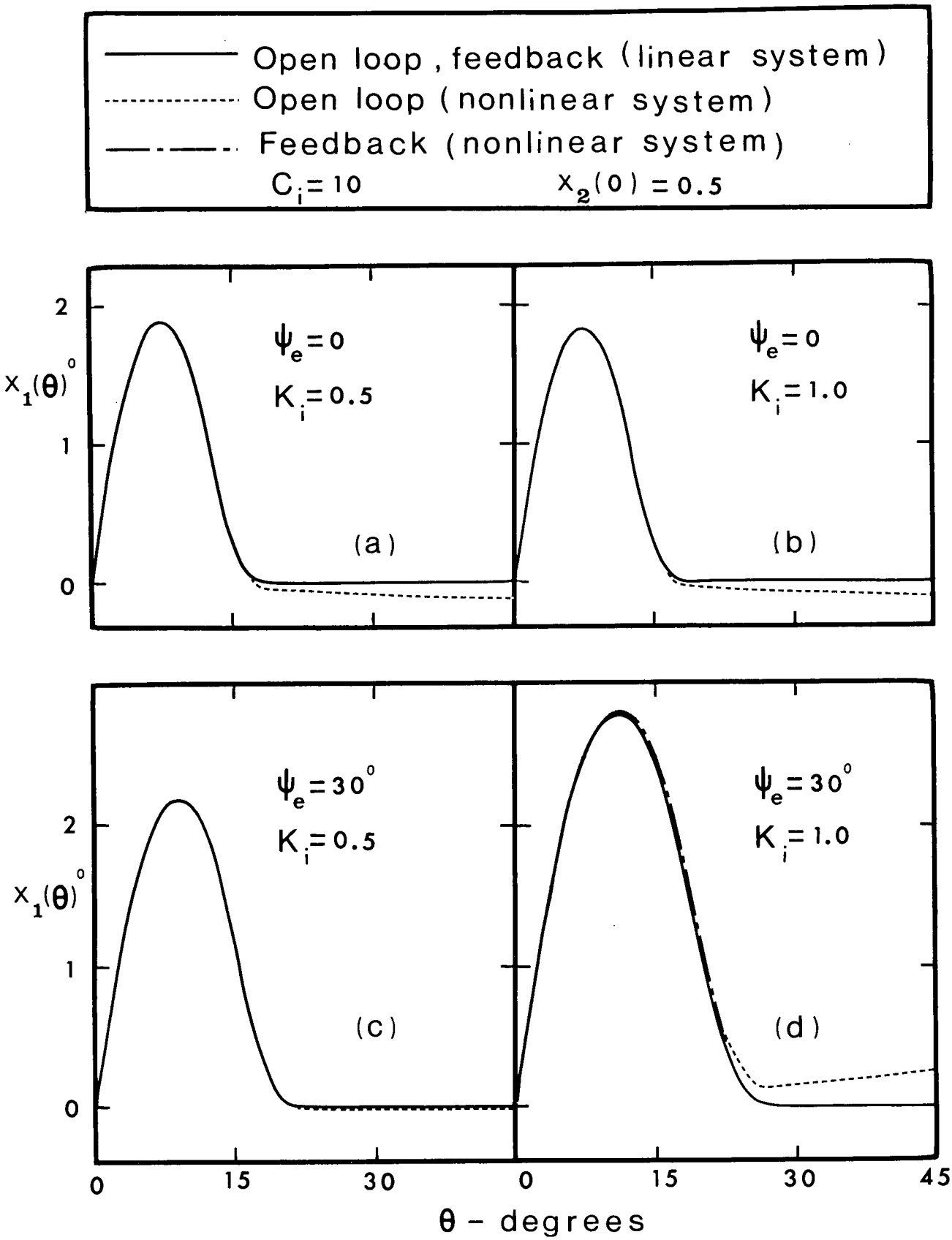

Figure 6.4 System response to impulsive disturbance

this, the nonlinear system state approaching the origin asymptotically using a number of switches of the control. In order to avoid any relay-chatter, it appears advisable to use only a single switch for the actual nonlinear system as well and employ a passive device to damp the small residual motion in the neighbourhood of the origin.

Figures 6.4c and d present the system response for a satellite stabilized in an arbitrary pitch attitude. Note that the gravity gradient torque now represents a destabilizing effect, which the controller must neutralize in addition to countering the disturbance. The longer damping time required with a higher value of the inertia parameter clearly reflects a greater reduction in the value of C^* for increased K_i.

The system response may now be projected for the pitch control of the CTS. At synchronous altitude, the value of $C_i \simeq 10$ corresponds to $A_i \simeq 2.5$ ft^2 and $\varepsilon_i = 10$ ft. When subjected to an extremely severe impulsive disturbance of $x_2(0) = 0.5$, a damping time of the order of 20° of the orbit is attained (Figure 6.4). A disturbance $x_2(0) = 0.1$ on the other hand would be damped out in approximately 4°. (Figure 6.3b). The system thus appears promising.

It should be pointed out here that the constraint $|Q_\psi| \leq (2/3\sqrt{3})C$ represents the most adverse situation as $|Q_\psi|$ may attain a value as large as C during certain orbital positions (Figure 6.2a). The performance of the controller,

therefore, would always exceed the responses presented here (Figure 6.4).

6.4 Concluding Remarks

(i) The analysis clearly demonstrates the feasibility of the time-optimal pitch control of satellites using the solar pressure.

(ii) The controller is capable of damping extremely severe disturbances in a few degrees of the satellite's orbital travel. The transient amplitude is also small.

(iii) The controller is able to provide nominal control at an orientation which is not an equilibrium position of the uncontrolled system.

(iv) The optimal control strategy, developed for the linearized system, may be applied effectively to the actual nonlinear system.

7. CLOSING COMMENTS

7.1 Summary of the Conclusions

The significant conclusions based on the preceding investigation may be summarized as follows:

(i) The solar radiation pressure, normally neglected in the analysis of spinning satellites, can affect the librational performance substantially. It merits the same consideration as the inertia properties, spin rate and eccentricity during the design of an attitude control system.

(ii) The environmental forces can be used quite effectively to provide three-axis libration damping and attitude control of spinning spacecraft.

(iii) As substantial control moments are available even with the use of moderate controller sizes, it does not appear necessary to spin a satellite from attitude control considerations. Of course, the presence of spin would improve the nutation damping performance.

(iv) A logical procedure is established for the development of an effective solar pressure control system. This should prove useful in evolving a suitable controller depending upon the mission requirements.

(v) The magnetic roll-yaw controller, in conjunction with the solar pitch controller, provides an efficient three-axis control system.

(vi) The hydrid aerodynamic-solar system offers effective control of near-earth satellites in elliptic trajectories which promise an increased life-span.

(vii) Utilization of the maximum available control moments, through bang-bang operation, leads to smaller damping times compared to the linear control law with saturation constraints. The near-optimum performance resulting for a wide range of system parameters and initial disturbances is particularly attractive.

(viii) Approximate analytical techniques can be used quite effectively during preliminary stages of satellite design. For small amplitude motion, usually the case of interest, they can predict the libration amplitude and frequency with considerable accuracy.

(ix) The attitude control systems analyzed here are semi-passive, as they do not involve any mass expulsion schemes and/or active gyros requiring large power consumption. This promises an increased satellite life-span.

7.2 Recommendations for Future Work

The investigation reported here suggests several topics for future exploration. Only some of the important problems are mentioned here:

(i) The feasibility of using environmental forces to advantage having been established here, it appears logical to direct efforts at improving the efficiency of these systems. The design approach suggested in Chapter 3 could be applied to devise alternative controller configurations. An extension of the approach in Chapter 6 to the synthesis of optimal or suboptimal control laws for the coupled motion is likely to improve the control performance.

(ii) A detailed hardware oriented study would permit precise comparison of the methods proposed here with the currently used active control systems. Such analyses should also include any inertia variations and reaction forces arising from control system operation.

(iii) With ever increasing energy requirements, the use of large solar panels by the future generation of satellites is likely to be indispensable. Substantial energy savings may result if the semi-

passive attitude control systems utilizing the environmental forces could be extended to flexible satellite configurations. The dynamical problem is going to be more involved. Hence, more sophisticated controllers and control strategies would be required as the disturbances, such as, panel vibration, differential thermal heating, etc., are of the continuous type. The problem appears to be quite useful as well as challenging.

(iv) The possibility of employing the environmental forces for orbital transfer and trajectory control appears interesting. As the concept promises considerable energy saving and reduction in payload (no mass expulsion is required), it could be of immense value in interplanetary travel as well where long time durations are involved. It presents an exciting possibility of achieving controlled variations in the orbital parameters of a space-vehicle. Optimization of system performance in the foregoing represents a vast challenging area that has remained virtually unexplored.

BIBLIOGRAPHY

1. Thomson, W.T., "Spin Stabilization of Attitude against Gravity Torques," The Journal of the Astronautical Sciences, Vol. 9, No. 1, January 1962, pp. 31-33.

2. Pringle, R., Jr., "Bounds on the Librations of a Symmetrical Satellite," AIAA Journal, Vol. 2, No. 5, May 1964, pp. 908-912.

3. Kane, T.R. and Shippy, D.J., "Attitude Stability of a Spinning Unsymmetrical Satellite in a Circular Orbit," The Journal of the Astronautical Sciences, Vol. 10, No. 4, Winter 1963, pp. 114-119.

4. Kane, T.R. and Barba, P.M., "Attitude Stability of a Spinning Satellite in an Elliptic Orbit," Journal of Applied Mechanics, Vol. 33, June 1966, pp. 402-405.

5. Wallace, F.B., Jr., and Meirovitch, L., "Attitude Instability Regions of a Spinning Symmetric Satellite in an Elliptic Orbit," AIAA Journal, Vol. 5, No. 9, September 1967, pp. 1642-1650.

6. Neilson, J.E., "On the Attitude Dynamics of Slowly-Spinning Axisymmetric Satellites under the Influence of Gravity-Gradient Torques," Ph.D. Thesis, University of British Columbia, November 1968.

7. Modi, V.J. and Neilson, J.E. "Attitude Dynamics of Slowly-Spinning Axisymmetric Satellites under the Influence of Gravity-Gradient Torques," Proceedings of the xxth International Astronautical Congress, Pergamon Press Ltd., Oxford, 1972, pp. 563-596.

8. Modi, V.J. and Neilson, J.E. "Roll Dynamics of a Spinning Axisymmetric Satellite in an Elliptic Orbit," Journal of the Royal Aeronautical Society, Vol. 72, No. 696, December 1968, pp. 1061-1065.

9. Modi, V.J. and Neilson, J.E. "On the Periodic Solutions of Slowly-Spinning Gravity-Gradient Systems," Celestial Mechanics - An International Journal of Space Dynamics, Vol. 5, No. 2, 1972, pp. 126-143.

10. Likins, P.W., "Effects of Energy Dissipation on the Free-Body Motions of Spacecrafts," No. 32-860, Jet Propulsion Laboratory Technical Report, 1966.

11. Roberson, R.E., "Torques on a Satellite Vehicle from Internal Moving Parts," Journal of Applied Mechanics, Vol. 25, 1958, pp. 196-200.

12. Landon, V.D. and Stewart, B., "Nutational Stability of an Axisymmetric Body Containing a Rotor," Journal of Spacecraft and Rockets, Vol. 1, No. 6, December 1964, pp. 682-684.

13. Iorillo, A.J., "Nutation Damping Dynamics of Axisymmetric Rotor Stabilized Satellites," American Society of Mechanical Engineers, Winter Meeting, November 1965.

14. Likins, P.W., "Attitude Stability Criteria for Dual-Spin Spacecraft," Journal of Spacecraft and Rockets, Vol. 4, No. 12, December 1967, pp. 1638-1643.

15. Mingori, D.L., "Effects of Energy Dissipation on the Attitude Stability of Dual-Spin Satellites," AIAA Journal, Vol. 7, No. 1, January 1969, pp. 20-27.

16. Pringle, R., Jr., "Stability of the Force-Free Motions of a Dual-Spin Spacecraft," AIAA Journal, Vol. 7, No. 6, June 1969, pp. 1054-1063.

17. Cloutier, G.J., "Stable Rotation States of Dual-Spin Spacecraft," Journal of Spacecraft and Rockets, Vol. 5, No. 4, April 1968, pp. 490-92.

18. Cloutier, G.J., "Nutation Damper Design Principles for Dual-Spin Spacecraft," The Journal of the Astronautical Sciences, Vol. 16, No. 2, March-April 1969, pp. 79-87.

19. Sen, A.K., "Stability of a Dual-Spin Satellite with a Four-Mass Nutation Damper," AIAA Journal, Vol. 8, No. 4, April 1970, pp. 822-823.

20. Vigneron, F.R., "Stability of a Dual-Spin Satellite with Two Dampers," Journal of Spacecraft and Rockets, Vol. 8, No. 4, April 1971, pp. 386-389.

21. Bainum, P.M., Fuechsel, P.G., and Mackison, D.L. "Motion and Stability of a Dual-Spin Satellite with Nutation Damping," Journal of Spacecraft and Rockets, Vol. 7, No. 6, June 1970, pp. 690-696.

22. Bainum, P.M., Fuechsel, P.G., and Fedor, J.V., "Stability of a Dual-Spin Spacecraft with a Flexible Momentum Wheel," Journal of Spacecraft and Rockets, Vol. 9, No. 9, September 1972, pp. 640-646.

23. Kane, T.R. and Scher, M.P., "A Method of Active Control Based on Energy Considerations," Journal of Spacecraft and Rockets, Vol. 6, No. 5, May 1969, pp. 633-636.

24. Mingori, D.L., Harrison, J.A.,and Tseng, G.T., "Semipassive and Active Nutation Dampers for Dual-Spin Spacecraft," Journal of Spacecraft and Rockets, Vol. 8, No. 9, May 1971, pp. 448-455.

25. Kane, T.R. and Mingori, D.L., "Effect of a Rotor on the Attitude Stability of a Satellite in a Circular Orbit," AIAA Journal, Vol. 3, No. 5, May 1965, pp. 936-940.

26. White, E.W. and Likins, P.W., "The Influence of Gravity Torque on Dual-Spin Satellite Attitude Stability," The Journal of the Astronautical Sciences, Vol. 16, No. 1, January-February 1969, pp. 32-37.

27. Roberson, R.E. and Hooker, W.W., "Gravitational Equilibria of a Rigid Body Containing Symmetric Rotors," Proceedings of the xviith International Astronautical Congress, Gordon and Breach Inc., New York, 1967, pp. 203-210.

28. Longman, R.W. and Roberson, R.E., "General Solutions for the Equilibria of Orbiting Gyrostats Subject to Gravitational Torques," The Journal of the Astronautical Sciences, Vol. 16, No. 2, March-April 1969, pp. 49-58.

29. Yu, E.Y., "Attitude Stability of an Orbiting Vehicle Containing a Gyrostat," Journal of Spacecraft and Rockets, Vol. 6, No. 8, August 1969, pp. 948-951.

30. Proceedings of the Symposium on Attitude Stabilization and Control of Dual-Spin Spacecraft, TR 0158(3307-01) -16, November 1967, Aerospace Corp., El Segundo, Calif., pp. 73-109.

31. Johnson, C.R., "Tacsat 1 Nutation Dynamics," AIAA Paper 70-455, Los Angeles, Calif., 1970.

32. Likins, P.W., Tseng, G.T., and Mingori, D.L., "Stable Limit Cycles due to Nonlinear Damping in Dual-Spin Spacecraft," Journal of Spacecraft and Rockets, Vol. 8, No. 6, June 1971, pp. 568-574.

33. Mingori, D.L., Tseng, G.T., and Likins, P.W., "Constant and Variable Amplitude Limit Cycles in Dual-Spin Spacecraft," Journal of Spacecraft and Rockets, Vol. 9, No. 11, November 1972, pp. 825-830.

34. Proceedings of the Symposium on Gravity Gradient Attitude Stabilization, The Aerospace Corp., December 1968.

35. Shrivastava, S.K., Tschann, C., and Modi, V.J., "Librational Dynamics of Earth Orbiting Satellites - A Brief Review," Proceedings XIV Congress of Theoretical and Applied Mechanics, Indian Society of Theoretical and Applied Mechanics, Kharagpur, December 1969, pp. 284-306.

36. Roberson, R.E., "Attitude Control of a Satellite Vehicle - An Outline of the Problem," Proceedings of the VIIIth International Astronautical Congress, Wein-Springer-Verlag, Berlin, 1958, pp. 317-319.

37. Wiggins, L.E., "Relative Magnitudes of the Space-Environment Torques on a Satellite," AIAA Journal, Vol. 2, No. 4, April 1964, pp. 770-771.

38. Clancy, T.F. and Mitchell, T.P., "Effects of Radiation Forces on the Attitude of an Artificial Earth Satellite," AIAA Journal, Vol. 2, No. 3, March 1964, pp. 517-524.

39. Modi, V.J. and Flanagan, R.C., "Effect of Environmental Forces on the Attitude Dynamics of Gravity Oriented Satellites: Part I - High Altitude Orbits," Aeronautical Journal, Royal Aeronautical Society, Vo. 75, November 1971, pp. 783-793.

40. Modi, V.J. and Kumar, K., "Librational Dynamics of Gravity Oriented Satellites under the Influence of Solar Radiation Pressure," Proceedings of the International Symposium on Computer-Aided Engineering, University of Waterloo, May 1971, pp. 359-377.

41. Debra, D.B., "The Effect of Atmospheric Forces on Satellite Attitude," The Journal of Aeronautical Sciences, Vol. 6, 1959, pp. 40-45.

42. Schrello, D.M., "Aerodynamic Influence on Satellite Librations," ARS Journal, Vol. 31, No. 3, March 1961, pp. 442-444.

43. Garber, T.B., "Influence of Constant Disturbance Torques on the Motion of Gravity Gradient Stabilized Satellites," AIAA Journal, Vol. 1, No. 4, 1963, pp. 968-969.

44. Meirovitch, L. and Wallace, F.B., Jr., "On the Effect of Aerodynamic and Gravitational Torques on the Attitude Stability of Satellites," AIAA Journal, Vol. 4, No. 12, December 1966, pp. 2196-2202.

45. Garwin, R.L., "Solar Sailing - A Practical Method of Propulsion Within the Solar System," Jet Propulsion, Vol. 28, No. 3, March 1958, pp. 188-190.

46. Sohn, R.L., "Attitude Stabilization by Means of Solar Radiation Pressure," ARS Journal, Vol. 29, No. 5, 1959, pp. 371-373.

47. Galitskaya, E.B. and Kiselev, M.I., "Radiation Control of the Orientation of Space Probes," Cosmic Research, Vol. 3, No. 3, May-June 1965, pp. 298-301.

48. Mallach, E.G., "Solar Pressure Damping of the Librations of a Gravity Oriented Satellite," AIAA Student Journal, Vol. 4, No. 4, December 1966, pp. 143-147.

49. Modi, V.J. and Flanagan, R.C., "Librational Damping of a Gravity Oriented System using Solar Radiation Pressure," Aeronautical Journal, Royal Aeronautical Society, Vol. 75, No. 728, August 1971, pp. 560-564.

50. Modi, V.J. and Tschann, C., "On the Attitude and Librational Control of a Satellite using Solar Radiation Pressure," Astronautical Research 1970, Proceedings of the XXI Congress of the International Astronautical Federation, Editor-in-chief: L.G. Napolitano, North-Holland Publishing Co., Amsterdam, 1971, pp. 84-100.

51. Modi, V.J. and Kumar, K., "Coupled Librational Dynamics and Attitude Control of Satellites in Presence of Solar Radiation Pressure," Astronautical Research 1971, Proceedings of the XXII Congress of the International Astronautical Federation, Editor-in-chief: L.G. Napolitano, D. Reidel Publishing Co., Dordrecht, Holland, 1973, pp. 37-52.

52. Ule, L.A., "Orientation of Spinning Satellites by Radiation Pressure," AIAA Journal, Vol. 1, No. 7, July 1963, pp. 1575-1578.

53. Peterson, C.A., "Use of Thermal Re-Radiative Effects in Spacecraft Attitude Control," CSR-TR-66-3, May 1966, Massachusetts Institute of Technology Center for Space Research, Cambridge, Mass.

54. Colombo, G., "Passive Stabilization of a Sunblazer Probe by Means of Radiation Pressure Torque," CSR-TR-66-5, 1966, Massachusetts Institute of Technology Center for Space Research, Cambridge, Mass.

55. Falcovitz, J., "Attitude Control of a Spinning Sun-Orbiting Spacecraft by Means of a Grated Solar Soil," CSR-TR-66-17, December 1966, Massachusetts Institute of Technology Center for Space Research, Cambridge, Mass.

56. Crocker, M.C. II, "Attitude Control of a Sun-Pointing Spinning Spacecraft by Means of Solar Radiation Pressure," Journal of Spacecraft and Rockets," Vol. 7, No. 3, March 1970, pp. 357-359.

57. Scull, J.R., "Mariner IV Revisited, or the Tale of the Ancient Mariner," presented at the 20th Congress of the International Astronautical Federation, Argentina, October 1969.

58. Alper, J.R. and O'Neill, J.P., "A New Passive Hysteresis Damping Technique for Stabilizing Gravity-Oriented Satellites," Journal of Spacecraft and Rockets, Vol. 4, No. 12, December 1967, pp. 1617-1622.

59. Bainum, P.M. and Mackison, D.L., "Gravity-Gradient Stabilization of Synchronous Orbiting Satellites," Journal of the British Interplanetary Society, Vol. 21, 1968, pp. 341-369.

60. Vrablik, E.A., Black, W.L., and Travis, L.J., "LES-4 Spin Axis Orientation System," TN 1965-48, 1965, Lincoln Lab., Massachusetts Institute of Technology, Cambridge, Mass.

61. Sonnabend, D., "A Magnetic Control System for an Earth Pointing Satellite," Proceedings of the Symposium on Attitude Stabilization and Control of Dual-Spin Spacecraft, Rept. RT-0158(3307-01)-16, November 1967, Aerospace Corp., El Segundo, Calif., pp. 121-144.

62. Fischell, R.E., "Spin Control for Earth Satellites," Peaceful Uses of Automation in Outer Space, edited by J.A. Aseltine, Plenum Press, New York, 1966, pp. 211-218.

63. Wheeler, P.C., "Spinning Spacecraft Attitude Control via the Environmental Magnetic Field," Journal of Spacecraft and Rockets, Vol. 4, No. 12, December 1967, pp. 1631-1637.

64. Sorensen, J.A., "A Magnetic Attitude Control System for an Axisymmetric Spinning Spacecraft," Journal of Spacecraft and Rockets, Vol. 8, No. 5, May 1971, pp. 441-448.

65. Shigehara, M., "Geomagnetic Attitude Control of an Axisymmetric Spinning Satellite," Journal of Spacecraft and Rockets, Vol. 9, No. 6, June 1972, pp. 391-398.

66. Hecht, E. and Manger, W.P., "Magnetic Attitude Control of the TIROS Satellites," Torques and Attitude Sensing in Earth Satellites, edited by S. Fred Singer, Academic Press, New York, 1964, pp. 127-135.

67. Lindorfer, W. and Muhlfelder, L., "Attitude and Spin Control for TIROS Wheel," AIAA/JACC Guidance and Control Conference, Seattle, Wash., 1966, pp. 448-461.

68. Wall, J.K., "The Feasibility of Aerodynamic Attitude Stabilization of a Satellite Vehicle," presented at ARS Controllable Satellite Conference, M.I.T., April 1959.

69. Schrello, D.M., "Passive Aerodynamic Attitude Stabilization of Near Earth Satellites, Vol. I, Libration due to Combined Aerodynamic and Gravitational Torques," WADD Tech. Report 61-133, Vol. I, July 1961.

70. Sarychev, V.A., "Aerodynamic Stabilization System of the Satellites," Proceedings of the International Colloquium on Attitude Changes and Stabilization of Satellite, Paris, October 1968, pp. 177-179.

71. Ravindran, R., "Optimal Aerodynamic Attitude Stabilization of Near Earth Satellites, Ph.D. Thesis, University of Toronto, April 1971.

72. Modi, V.J. and Shrivastava, S.K., "On Librations of Gravity-Oriented Satellites in Elliptic Orbits through Atmosphere," AIAA Journal, Vol. 9, No. 11, November 1971, pp. 2208-2216.

73. Modi, V.J. and Shrivastava, S.K., "On the Optimized Performance of a Semi-Passive Aerodynamic Controller," AIAA Journal, Vol. 11, No. 8, August 1973, pp. 1080-1085.

74. Butenin, N.V., Elements of the Theory of Nonlinear Oscillations, Blaisdell Publishing Company, New York, 1965, pp. 201-217.

75. Modi, V.J. and Brereton, R.C., "Periodic Solutions Associated with the Gravity-Gradient-Oriented System. Part I: Analytical and Numerical Determination," AIAA Journal, Vol. 7, No. 7, July 1969, pp. 1217-1225.

76. Modi, V.J. and Brereton, R.C., "Periodic Solutions Associated with the Gravity-Gradient-Oriented System. Part II: Stability Analysis," AIAA Journal, Vol. 7, No. 8, August 1969, pp. 1465-1468.

77. Minorsky, N., Nonlinear Oscillations, D. Van Norstrand Company Inc., Princeton, 1962, pp. 127-133, 390-415.

78. Moran, J.P., "Effects of Plane Librations on the Orbital Motion of a Dumbbell Satellite," ARS Journal, Vol. 31, No. 8, August 1961, pp. 1089-1096.

79. Yu, E.Y., "Long-Term Coupling Effects Between the Librational and Orbital Motions of a Satellite," AIAA Journal, Vol. 2, No. 3, March 1964, pp. 553-555.

80. Ehricke, K.A., Principles of Guided Missile Design, D. Van Nostrand Co. Inc., New Jersey, 1960, pp. 241-256.

81. RCA, "RCA Flywheel Stabilized, Magnetically Torqued Attitude Control System for Meteorological Satellites, CR-232, 1965, NASA.

82. Schaaf, S.A. and Chambré, P.L., Flow of Rarefied Gases, Princeton University Press, 1961, pp. 17-24.

83. Jensen, J., Townsend, G., Kork, K., and Kraft, D., Design Guide to Orbital Flight, McGraw Hill, New York, 1962, pp. 179-264.

84. Jacchia, L.G., "Static Diffusion Models of the Upper Atmosphere with Empirical Temperature Profiles," Smithsonian Contributions to Astrophysics, Vol. 8, No. 9, 1965, Smithsonian Institution, Washington, D.C., pp. 215-257.

85. Pontryagin, L.S., Boltyanskii, V.G., Gamkrelidze, R.V., and Mischenko, E.F., The Mathematical Theory of Optimal Processes, Pergamon Press Ltd., New York, 1964, pp. 26-34.

APPENDIX I

The expressions for the frequencies ω_1 and ω_2 are given by,

$$\omega_1 = f_1(a,b,I,\sigma,e,C,G)$$

$$= F(a,b,\alpha_1,\alpha_2,k_1,k_2,\ell_1,\ell_2,C,G,A_1,B_1)$$

$$= k_1-\{1/(k_1^2-k_2^2)\}\Big[C(1+3e)\{(5A_1+7B_1-4G)\ell_1\alpha_1^2+(7A_1+B_1-4G)\ell_2\}/$$

$$16\alpha_1+\ell_1[\{I(\sigma+1)(1+2e)-4\}\{k_1(3\alpha_1^2a^2+2\alpha_2^2b^2+2B_1^2)+4k_2\alpha_1\alpha_2b^2\}/$$

$$16+\{I(\sigma+1)(1+2e)+2(3I-4)\}\alpha_1(a^2+4b^2+4A_1^2)/32+\{I(\sigma+1)(1+2e)-4\}\times$$

$$\alpha_1(\alpha_1^2a^2+2\alpha_2^2b^2+2B_1^2)/16-\{3\alpha_1k_1^2a^2/8+\alpha_1k_2^2b^2/4+\alpha_1A_1^2/4+\alpha_2k_1k_2b^2/2\}$$

$$-k_1(a^2+b^2+A_1^2)/4]+(\ell_2/\alpha_1)[\{I(\sigma+1)(1+2e)+4(3I-4)\}\times$$

$$(a^2+2b^2+2A_1^2)/16-\{I(\sigma+1)(1+2e)\}\alpha_1k_1(\alpha_1^2a^2+\alpha_2^2b^2+B_1^2)/8$$

$$-[I(\sigma+1)\ (1+2e)\}(\alpha_1^2a^2+4\alpha_2^2b^2+4B_1^2)/32-\alpha_1^2k_1^2a^2/8$$

$$-\alpha_1\alpha_2k_1k_2b^2/2+\alpha_1k_1A_1B_1/2-\alpha_2k_2b^2/2-\alpha_1k_1(3a^2+2b^2+2A_1^2)/8]\Big]$$

$$\omega_2 = F(b,a,\alpha_2,\alpha_1,k_2,k_1,\ell_1,\ell_2,C,G,A_1,B_1)$$

APPENDIX II

The functions F_i and G_i (i=1,2,3,4) are given by,

$$F_1 = \Big[-I(\sigma+1)\{(1+e)/(1+e\cos\theta)\}^2\cos\gamma_p-\{3(I-1)/(1+e\cos\theta)$$

$$-1\}\cos\beta_p(\cos^2\gamma_p-\sin^2\gamma_p)-[\{2e\sin\theta/(1+e\cos\theta)\}\sin\beta_p$$

$$-2\beta_p'\cos\beta_p]\sin\gamma_p-\{(1+e)^3/(1+e\cos\theta)^4\}C\cos\theta\times$$

$$[\{(\sin\gamma_p\sin\beta_p\cos\theta-\cos\beta_p\sin\theta)\sin\beta_p-\sin\gamma_p\cos\theta\}\cos^2\gamma_p\cos\theta/$$

$$\{(\sin\gamma_p\sin\beta_p\cos\theta-\cos\beta_p\sin\theta)^2+(\cos\gamma_p\cos\theta)^2\}^{1/2}-$$

$$\{(\sin\gamma_p\sin\beta_p\cos\theta-\cos\beta_p\sin\theta)^2+(\cos\gamma_p\cos\theta)^2\}^{1/2}\sin\gamma_p$$

$$-G|\sin\gamma_p\cos\beta_p\cos\theta+\sin\beta_p\sin\theta|\sin\gamma_p]\Big]\sec\beta_p$$

$$F_2 = [\{2e\sin\theta/(1+e\cos\theta)\}\cos\beta_p+2\beta_p'\sin\beta_p]\sec\beta_p$$

$$F_3 = [\{3(I-1)/(1+e\cos\theta)\}\sin\beta_p\sin\gamma_p\cos\gamma_p+\{2e\sin\theta/(1+e\cos\theta)\}\times$$

$$(\cos\beta_p\cos\gamma_p-\gamma_p'\sin\beta_p)+2\beta_p'\gamma_p'\cos\beta_p+\{\gamma_p''+(2\beta_p'-\sin\gamma_p)\times$$

$$\times\cos\gamma_P\}\sin\beta_P-\{(1+e)^3/(1+e\cos\theta)^4\}C\cos\theta(\sin\gamma_P\sin\beta_P\times$$

$$\cos\theta-\cos\beta_P\sin\theta)(\sin\gamma_P\cos\beta_P\cos\theta+\sin\beta_P\sin\theta)\cos\gamma_P/\{(\sin\gamma_P\times$$

$$\sin\beta_P\cos\theta-\cos\beta_P\sin\theta)^2+(\cos\gamma_P\cos\theta)^2\}^{1/2}]\sec\beta_P$$

$$F_4 = [I(\sigma+1)\{(1+e)/(1+e\cos\theta)\}^2+2\gamma_P'\sin\beta_P-2\cos\beta_P\cos\gamma_P]\sec\beta_P$$

$$G_1 = I(\sigma+1)\{(1+e)/(1+e\cos\theta)\}^2\sin\beta_P\sin\gamma_P+$$

$$2\{3(I-1)/(1+e\cos\theta)-1\}\sin\beta_P\cos\beta_P\sin\gamma_P\cos\gamma_P$$

$$-\{2e\sin\theta/(1+e\cos\theta)\}\cos\gamma_P-(\cos^2\beta_P-\sin^2\beta_P+1)\gamma_P'\sin\gamma_P$$

$$+\{(1+e)^3/(1+e\cos\theta)^4\}C\cos\theta[\{(\sin\gamma_P\sin\beta_P\cos\theta-\cos\beta_P\sin\theta)\times$$

$$\sin\beta_P-\sin\gamma_P\cos\theta\}(\sin\gamma_P\sin\beta_P\cos\theta-\cos\beta_P\sin\theta)\cos\gamma_P/$$

$$\{(\sin\gamma_P\sin\beta_P\cos\theta-\cos\beta_P\sin\theta)^2+(\cos\gamma_P\cos\theta)^2\}^{1/2}$$

$$+\cos\gamma_P\sin\beta_P\{(\sin\gamma_P\sin\beta_P\cos\theta-\cos\beta_P\sin\theta)^2+(\cos\gamma_P\cos\theta)^2\}^{1/2}$$

$$+G\cos\gamma_P\sin\beta_P|\sin\gamma_P\cos\beta_P\cos\theta+\sin\beta_P\sin\theta|]$$

$$G_2 = [-I(\sigma+1)\{(1+e)/(1+e\cos\theta)\}^2+2\gamma_P'\sin\beta_P]\cos\beta_P$$

$$+(\cos^2\beta_P-\sin^2\beta_P+1)\cos\gamma_P$$

$$G_3 = I(\sigma+1)\{(1+e)/(1+e\cos\theta)\}^2(\gamma_P'\sin\beta_P-\cos\beta_P\cos\gamma_P)$$

$$+[\{3(I-1)/(1+e\cos\theta)\}\sin^2\gamma_P+\cos^2\gamma_P-\gamma_P'^2](\cos^2\beta_P-\sin^2\beta_P)$$

$$-4\gamma_P'\sin\beta_P\cos\beta_P\cos\gamma_P+\{(1+e)^3/(1+e\cos\theta)^4\}C \times$$

$$[(\sin\gamma_P\sin\beta_P\cos\theta-\cos\beta_P\sin\theta)^2(\sin\gamma_P\cos\beta_P\cos\theta+\sin\beta_P\sin\theta)/$$

$$\{(\sin\gamma_P\sin\beta_P\cos\theta-\cos\beta_P\sin\theta)^2+(\cos\gamma_P\cos\theta)^2\}^{1/2}$$

$$+(\sin\gamma_P\cos\beta_P\cos\theta+\sin\beta_P\sin\theta)\{(\sin\gamma_P\sin\beta_P\cos\theta-\cos\beta_P\sin\theta)^2$$

$$+(\cos\gamma_P\cos\theta)^2\}^{1/2}+G(\sin\gamma_P\cos\beta_P\cos\theta+\sin\beta_P\sin\theta) \times$$

$$|\sin\gamma_P\cos\beta_P\cos\theta+\sin\beta_P\sin\theta|]$$

$$G_4 = 2e\sin\theta/(1+e\cos\theta)$$